DYNAMICS OF THE 5-HT_{3A} SEROTONIN RECEPTOR IN LIVING CELLS

THÈSE N^{O} 3384 (2005)

PRÉSENTÉE À LA FACULTÉ SCIENCES DE BASE

Institut des sciences et ingénierie chimiques

SECTION DE CHIMIE ET GÉNIE CHIMIQUE

ÉCOLE POLYTECHNIQUE FÉDÉRALE DE LAUSANNE

POUR L'OBTENTION DU GRADE DE DOCTEUR ÈS SCIENCES

PAR

Emmanuel GUIGNET

ingénieur chimiste diplômé EPF
de nationalité suisse et originaire d'Essertes (VD)

acceptée sur proposition du jury:

Prof. H. Vogel, directeur de thèse
Dr R. Hovius, rapporteur
Prof. K. Johnsson, rapporteur
Dr S. Lummis, rapporteur
Prof. G. Schütz, rapporteur

Lausanne, EPFL
2006

The present thesis has been conducted between June 2001 and October 2005 in the laboratory of physical chemistry of polymers and membranes (LCPPM) at the Swiss Federal Institute of Technology in Lausanne (EPFL) under the supervision of Professor Horst Vogel. The work has been financially supported by the Swiss National Science Foundation.

Parts of the thesis have been published in:

Emmanuel G. Guignet, Ruud Hovius and Horst Vogel. Reversible site-selective labeling of membrane proteins in live cells. Nature biotechnology, 22(4): 440-44, 2004.

Ruud Hovius, Bruno H. Meyer, Emmanuel G. Guignet and Horst Vogel. Fluorescent labelling of membrane proteins in living cells. Structural genomics on membrane proteins. K. Lundström, Ed. CRC Press. Chapter 12.

Publications in preparation:

Emmanuel G. Guignet, Jean-Manuel Segura, Ruud Hovius and Horst Vogel. Reversible site-selective labeling in live cells for single molecule spectroscopy: Diffusion of the 5-HT3 receptor.

Emmanuel G. Guignet, Christophe Danelon, Ruud Hovius and Horst Vogel. Fractional Gaussian noise of ionic channel current in a single activated serotonin receptor.

Contents

Summary

The 5-HT_3 serotonin receptor belongs to the cys-loop ligand-gated ion channel (LGIC) family. It is located in the central and peripheral nervous system and is implicated in certain pathologic situations. The 5-HT_3 receptor is investigated here, as a typical example of these LGIC's, to elucidate its structure and dynamics in living cells.

Distribution, receptor-ligand interaction and low-resolution structural information of the 5-HT_3 receptor were determined using a new method for protein labelling (chapter 2). This generic method does not require the fusion of bulky fluorophores or other moieties to the target molecule. Instead, small nickel-chelating nitrilotriacetate probes are used that bind specifically and reversibly to polyhistidine loops on the target proteins.

The lateral mobility of the 5-HT_3 in different functional states was investigated by single-molecule microscopy using the newly developed repetitive protein labelling method (chapter 3). A significant reduction of the lateral mobility of the desensitized receptor was observed indicating the role of serotonin in modulating the diffusion of the receptor, which might be important in the development of the synapse.

Conformational transitions of the 5-HT_3 receptor were investigated by tethering a fluorophore to a single cysteine side chain introduced at the 20' position in the TM2 region (chapter 4). During serotonin application, fluorescence decreased by $\sim$18% indicating a change of the fluorophore environment. Eighteen single cysteine receptors were characterized for functionality and cysteine accessibility.

Finally, electrical current through single activated 5-HT_3 mutant receptors was measured (chapter 5). Five different conductance levels were determined and noise analysis of current fluctuations in the open states of the activated receptor revealed a $1/f^{\alpha}$ dependence with $\alpha < 1$. According to a proposed model, the oscillating domain responsible of the current fluctuations contains charged amino acids.

These results contribute to a more comprehensive model of the dynamics both of the 5-HT_3 receptor and 5-HT_3 receptor within cells.

Version abrégée

Le récepteur de la sérotonine 5-HT_3 appartient à la famille des canaux ioniques activés par un ligand de type cys-boucle. Il est localisé dans le système nerveux central et périphérique, et est impliqué dans différentes pathologies. Le récepteur 5-HT_3 est utilisé ici comme exemple typique de ces canaux ioniques activés par un ligand pour élucider sa structure et sa dynamique dans des cellules vivantes.

La distribution, l'interaction ligand-récepteur ainsi que des informations structurelles à faible résolution ont été déterminées en utilisant une nouvelle méthode de marquage de protéines (chapitre 2). Cette méthode générique ne requiert pas la fusion de fluorophores volumineux à la molecule d'intérêt. De petites sondes de nitrilotriacetate chélatant du nickel suffisent à lier de manière spécifique et réversible les boucles de polyhistidines de la molécule d'intérêt .

La mobilité latérale du 5-HT_3 dans différents états fonctionnels a été étudiée par microscopie de molécule unique en utilsant la nouvelle méthode de marquage répétitif de protéines (chapitre 3). Une diminution significative de la mobilité latérale du récepteur désensibilisé a été observée indiquant le rôle de la sérotonine comme modulateur de la diffusion du récepteur, ce qui doit être important dans le développement des synapses.

Les transitions conformationnelles du récepteur 5-HT_3 ont été étudiées en attachant un fluorophore à la chaîne latérale d'une cystéine unique introduite à la position 20' du second segment transmembranaire (chapitre 4). Pendant l'application de sérotonine, la fluorescence a diminué de 18% indiquant un changement de l'environnement du fluorophore. Dix-huit récepteurs contenant une seule cystéine ont été caractérisés pour leur fonctionnalité et l'accessibilité de la cystéine.

Finallement, le courant électrique traversant un seul mutant du récepteur 5-HT_3 a été mesuré (chapitre 5). Cinq niveaux différents de conductance ont été déterminés et l'analyse de bruit des fluctuations de courant dans les états ouverts du récepteur activé a indiqué une dépendance du bruit de $1/f^{\alpha}$ avec $\alpha < 1$. Selon

un modèle proposé, le domaine d'oscillation responsable des fluctuations de courant contient des acides aminés chargés.

Ces résultats contribuent à un modèle plus complet de la dynamique du récepteur lui-même ainsi que la dynamique du récepteur dans les cellules.

Chapter 1

General introduction

Investigating and understanding the function, structure, interactions and dynamics of proteins that regulate biochemical networks of cells and organisms are of great importance because they are central to life. They deliver a fundamental view at the molecular level on how a cell works and the correlation between disfunction of biomolecules and disease. Therefore, these studies are of interest for medicine as well as pharmaceutical industry, allowing the design of new selective and specific drugs and new therapeutic methods.

Ligand-gated ion channels (LGIC) are excellent drug targets. They are responsible for electrical signaling in muscles, nerves and synapses and are therefore associated with a wide range of important pathologies. The investigation of the serotonin type 3A receptor, a representative member of the LGIC family, is going to contribute to the understanding of the molecular structural dynamics of this marvellous machinery, which is the scope of this thesis.

This introduction presents general information on the domain of ion channels and ligand-gated ion channels with emphasis of the serotonin type 3 receptor.

1.1 The concept of transmembrane signalling

The ability of cells to receive and respond to signals origenating in the plasma membrane is fundamental to life. Bacterial cells receive constant input from membrane receptors to sample the surrounding medium for pH, osmotic strength, availability of food, oxygen and light. These signals elicit appropriate responses, such as motion towards food or away from toxic substances (chemotaxis). In multicellular organisms, cells that have different functions exchange a wide variety of signals. Plant cells respond to growth hormones and to variation in sunlight. Animal cells exchange in-

formation about their correct placement in a developing embryo, the concentration of ions and glucose in extracellular fluids and interdependent metabolic activities taking place in different tissues. The signal in animals may be autocrine (acting on the same cell that produces them), paracrine (acting on a near neighbor), or endocrine (carried through the bloodstream from the signal producing cell to a distant target cell). In all three cases, the signal is detected by a specific receptor and is converted to a cellular response.

Although the number of biological signals is large (antigens, growth factors, hormones, light, mechanical touch, neurotransmitters, odorants, pheromones, tastants, ...), as is the variety of biological responses to these signals, organisms use just a few evolutionary conserved mechanisms to detect extracellular signals and transduce them into intracellular changes.

Signal transduction is remarkably specific and exquisitely sensitive. Three factors account for the extraordinary sensitivity of signal transducers: the high affinity and specificity of receptors for signal molecules, the cooperativity in the ligand-receptor interaction and the amplification of the signal. The high affinity of signal transducers is achieved by precise molecular complementarity between the signal and receptor molecules, mediated by the same kinds of weak (noncovalent) forces that occur in enzyme-substrate and antigen-antibody interactions. In multicellular organisms, specificity is further promoted because the receptors for a given signal, or the intracellular targets of a given signal pathway, are present only in certain cell types.

In other words, and in a very broad sense, a receptor can be regarded as a molecular switch which controls the delivery of a message. Being a protein, a receptor is not a rigid structure, but exists in a variety of more or less stable conformational states that are in thermodynamic equilibrium [1, 2].

The investigated serotonin type 3A receptor (5-HT_{3A}), a member of the ligand-gated ion channel (LGIC) family, is a channel gated (*i.e.* opened) by the binding of the neurotransmitter serotonin. The signal generated through receptor activation is a depolarization of the cellular membrane caused by cation flux down their electrochemical gradient triggering a cascade of intracellular events.

1.2 Serotonin: discovery, structure and function

Serotonin or 5-hydroxytryptamine (5-HT), a biogenic monoamine, is widely distributed both in animal and plant kingdoms. In mammals, high concentrations of 5-HT are found in the enterochromaffin cells of gastrointestinal mucosa, in the central ner-

vous system and in blood platelets. 5-HT was first detected in the gastrointestinal tract and blood serum.

The premise for the discovery of serotonin is a very old observation, going back to 1868 [3,4]. When physiologists tried to perfused isolated organs with serum or defibrinated blood, they invariably encountered a disturbing vasoconstriction. This was studied later in more detail by a number of investigators who gave the responsible compound various names, such as serum vasoconstriction, adrenaline-like substance of blood, Spätgift, etc [5]. The origin of this vasoconstrictor principle from platelets was recognized very early. It is in 1948 that Rapport and Page resumed the problem with more advanced methodology [6]. Starting from the serum obtained from two tons of beef blood [7], they succeeded in isolating a creatinine serum vasoconstrictor complex, having a pharmacological component. The constitutional formula 5-hydroxytryptamine was suggested for the vasoconstrictor principle, which was given the name serotonin. This name indicates that its source is serum and its activity is one causing constriction and blood pressure increase [8].

Independently, Erspamer had discovered in 1940 a factor called enteramine, in gut mucosa that was later shown to be identical to serotonin. In 1951 synthesis by Hamlin and Fischer confirmed the chemical structure of serotonin [9]. It had become clear that 5-HT is not only present in the serum and that its action is certainly not limited to constriction of the smooth muscles [10].

Physiological functions of 5-HT include regulation of blood pressure, cardiac function, gastric and enteric motility, nociception and sleep. Although only 1-2% of the total body content of 5-HT is present in the brain, the action of 5-HT as chemical messenger (neurotransmitter) between neurons in the central nervous system has received much attention. Malfunction of the 5-HT system has been implicated to play a role in the aetiology of several neuronal disorder like depression, schizophrenia, aggression, anxiety, stress, withdrawal effect from addiction, eating disorders and migraine [11–16].

The biosynthesis of serotonin starts from the essential amino acid L-tryptophan following a simple pathway (figure 1.1). Its synthesis is similar to that found for catecholamines, a family of compounds including dopamine, norepinephrine, and epinephrine derived from the amino acid tyrosine. Serotonin is formed by the 5-hydroxylation of tryptophan to form 5-hydroxytryptophan followed by the rapid decarboxylation of 5-hydroxytryptophan to give 5-hydroxytryptamine (5-HT) also called serotonin. The first and rate-limiting reaction in this sequence is catalyzed by tryptophan-5-hydroxylase, an enzyme which belongs to the family of amino acid hydroxylases [17]. The 5-hydroxylase utilizes two substrates, L-tryptophan and

molecular oxygen, as well as a reduced pterin cofactor (L-*erythro*-5,6,7,8-tetrahydrobiopterin), which serves as an electron donor [18]. The second step in the reaction pathway requires the aromatic L-alpha amino acid decarboxylase; a soluble pyridoxal-5'-phosphate (PLP) dependent enzyme, with a wide substrate specificity. 5-hydroxytryptophan, which occurs in trace amount, is one of its preferred substrates and is rapidly decarboxylated to 5-HT in serotonergic neurons. As with other transmitters, serotonin is sequestered in storage vesicles where it is held prior to release [19]. Serotonin that is not sequestered is rapidly metabolized to 5-hydroxyindoleacetic acid through the actions of monoamine oxidase, which oxidatively deaminates the amine to 5-hydroxyindoleacetaldehyde, and aldehyde dehydrogenase which oxidizes the aldehyde to the corresponding acid (for review see [20]).

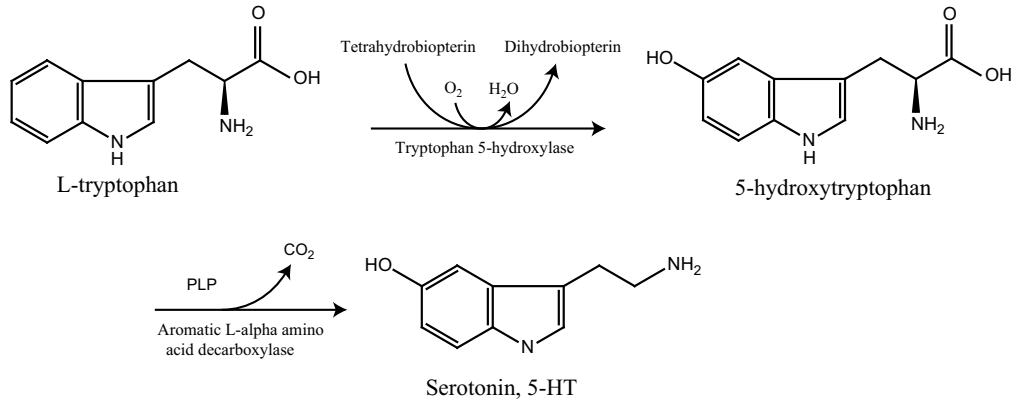

Figure 1.1: Serotonin biosynthesis. *Two steps are required to convert L-tryptophan into serotonin. These steps are catalyzed by specific enzymes, the tryptophan-5-hydroxylase and the aromatic L-alpha amino acid decarboxylase.*

1.3 Receptor classification

The current classification of receptors, proposed by the International Union of Pharmacology Committee for Receptor Nomenclature and Drug Classification (NC-IUPHAR), gives to pharmacologists a common language that avoid ambiguity and inconsistent terminology, as well as a systematic scheme of classification, which is in itself an important generic research approach in biological science.

Criteria for receptor characterization are based on a combination of information derived from the receptor's amino acid sequence, pharmacology and signal transduction mechanisms [21–24]. Of these essential criteria, amino acid sequences of proteins provide a basis for classification into superfamilies. Many receptor proteins with similarities between their primary sequence, differ pharmacologically but

are functionally similar, as they share a single molecular signal transduction mechanism. This *common structure-common function* concept is not unique to receptors, but arises from the observation that families of proteins are probably derived from a common ancestral gene [25].

Out of this classification from the IUPHAR are four main receptor structure classes: ion channels and ligand-gated ion channels (LGIC's), G protein-coupled receptors (GPCR's) (seven-transmembrane domain), enzyme-associated receptors with subunits having one membrane-inserted domain, transcription factor receptors. Each of theses classes includes superfamilies of receptors. For instance, the serotonin type 3 receptor belongs to the cys-loop superfamily, which is a member of the ligand-gated ion channel group. Therefore, the 5-HT_3 receptor shares similar features with the other members of the superfamily. For more information regarding the classification procedures, receptors numbering and codes, visit the IUPHAR web page (http://www.iuphar.org).

1.4 Receptors activated by serotonin

Gaddum and Picarelli [26] in 1957 were the first to suggest the existence of more than one type of 5-HT receptor. They demonstrated that functional responses of guinea pig ileum (a region in the bowel) could be partially blocked by morphine (M), whilst the remainder of the response was inhibited by dibenzyline (D). They proposed therefore a subdivision of these novel receptors naming them M and D respectively. Actually, neither morphine nor dibenziline is a specific 5-HT antagonist. Morphine blocks nerve-mediated excitatory responses to 5-HT because it inhibits the release of acetylcholine, which is a final common excitatory neurotransmitter to enteric smooth muscle [27, 28]. Dibenzyline is an alkylating agent that inactivates non-specifically a number of receptors on smooth muscle cells. Despite the fact that the drugs used to distinguish receptor subtypes were physiological antagonists, they did establish that there are separate neuronal and muscle 5-HT receptors in the bowel. More recent research has not only led to the development of specific antagonists that actually act on 5-HT receptors, but to the realization that there is not only one neuronal and one muscular receptor subtype for 5-HT but many of them [15]. In 1986, Bradley *et al.* [29] established a classification scheme for the subtypes of 5-HT receptors known until then. He based his rational on binding studies of selective pharmacological agents. In the years following this classification, the application of molecular biological technology had a major impact in the 5-HT field, allowing the discovery of many additional 5-HT receptors. Up to now, seven types have

been reported, 5-HT_{1-7} comprising 14 structurally and pharmacologically distinct mammalian 5-HT receptors. The Gaddum's D and M forms of serotonin receptors are now, according to this nomenclature, related to the 5-HT_2 and 5-HT_3 receptors respectively.

Intense scrutiny has now revealed much about the functional properties of different 5-HT receptors subtypes. At the molecular level, it has been established, largely using recombinant receptor models and hydropathy profiles, that the 5-HT receptors are seven transmembrane spanning, G-protein coupled receptors (GPCR) 5-HT_1, 5-HT_2, 5-HT_4, 5-HT_5, 5-HT_6 and 5-HT_7, with the exception of the 5-HT_3 receptor, which is a ligand-gated ion channel. These families can be then divided into subclasses denoted by letters (table 1.1). In the brain, the function of many 5-HT receptors can now be unequivocally associated with specific physiological responses, ranging from modulation of neuronal activity and transmitter release to behavioral changes (for review [30–32]).

Among these receptors, the 5-HT_3 receptor takes a special place. It is phylogenetically much older than the other serotonin receptors, all of which have developed from a single primordial 5-HT receptor and belong to the G-protein coupled receptor family.

Table 1.1: Classification of the 5-HT receptors.

	Subtypes	Major signalling pathway
5-HT_1	5-HT_{1A}, 5-HT_{1B}, 5-HT_{1D}, 5-HT_{1E}, 5-HT_{1F}	cAMP
5-HT_2	5-HT_{2A}, 5-HT_{2B}, 5-HT_{2C}	IP_3
5-HT_3	5-HT_{3A}, 5-HT_{3B}, 5-HT_{3C}, 5-HT_{3D}, 5-HT_{3E}	Ion channel
5-HT_4	-	cAMP
5-HT_5	5-HT_{5A}, 5-HT_{5B}	cAMP?
5-HT_6	-	cAMP
5-HT_7	-	cAMP

1.5 Ligand-gated ion channels

1.5.1 Fast signal transduction at the synapse

Excitation of sensory cells, neurons and myocytes depends on ion channels, signal transducers that provide a regulated path for the movement of inorganic ions as Na^+, K^+, Ca^{2+} and Cl^- across the plasma membrane in response to various stimuli. Signaling in the nervous system is accomplished by networks of neurons, specialized

cells that carry an electrical impulse (action potential) from one end of the cell (the cell body) through an elongated cytoplasmic extension (the axon). An electrical impulse, or action potential, propagating along an excited neuron triggers release of neurotransmitters molecules at the synapse of the presynaptic cell (figure 1.2). The neurotransmitters then act transiently and specifically on receptors expressed on the surface of the receiving postsynaptic cell [11]. Upon binding of the neurotransmitters to ion channels, a brief flux of ions across the post synaptic membrane is generated, changing the postsynaptic membrane potential. The amplitude, duration and direction of this ion flux, as well as the nature of the ions traversing the postsynaptic membrane, determines whether this response will in turn either activate voltage sensitive membrane conductance and thus initiate action potentials, or instead reduce the cell's electrical activity. Inhibitory (hyperpolarization of the cell membrane) and excitatory (depolarization of the cell membrane) synaptic neurotransmission is mediated by ligand-gated anion (γ-amino-butyric acid type A and C, and glycine receptors) and by cation channels (nicotinic acetylcholine, serotonin type 3, purinergic type 2x and ionotropic glutamate receptors), respectively.

1.5.2 Structure and classification of plasma membrane ligand-gated ion channels

The superfamily of LGIC present in the plasma membrane consists of a group of receptors such as the nicotinic acetylcholine receptor (nACh), the serotonin type 3 receptor (5-HT_3), the ionotropic type A and C γ-aminobutyric acid receptors ($GABA_A$, $GABA_C$), the glycine receptor, the purinergic receptor (P_{2x}), the ionotropic glutamate receptor and the zinc activated channel (ZAC), which share functional features. On the basis of the distribution of hydrophilic and hydrophobic amino acids residues in the protein sequences (hydropathy profiles), proteolysis and binding experiments, three different categories of ligand-gated ion channels have been proposed (figure 1.3). The transmembrane subunits are supposed to be arranged in a ring forming the ion channel in the center.

The P_{2x} ionotropic receptor family are cation selective, ligand-gated ion channel that open in response to the binding of extracellular ATP. P_{2x} receptors do not exhibit significant sequence homology with any of the other ligand-gated ion channels and are therefore considered to represent a separate class of ligand-gated ion channels [33]. The absence of a cleaved N-terminal signal sequence places the N-terminus facing the cytoplasmic site of the membrane. Protein topology predicts only two membrane spanning segments, TM1 and TM2 connected by an extracellu-

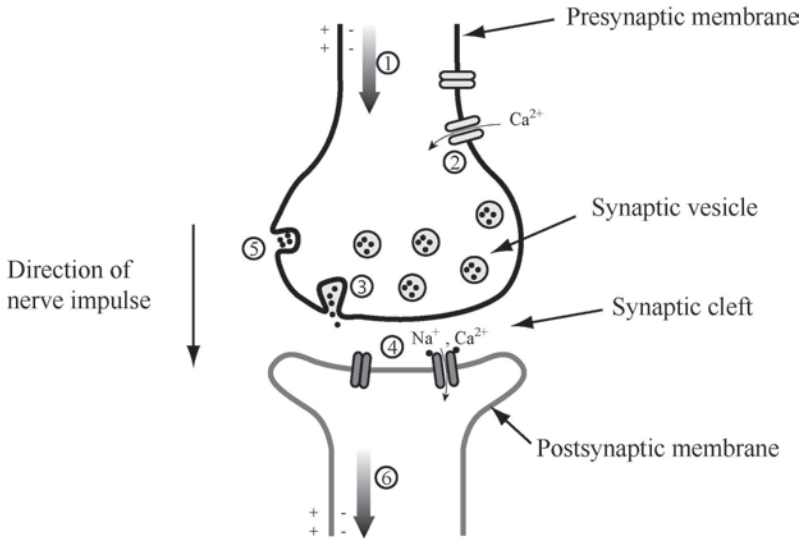

Figure 1.2: Schematic view of a synapse. *The plasma membrane of presynaptic neuron is initially polarized (inside negative) through the action of Na^+K^+ ATPase, which pumps 3 Na^+ out for every 2 K^+ pumped into the neuron. A stimulus to this neuron causes an action potential (1) to move along the axon (arrow) by the consecutive opening of Na^+- and K^+-channels. When the wave of depolarization reaches the axon tip, voltage-gated Ca^{2+} channels open (2), allowing Ca^{2+} entry into the presynaptic neuron. The resulting increase of $[Ca^{2+}]$ triggers exocytic release of neurotransmitters in the synaptic cleft (3). The neurotransmitters bind to a receptor on the postsynaptic neuron, causing its ligand-gated ion channel to open (4). Extracellular Na^+ and Ca^{2+} enter through this channel, depolarizing the postsynaptic cell (6). The electrical signal has thus passed the cell body of the postsynaptic neuron and will move along its axon to a third neuron by this same sequence of events. Neurotransmitters in the synaptic cleft are removed through two pathways, uptake of the neurotransmitters by endocytosis in the presynaptic neuron (5) or degradation by specific enzymes.*

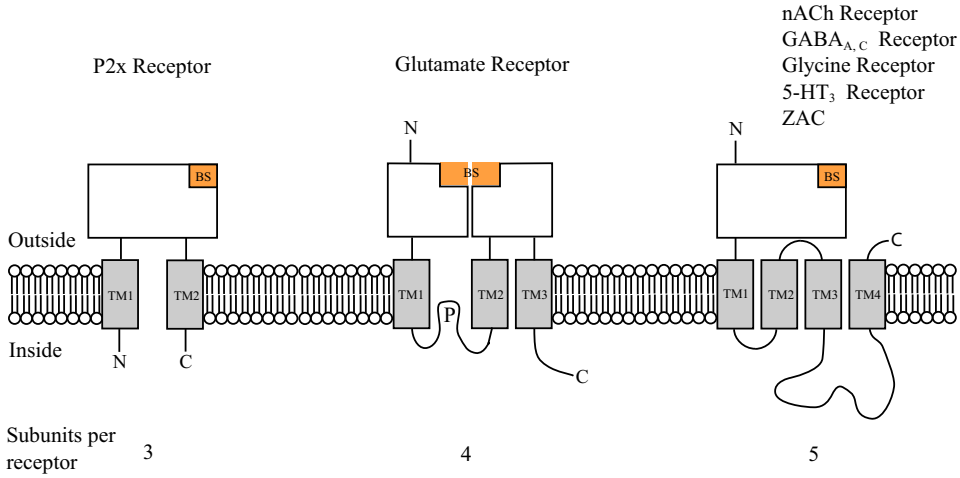

Figure 1.3: Protein topology and models of ligand-gated ion channel families. *Based on the distribution of hydrophilic and hydrophobic residues in the protein sequences and on biochemical experiments, three families of ligand-gated ion channel receptors can be distinguished according to predicted structure. TM stands for transmembrane region and BS for binding site.*

lar loop; the mature P_{2x} receptor is homotrimeric [34, 35].

Glutamate receptors (GluR) form a separate class and are grouped into three broad subtypes [36]; the kainic acid, the α-amino-3-hydroxy-5-methyl-4-isoxazole propionic acid (AMPA) and the N-methyl-D-aspartic acid (NMDA), based on amino acid sequence and agonist pharmacology. A typical GluR subunit consists of an amino-terminal domain, a ligand binding domain composed of the juxtaposition of two extracellular domains [37], three transmembrane domains with a re-entrant pore loop and a carboxy terminal domain. The re-entrant pore is located between the first and the second transmembrane domain. This so-called P-loop sequence lines the channel and determines many of its electrophysiological properties. The receptor is a tetramer assembled as dimers of dimers [38–41].

For the nACh, glycine, $GABA_A$, $GABA_C$, ZAC and the 5-HT_3 receptors, it is suggested that all members of this superfamily fold into four transmembrane domains (TM1-TM4) with the N- and C-termini both located extracellularly [42–45]. In all these members, a region of strong conservation in the extended N-terminal extracellular domains can be recognized. This region is characterized by a pair of cysteine residues, whose positions are conserved between different subunits of the ligand-gated ion channel. These residues may form disulfide bridges essential for the stabilization of the tertiary structure/subunit assembly. The number of amino-acids between the two cysteins is also conserved. This region is used as a fingerprint for

this class of receptor that is thus called the cys-loop family. All these receptors form homo- or heteropentamers indicating that the members of this ligand-gated ion channel superfamily share a conserved quaternary structure. In all cys-loop members, the pore formed by the co-assembly of five subunits is lined by residues from five TM2 domains, and is located along the pseudo axis of symmetry of the receptor complex.

The alignment of TM2 domains and flanking region of the cys-loop LGIC family reveals conservation of the residues between and within the two ion selectivity classes (anion and cation channels). The leucine residue in the 9' position is the only fully conserved residue (only in the 5-HT_{3B} holds a valine residue) and is considered as a signature for this class of receptors [46].

Coassembly of subunits beyond the boundaries of ligand-gated ion channel families have been shown to form functional receptor. For instance, heteromeric 5-HT_3/α_4 nACh has similar pharmacological profiles to the homomeric 5-HT_{3A} receptor, but distinct sensitivities to antagonists [47]. Moreover, as ligand-gated ion channels are close relatives in the gene superfamily, it was also possible to generate chimeras. The first reported one is a chimeric nicotinic-serotonergic receptor, a homopentamer containing at the N-terminal part the nicotinic α_7-subunit and the complementary C-terminal domain of the 5-HT_{3A} subunit that is gated by nicotinic ligands [48]. Other similar homopentameric chimeras were constructed like $GABA_A$/glycine receptor [49], AChBP/5-HT_{3A} receptor [50] and AChBP/glycine receptor [51]; acetylcholine binding protein (AChBP) is a homopentamer homologous to the extracellular domain of nACh receptors, the structure of which has been determined at atomic resolution [52]. These chimeras were mainly designed to understand the mechanism of allosteric coupling between the ligand-binding domain and the ion channel of cys-loop ligand-gated ion channels.

1.5.3 Functional states of the ligand-gated ion channels

From a general point of view, ligand-gated ion channels open within a fraction of seconds after binding of agonist-type ligands and close thereafter into a state where channel opening is blocked while the ligand is still bound. After removing the ligands, the receptor can be activated as before. Such behavior is described in general by three distinctive functional states , the resting state or basal state (closed) (B), the open state (A) and the desensitized state (closed) (D) as illustred in figure 1.4. The basal state is the most stable state in the absence of agonist and the desensitized state is the most stable state in the presence of the agonist.

The open state is metastable in that its concentration rises transiently and reaches a very low value at equilibrium. The role of desensitization is uncertain but there are indications that its kinetics can determine the size, timecourse and frequency of transmitted signals [53]. Ligand-gated ion channels are allosteric; the oligomeric channel contains multiple agonist-binding sites, non-competitive-antagonist sites, and gates that interact at a distance through changes of the quaternary structure of the receptor. They also open, albeit rarely, and desensitize in the absence of agonist. Their behavior can therefore be described by the Monod-Wyman-Changeux (MWC) model of allosteric interaction [54].

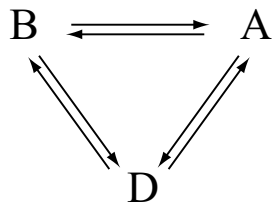

Figure 1.4: Simple three states allosteric model. *The simplest allosteric model describing the functional states of the ligand-gated ion channels. It consists of a basal state B, an open state A and a desensitized state D. Transition probabilities between these states are modulated by ligand binding.*

1.6 The 5-HT$_3$ receptor

1.6.1 Physiology and pathophysiology of the 5-HT$_3$ receptor

The serotonin type 3 receptor is a ligand-gated cation channel located in the central and peripheral nervous system. It has also been found in a variety of other cells like mononuclear cells, lymphocytes and intestinal enterochromaffine cells. In the periphery, 5-HT$_3$ receptors have been detected on pre- and postganglionic autonomic neurons and on neurons of the sensory and enteric nervous system (myenteric and submucosal plexus). A high density of 5-HT$_3$ receptors has been found in the following central nervous system locations (mostly on GABAergic neurons): area postrema, nucleus tractus solitarii, nucleus accumbens, nucleus caudatus, nucleus dorsalis nervi vagi, amygdala, hippocampus, entorhinal cortex, frontal cortex, cingulate cortex and dorsal horn ganglia [55, 56].

5-HT$_3$ receptors are found in the brain predominantly in presynaptic regions associated with axons and nerve terminals (70-80%) except in hippocampus, where they are mostly postsynaptic receptors located on somatodendritic regions [57]. The

predominant localization on nerve endings is consistent with a physiological role of 5-HT_3 receptors in the control of neurotransmitter release [58]. On the molecular level, activation of presynaptic 5-HT_3 receptors followed by rapid depolarization of the peripheral or central neuron causes a rapid rise in cytosolic Ca^{2+} concentration by inducing calcium influx and mobilization of intracellular calcium stores as well as modulating the release of various neurotransmitters and neuropeptides such as dopamine, cholecystokinin, acetylcholine, γ-aminobutyric acid (GABA), substance P or serotonin itself [59]. They have been demonstrated to be involved in sensory transmission, regulation of autonomic functions, integration of the vomiting reflex, pain processing and control of anxiety.

While the physiologic functions of the 5-HT_3 receptor are discrete and difficult to detect, the receptor plays a key role in certain pathologic situations related to increased serotonin release. 5-HT_3 receptor antagonists revealed a remarkable range of activities [60]. They do not modify any aspect of normal animal behavior or induce pronounced changes of physiological functions in healthy subjects except for intestinal transit. Clinical efficacy was shown for various forms of emesis like chemotherapy-induced, radiotherapy-induced, and postoperative emesis, diarrhoea-predominant irritable bowel syndrome, skin burn wounds, anxiety, chronic fatigue syndrome, alcohol abuse and in pain syndromes such as fibromyalgia and migraine [61–63]. 5-HT_3 antagonists are also suggested to be effective for the treatment of other rheumatotic diseases such as rheumatoid arthritis, tendinopathies, periarthropathies and myofascial pain as well as for chronic heart pain and bulimia [64–66]. A better understanding of the role played by the 5-HT_{3A} receptor is likely to result from new molecular tools, such as gene knock-out mice, especially inducible mice in which a specific genetic alteration can be restricted both temporally and anatomically [67–69].

1.6.2 5-HT_3 receptor subtypes and 5-$HT_{3A/3B}$ properties

5-HT_3 receptors, like other members of the cys-loop family (nACh, $GABA_A$ and glycine receptors), exist as homo- and hetero-pentamers in the membrane. Up to now, five different human 5-hydroxytryptamine type 3 receptor-like genes have been cloned; 5-HT_{3A}, 5-HT_{3B}, 5-HT_{3C}, 5-HT_{3D} and 5-HT_{3E} (table 1.1). No functional data are available for 5-HT receptor genes C, D and E except that 5-HT_{3D} expression is restricted to kidney, colon and liver and 5-HT_{3E} expression to colon and intestine, whereas all other genes are widely expressed in many tissues including brain [70,71]. Concerning the human 5-HT_{3C}, its sequence has been patented and hardly any detail

is published [72]. Much is known about the 5-HT$_{3A}$ and 5-HT$_{3B}$. By contrast to the 5-HT$_{3A}$ subunit, the 5-HT$_{3B}$ subunit appears to be much more complex, because its TM2 segment lacks any structural homology to that of other ligand-gated ion channels.

In contrast to the 5-HT$_{3A}$ subunit, 5-HT$_{3B}$ subunit does not form functional homopentameric channel because of its retention in the endoplasmic reticulum (ER) [73]. This retention has been attributed to an ER retention signal located within the first cytoplasmic loop between TM1 and TM2 [74]. The presence of the 5-HT$_{3B}$ subunit modulates the biophysical properties of the channel, presumably by forming hetero-pentamers with the 5-HT$_{3A}$ subunit [75–77]. Electrophysiological and pharmacological studies showed that native receptors are distinct from the homopentameric receptor expressed in heterologous systems [42, 78, 79] suggesting the presence of another subunit before the discovery of the 5-HT$_{3B}$. Combinations of 5-HT$_{3A}$ and 5-HT$_{3B}$ subunits produce receptors with several distinctive properties. Heteromeric receptors are less potently activated by 5-HT than are homomeric receptors (table 1.2); homomeric receptors have a higher permeability to Ca^{2+} relative to monovalent cations than do heteromeric receptors; and heteromeric receptors have a significantly greater single channel conductance than do homomeric receptors [75].

In addition to these known 5-HT$_3$ subunits, two splice variants further increase functional diversity of these receptors. These two 5-HT$_{3A}$ subunits differ in the presence of six amino acids in the large intracellular loop and have different expression profiles during development [80, 81]. However, thus far, physiologically relevant functional differences between the splice variants have not been shown. It is possible that additional undiscovered 5-HT$_3$ receptor subunits exist.

A new type of ionotropic 5-HT receptor has been reported in the nematode *Caenorhabditis elegans*. It is a 5-HT-gated chloride channel encoded by the gene *mod*-1 for modulation of locomotion defective. The predicted MOD-1 protein is related to the members of the cys-loop family of ligand-gated ion channels, in particular to GABA and glycine-gated chloride channels but functions as a 5-HT receptor [82]. Other anion-selective cys-loop ligand-gated ion channels have been found in *C. elegans* [83].

1.6.3 Pharmacology of the 5-HT$_3$ receptor

The efficiency of serotonin for the agonist recognition site of the 5-HT$_3$ receptor is relatively low (table 1.2). 5-HT might not be the only endogenous ligand as dopamine (DA) is a low-affinity agonist of 5-HT$_3$ receptors [84]. Of the various 5-HT$_3$ recep-

tor agonists known, 2-methyl-5-HT, phenylbiguanide and *m*-chlorophenylbiguanide (mCPBG) are the more commonly used. However, highly selective 5-HT_3 receptor agonists have not been found. Non-selective effects, observed at agonist concentrations similar to those required for 5-HT_3 receptor activation, include reversal of DA transport (for serotonin, phenylbiguanide, mCPBG and cocaine) [85,86] and partial agonism or antagonism of α_2 adrenoreceptors (mCPBG for instance) [87,88].

Numerous highly potent antagonists of 5-HT_3 receptors have been developed. Several common 5-HT_3 receptor antagonists are listed in table 1.2. In general, these compounds are highly selective for 5-HT_3 receptors and non-selective effects appear to occur only at concentrations 100-fold or more in excess of those required to antagonize the 5-HT_3 receptor. The non-selective effects of 5-HT_3 receptor antagonists are of variable nature and include antagonism of receptors other than 5-HT_3 receptors [89,90], agonism of 5-HT_4 receptors [91], and local anaesthetic-like block of ligand- and voltage-gated ion channels [92].

A notable property of 5-HT_{3A} receptors is the potentiation of agonist effects by alcohols and anaesthetic agents [93] which might complicate the comparison of *in vitro* data with data obtained *in vivo* from anaesthetized animals. For extensive details on 5-HT receptor pharmacology, see [24].

Table 1.2: Comparison of the pharmacological properties of the homooligomeric 5-HT_{3A}, the heterooligomeric 5-$HT_{3A/3B}$ and the 5-HT_3 in N1E-115 neuroblastoma cells.

	5-HT_{3A}	**5-$HT_{3A/3B}$**	**5-HT_3 N1E-115**
Agonists	[1]**pEC_{50}**	[2]**pEC_{50}**	[3]**pEC_{50}**
5-HT	5.63	5.22	5.38
2-methyl-5-HT	4.83	5.31	4.76
1-phenylbiguanide	4.52		ND
m-chlorophenylbiguanide	6.06	5.68	5.85
Antagonists	**pIC_{50}**	**pIC_{50}**	**pIC_{50}**
ondansetron	8.92		9.60
granisetron	9.85		9.90
D-tubocurarine	8.85		9.09
cocaine	5.63		5.14

pEC_{50} = -$\log_{10}EC_{50}$(M); pIC_{50} = -$\log_{10}IC_{50}$(M); ND for not determined.

[1]Data from [75], [94] and [95].

[2]Data from [75]

[3]Data from [96] and [97].

1.6.4 Molecular structure of the 5-HT$_3$ receptor

Much of the work on the structure of the cys-loop ligand-gated ion channel family has been performed on nicotinic acetylcholine (nACh) receptors for historical and practical reasons. The nACh receptor is present in high amounts in the electric organs of *Torpedo* electric ray, suitable for electron microscopy [98], and is therefore a never failing and easy source for experimental investigation. Moreover, toxins that specifically inhibit the gating of the nACh channel are present in high amounts in nature in the venom of the snakes *Bungarus multicincus* (α-bungarotoxin) and cobra and of marine snails *Conus* genus (α-conotoxin) [99, 100]. All these factors contributed to the popularity of this receptor in the scientific community since they facilitate biochemical and biophysical investigations. Moreover, the structure of a protein homologous to the extracellular domain of the receptor, named the acetylcholine binding protein (AChBP), has been resolved at the atomic level recently [52]. This structure leads to a good idea how the whole extracellular part might look and has significantly advanced the understanding of the ligand binding domain [101]. Therefore, the nACh receptor is the prototype of the cys-loop receptor family in terms of biochemistry, electrophysiology and structure.

The amino-acid sequence of the 5-HT$_{3A}$ receptor subunit displays strong sequence similarity with the Torpedo nACh receptor α-subunit (27% identity), as well as the β_1-subunit of the bovine GABA$_A$ receptor (22% identity) [102]. The most closely related ligand-gated ion channel is the neuronal nACh receptor α_7-subunit, an homo-pentameric receptor, that shares 30% identity [103]. The AChBP shares 23% and 19% amino-acid identity with the extracellular domain of α_7 nACh receptor and 5-HT$_{3A}$ receptor, respectively. These high amino-acid homologies between members of the cys-loop LGIC family allow reliable structural extrapolation from resolved structures of a member to an other.

5-HT$_3$ receptors are formed by the assembly of five subunits, each with a large N-terminal domain and four putative transmembrane domains (figure 1.3). Five different subunits are known (5-HT$_{3A}$ to 5-HT$_{3E}$) that can co-assemble to make functional hetero-pentamers (only known for subunits A and B). However, nothing is known about the stoichiometry of these different subunits with the exception of the hetero-pentamer 5-HT$_{3A/3B}$, where the stoichiometry has rencently been revealed to be 2A:3B showing the arrangement B-B-A-B-A around the receptor rosette [104]. 5-HT$_{3A}$ forms functional homo-pentamers the properties of which are modified by the presence of the 5-HT$_{3B}$ subunit [75–77].

The 5-HT$_{3A}$ sequence consists of 487 amino acids (length of the unprocessed

precursor) resulting in a 54 kDa molecular weight for the mature protein [42, 105]. Each subunit contains seven cysteins (two forming the disulfide bridge of the cys-loop) and thirteen tryptophans. Initial studies showed that the molecular target size of the 5-HT_3 receptor expressed in NCB-20 cells is approximately 250 kDa, suggesting that the functional receptor is a multimeric structure [106]. This suggestion was confirmed by low resolution electron microscopy studies showing that the 5-HT_3 receptor, purified from NG108-15 mouse neuroblastoma x rat glioma cells, is composed of five subunits arranged symmetrically around a central cavity of 2 to 3 nm in diameter; the 5-HT_3 receptor can be modelled as a cylinder 11 nm in length and 8 nm in diameter with a closed end and a central cavity 3 nm in diameter [107]. No atomic resolution structure has been obtained yet for the 5-HT_3 receptor due to the difficulties inherent in crystallization of ion channels. Information is limited to the extrapolation of the known homologous structure like AChBP [52] and the recently proposed structure of the nAChR of Unwin and coworkers [108,109] is deduced from increasingly higher resolution computer-enhanced cryo-electron microscopy images (figure 1.5).

1.7 Scope of the thesis

Still today, many questions in the field of ligand-gated ion channels remain to be resolved: For instance, how ligand binding to the receptor is transduced into an opening of the ion channel, what are the structural and conformational dynamic changes of the receptor when activated, how does the receptor behave in a cell plasma membrane, does it freely diffuse or not, are there different open states of the channel ...? Even if structural data of homologous proteins of the 5-HT_3 receptor increase our structural perception of the LGIC receptor, they are by far not sufficient to draw a clear picture of these receptors in the different conformational states. The most advanced published structure of a ligand-gated ion channel is the one presented by Unwin of the *Torpedo* nACh receptor [109] at 4 Å resolution which is not sufficient to distinguish individual amino-acid positions (figure 1.5).

The mentioned questions are addressed throughout the next chapters and some of them are answered, or partially answered. To address these issues, two main tools have been used. (i) Electrophysiology, because it records the flow of ions across the pore in living cells down to single channel sensitivity and is therefore a tool of choice to investigate LGIC. (ii) Fluorescence as an optical technique because it allows investigations under biological conditions. The measurement itself is nondestructive and noninvasive. Moreover, fluorescence techniques are very sensitive down to the

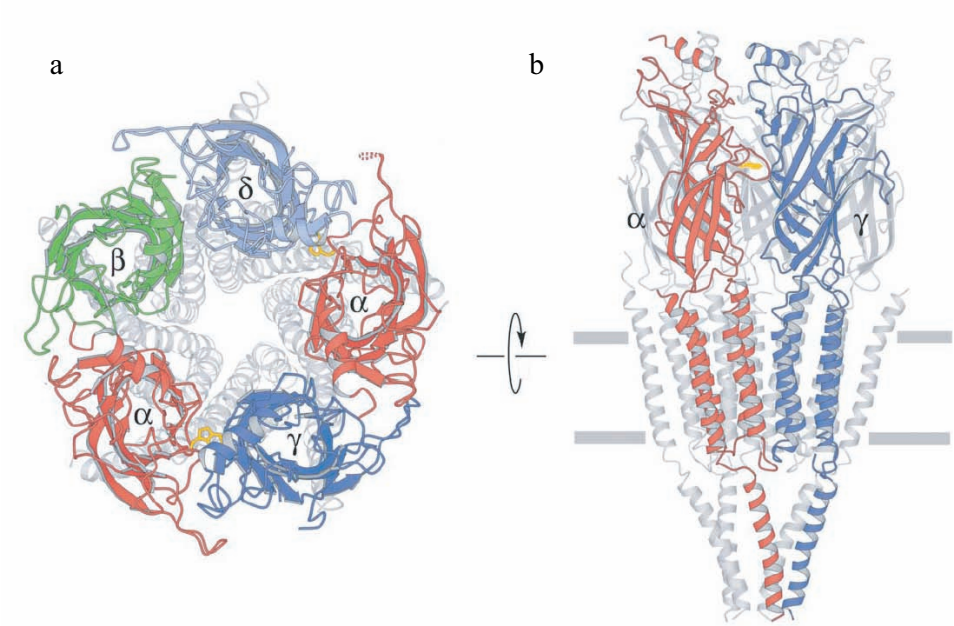

Figure 1.5: Refined structure of the Torpedo nACh receptor at 4 Å resolution [109]. *Ribbon diagram of the whole receptor, as viewed from the synapse cleft (a) and after 90° rotation, i.e. parallel with the membrane plane (b). Only the ligand-binding domain is highlighted in (a) and only the front row subunits are highlighted in (b). The greek letters denote the different subunits of the* Torpedo *nACh receptor. αTrp149 residues, interacting with ligand in the binding pocket, is highlighted in yellow. The receptor has a five-fold symmetry with a central pore formed by the assembly of five subunits where residues of the TM2 domains line the channel (a). The receptor is made of three main parts, the extracellular domain containing the binding site, the transmembrane domain composed of α-helices forming the channel, and the intracellular part (see figure 1.3 for comparison).*

single fluorophore detection and allow the visualization of multiple phenomena like protein-protein interactions, diffusion, rotations, environmental changes,..., and is therefore well suited for *in vivo* investigation of the 5-HT_3 receptor.

First, a new and generic fluorescence labelling method is developed and applied to the 5-HT_{3A} receptor yielding molecular structural information in live cells. This technique offers several advantages compared to other labelling procedures: Small size of the tag and probe, reversible labelling and fast kinetic measurements (chapter 2). Here, this labelling method is used for imaging single receptor molecules in live cells, which allows to measure the diffusion of single receptors in the plasma membrane (chapter 3). Regarding the structural dynamics of this protein, fluorescent reporters are site-specifically incorporated into the channel region using the so-called substituted-cysteine accessibility method, which allows to detect conformational changes of the receptor (chapter 4). Finally, electrophysiology experiments on the single channel level reveal subconductive states of a high conducted mutant receptor (chapter 5).

Chapter 2

Reversible site-specific labelling of membrane proteins in living cells: Structure of the 5-HT_{3A} receptor

Abstract — Chemical and biological labelling is fundamental for the elucidation of the function of proteins within biochemical cellular networks using bioanalytical techniques. In particular, fluorescent probes allow fast, real-time imaging of molecules and molecular assemblies. A new generic method to label *in vivo* proteins selectively, rapidly (seconds) and reversibly, with small molecular probes that can have a wide variety of properties is presented in this chapter. These probes comprise a chromophore and a metal-ion-chelating nitrilotriacetate (NTA) moiety, which binds reversibly and specifically to engineered oligohistidine sequences in proteins of interest. The feasibility of the approach is demonstrated, *in vitro* and *in vivo*, by binding NTA-chromophore conjugates to a purified fluorescent protein and to a representative ligand-gated ion channel and G protein-coupled receptor, each containing a polyhistidine sequence. The ionotropic 5-HT_{3A} serotonin receptor is investigated by fluorescence measurements to characterize in live cells the probe-receptor interactions, yielding structural information and plasma membrane distribution of the receptor.

2.1 Introduction

Elucidating the distribution, dynamics, interactions and chemical environments of proteins inside living cells is critical for understanding the biomolecular mechanisms of cellular functions. For instance, labelling proteins with fluorescent probes allows detection of molecular interactions, mobility and conformational changes of proteins in live cells [110–112]. For this to be feasible, the probes should be well addressed and not perturbing in order to investigate the more sophisticated function of proteins in their natural environment. Several methods have been developed to site-specifically introduce probes into proteins in live cells.

The most prominent method of protein labelling is to genetically encode green fluorescent protein (GFP) as a fusion to the protein of interest [113]. GFP has been fused to a variety of protein targets with little or none interference in native protein functionally. Unfortunately, fluorescent proteins are inherently limited by their spectral characteristics and dimensions (∼27 kDA) even with all the different variants developed [114]. The need for chemically diverse protein labels has led researchers to develop various ways to label proteins with small molecule probes having a wide range of properties. Whereas the strength of the reporters like GFP lies on the perfect specificity of genetic fusion, the chemoselective reaction of a small-molecule probe with a single functional group on a single protein in a native environment poses an enormous problem; it has to exclude thousand of other competing proteins as well as DNA, RNA, carbohydrates and small molecules.

For labelling proteins with small molecule probes *in vitro*, the unique reactivity of cysteine has been exploited and less commonly the N-terminus of proteins. These strategies can not be used for cellular labelling, because nearly all endogenous proteins bear cysteine sidechains and a free N-terminus. Thus, strategies for achieving specificity have relied upon unique combinations of amino-acids (i.e. peptide or protein sequences fused to the protein under investigation) that recruit the small molecule probe of interest. For some methods the information contained in the targeting sequence alone is sufficient to confer specificity. In other cases, an enzyme mediates the conjugation of the probe to the target sequence.

The most straightforward method for targeting a small molecule to a protein is to use a binding interaction sequence that is genetically fused to the protein of interest. Cell surface exposed epitopes fused to proteins target various hapten antibodies with high affinity and specificity. Fluorescent labelling is done using either fluorescently labelled primary or secondary antibodies directed against the Fc domain of the primary one [115]. Intracellular epitopes can only be accessed

by cell permeabilization. More recent approaches have employed the dihydrofolate reductase (DHFR), a monomeric 18 kDa protein, as a fusion protein that binds with subnanomolar affinity to its inhibitor methotrexate and its fluorescent derivatives in DHFR-deficient CHO cells [116]. Similarly, the FK506 immune-suppressant binding protein (FKBP), that binds with high affinity fluorescein FK analogue (SLF'), was used in mammalian cell lines [117]. Labelling with these tags is highly specific, and the method is versatile because it can accommodate probes of many different properties. However, like GFP, the protein tags are large.

Stabilizing the protein-probe binding event through covalent interaction, was performed using enzymes with single turn-over. O^6-alkylguanine-DNA-alkyltransferase (hAGT), the human DNA repair protein, fused to the protein of interest binds various O^6-benzylguianine suicide substrates through the alkylation of a cysteine residue. A range of fluorescent groups and biotin have thus been introduced [118–120]. A similar strategy named "Halo Tag^{TM}" launched by Promega used an optimized dehalogenase as fusion protein, which can irreversibly be labelled by chloro-alkane derivatives carrying fluorescent probes. An elegant variation of these labelling approaches employed a modified shortened peptide derivative of the acyl carrier protein (ACP) as fusion protein for cell surface protein labelling. The post-translational modification of ACP by phosphopantetheine transferase (PPTase) lead to the transfer of the label added as coenzyme A adduct to a serine residue of ACP [121]; this method was recently extended to multicolor labelling [122]. All these three methods have an excellent specificity because the initial binding interactions orient the reactive groups and ensure site-specific interaction. Since nearly all biophysical probes can be appended without affecting the specificity or rate of the ligation chemistry, they are all quite versatile. Nevertheless, the size of the tag remains important.

The fusion of a peptide sequence to the protein of interest presents a much less invasive option than the fusion of a protein sequence. As with proteins, small molecules can be targeted to peptide via affinity binding interactions. Fluorogenic biarsenical (FlAsH) compounds were used to label six amino acids tetracysteine peptide (Cys-Cys-X-X-Cys-Cys, where X were initially undefined amino acids but are now preferably Pro-Gly). Upon binding to the tetrathiol sequence, the cell permeable probe becomes highly fluorescent [123]; the binding is reversed by ethanedithiol (EDT) in high excess. Even if the FlAsH methodology has already begun to make significant contributions to cell biology [124–126], several drawbacks limit its utility. Biarsenical compounds retain significant affinity for isolated thiols requiring complex washouts or presence of thiol compounds (μM-mM). A recently reported

methodology method for labelling 15 amino acids peptide sequence uses the *E. coli* enzyme biotin ligase (BirA), which sequence-specifically ligates a ketone isostere of biotin to the lysine residue of the acceptor peptide. The introduced ketone is then selectively labelled with hydrazine derivatives of fluorophores, yielding a hydrazone adduct [127]. This two steps approach has several short comings; the hydrazone adduct is unstable and has to be reduced by sodium cyanoborohydride to yield a stable bond, the coupling of biotin to the acceptor peptide is slow and high amounts of hydrazine derivatives are required. Surface protein labelling in living cells was therefore performed with fluorescently labelled streptavidin and streptavidin-conjugated quantum dots [128], both whose dimension do not confer any advantages towards previously mentioned methods.

Another very different approach is the suppressor tRNA technology that site-specifically incorporates unnatural amino-acids into proteins using the nonsense stop codon [129–131]. Biophysical probes like benzophenone, aryl azide cross-linkers, fluorophores have been incorporated at these sites *in vitro* and *in vivo*. The major advantages of unnatural amino acid labelling are the excellent specificity, versatility and minimal structural perturbation to the protein of interest. However, unnatural amino acid mutagenesis is not yet broadly applicable in all cell types. Another serious concern is that the introduction of modified amino-acids into nascent proteins is mainly limited by the acceptance of the ribosome which places a limit on the type of probes that can be directly introduced. For reviews on protein labelling, see [132–134].

Here, polyhistidine sequences are exploited as recognition elements for site-selective labelling (figure 2.1). These genetically encoded tags can be introduced into regions of the amino-acid sequence where they do not disturb the protein's structure and function such as at the termini or loops, as will be shown; the tags will not be tolerated within structurally important regions such as helical spanning parts. The probes contain a metal-ion chelating nitrilotriacetic (NTA) part covalently bound to a chromophore that can have a wide range of properties. The site-specific interaction between the peptide sequence and probe is non-covalent and can therefore be reversed by competition. Quenchers NTA-probes were first used to overcome the relatively low affinity (μM) towards the hexahistidine tag and to prove the feasibility of the method. Several factors involved in the interaction were then investigated like the length of the polyhistidine recognition peptide, the metal ion and, mono and divalent NTA-probes. Note that oligohistidine sequences have been widely applied in combination with NTA for purification [135], *in vitro* detection [136, 137] and surface immobilization of recombinant proteins [138]. NTA-chromophore con-

jugates overcome several limitations of currently used labelling methods and, being complementary and orthogonal to these methods, they open novel approaches to the efficient and quantitative investigation of proteins in live biological cells.

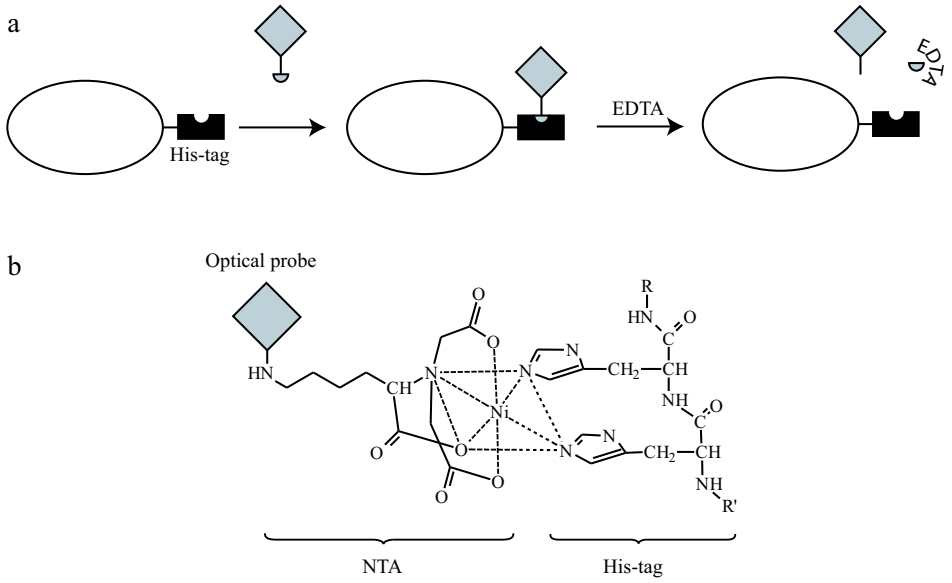

Figure 2.1: Principle of the reversible site-specific labelling with NTA-probes. *(a) A polyhistidine sequence genetically introduced to the protein of interest is recognized by the probe through the site-specific interaction between the tag and metal-NTA moiety. Complexing the metal with EDTA reverses the binding yielding the original tagged protein. (b) Structural interaction between the metal bound NTA-probe and a polyhistidine sequence. The NTA bound optical probe can have a vide range of properties since it does not interact with the recognized peptide sequence.*

2.2 Fluorescence resonance energy transfer

Throughout this chapter, fluorescence resonance energy transfer (FRET), which is the transfer of the excited state energy from the donor (D) to an acceptor (A), will be used for the characterization of the interaction between NTA-probes and polyhistidine tagged proteins. The donor molecule typically emit at shorter wavelengths with overlap with the absorption spectrum of the acceptor. Energy transfer occurs without the appearance of a photon and is the result of long-range of a dipole-dipole interactions between the donor and the acceptor. The rate of energy transfer depends upon the extent of spectral overlap of the emission spectrum of the donor with the absorption spectrum of the acceptor, the quantum yield of the donor, the

relative orientation of the donor and acceptor transition dipoles and the distance between the donor and acceptor molecule (figure 2.2). FRET provides signals sensitive to intra- and intermolecular distances in the 1-10 nm range, which are comparable to the dimensions of biological marcromolecules or distances involved in biological phenomena like molecular binding. Consequently FRET is capable of resolving molecular interactions and conformations with a spatial resolution far exceeding the inherent diffraction limit ($\sim \lambda/2$). The distance dependance of FRET, and since fluorescence is non-invasive for *in vivo* investigations, resulted in its widespread use in biophysics [139].

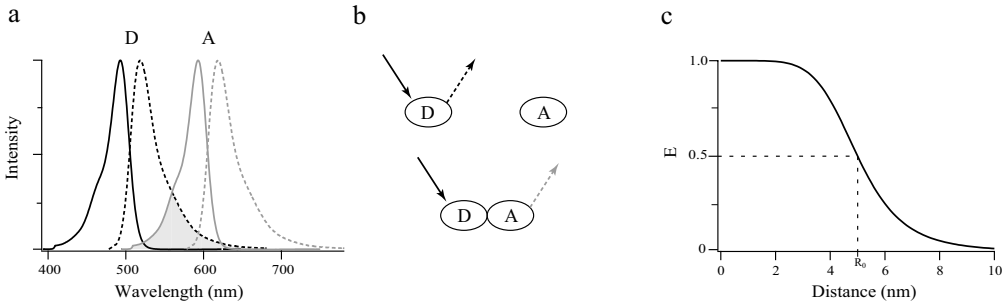

Figure 2.2: Energy transfer principle. *A prerequisite for FRET is that the absorption (−) and emission (−−) spectra of a pair of donor (D) and acceptor (A) overlaps (hatched area of (a)) and that D and A are in close proximity. Owing to FRET, the fluorescence of the donor is quenched and fluorescence of the acceptor is increased (b). The transfer efficiency E can then be calculated using equations 2.8 and 2.7. The transfer efficiency E depends on the distance separating D from A, described by equation 2.6 and illustrated in (c). FRET is most sensitive to distance variation when $r = R_0$ (maximal slope).*

Mathematical description [140, 141] — The rate of energy transfer from a donor to an acceptor separated by a fixed distance r is given by equation 2.1 and 2.3 where ϕ_{D} is the quantum yield of the donor in the absence of the acceptor, n is the refractive index of the medium, N_{Av} is the Avogadro's number, κ^2 is the orientation factor of the transition dipoles and J is the overlap integral.

$$k_{\mathrm{T}} = \frac{9000 \cdot \ln 10 \cdot \kappa^2 \cdot \phi_{\mathrm{D}}}{128 \cdot \pi^2 \cdot n^4 \cdot N_{\mathrm{Av}} \cdot r^6 \cdot \tau_{\mathrm{D}}} \cdot J \tag{2.1}$$

All the experimentally known parameters of equation 2.1 characterizing the D and A pair interaction are grouped into a term R_0 named the Förster distance (equation 2.2). k_{T} can then be written in terms of r, R_0 and τ_{D} as presented by equa-

tion 2.3. In this relation, the rate of transfer k_{T} is equal to the decay rate of the donor in the absence of the acceptor τ_{D} when D-A distance is equal to R_0, then the transfer efficiency is 50%.

$$R_0 = 9.78 \cdot 10^2 \times \left(J \cdot \kappa^2 \cdot n^{-4} \phi_{\mathrm{D}}\right)^{1/6} \tag{2.2}$$

$$k_{\mathrm{T}} = \frac{1}{\tau_{\mathrm{D}}} \cdot \left(\frac{R_0}{r}\right)^6 \tag{2.3}$$

The overlap integral J in equations 2.1 and 2.2 expresses the overlapping degree between the donor emission and the acceptor absorption. J is determined by equation 2.4 where F_{D} is the corrected fluorescence intensity of the donor with the total intensity normalized to unity and $\varepsilon_{\mathrm{A}}(\lambda)$ is the extinction coefficient of the acceptor at λ.

$$J = \int_0^\infty F_{\mathrm{D}}(\lambda) \cdot \epsilon_{\mathrm{A}}(\lambda) \cdot \lambda^4 d\lambda \tag{2.4}$$

The efficiency of energy transfer (E), which is the ratio of the transfer rate to the total decay rate of the donor, is expressed as:

$$E = \frac{k_{\mathrm{T}}}{{\tau_{\mathrm{D}}}^{-1} + k_{\mathrm{T}}} \tag{2.5}$$

Recalling that $k_{\mathrm{T}} = {\tau_{\mathrm{D}}}^{-1}(R_0/r)^6$, equation 2.5 is rearranged to yield equation 2.6. This equation shows, as equation 2.3, that the transfer efficiency is 50% when $r = R_0$ and that it is strongly distance dependent when r is close to R_0.

$$E = \frac{1}{1 + \left(\frac{r}{R_0}\right)^6} \tag{2.6}$$

In practice, the transfer efficiency is typically measured using the relative fluorescence intensity of the donor in the absence (F_{D}) and presence (F_{DA}) of the acceptor. The transfer efficiency can also be calculated from fluorescence lifetimes under these respective conditions (τ_{D} and τ_{DA}).

$$E = 1 - \frac{F_{\mathrm{DA}}}{F_{\mathrm{D}}} \tag{2.7}$$

$$E = 1 - \frac{\tau_{\mathrm{DA}}}{\tau_{\mathrm{D}}} \tag{2.8}$$

2.3 Materials and methods

2.3.1 Synthesis of NTA-probes

The reactions were performed in the dark at 22°C. The NTA-probes were purified by thin layer chromatography (TLC) on silica gel 60 plates 200 x 200 x 0.25 mm^3 (Merck, Darmstadt, Germany). The different products of the reactions were easily distinguishable since they are colored. The excess of NTA-lysine was revealed on TLC with ninhydrine, which reacts with primary amines yielding a red spot under warming. Extracted products were then aliquoted, lyophilized and stored at -80°C. Purity of all the products was verified by TLC using $CH_3CH_2CH_2CH_2OH$/ CH_3COOH/H_2O 2:1:1 as mobile phase. The solvents used were purchased from Fluka (Buchs, Switzerland) and were of the highest quality available. NTA-probe structures are presented in figure 2.3.

Ni-NTA-lysine, Co-NTA-lysine and Cu-NTA-lysine — 381 μmol of N-(5-amino-1-carboxypentyl) iminodiacetic acid [135] ('NTA-lysine') were dissolved in a 3.81 ml 0.1 μM $NiCl_2$ (Fluka) water solution; the pH was then adjusted to 8.0 with NaOH. After 30 min, the water was evaporated yielding blue-green crystals of Ni-NTA-lysine (MW 318). Co-NTA-lysine (MW 318) and Cu-NTA-lysine (MW 323) were prepared as for Ni-NTA-lysine with $CoCl_2$ and $CuCl_2$ (Fluka) yielding after evaporation purple and green crystals, respectively. Crystals were stored at 4°C.

QSY7-NTA-Ni — The succinimidyl ester of QSY7 (9-[2-[[4-[[(2,5-dioxo-1-pyrrolidinyl)oxy]carbonyl]-1-piperidinyl]sulfonyl]phenyl]-3,6 bis(methylphenylamino)- xanthylium chloride, Molecular Probes Invitrogen, CA, USA) and 5 equivalents Ni-NTA-lysine were dissolved in 50 mM $NaHCO_3$ pH 9.0 containing 50% acetonitrile. The reaction was incubated for 12 hours. The product QSY7-NTA-Ni, was purified by TLC eluted with $CHCl_3/CH_3OH/H_2O$ 65:24:4 (R_f = 0.27) and extracted with acetonitrile/H_2O 1:1. QSY7-NTA-Ni was distinguishable from QSY7-NTA by TLC eluted with Acetonitrile/H_2O 1:1 (R_f = 0.83 and 0.76 with and without nickel, respectively).

QSY7-NTA-Co & **QSY7-NTA-Cu** — QSY7-NTA-Co and QSY7-NTA-Cu were synthesized as described for QSY7-NTA-Ni with the exception that Ni-NTA-lysine was replaced by Co-NTA-lysine and Cu-NTA-lysine.

QSY9-NTA-Ni — QSY9-NTA-Ni was produced by coupling the succinimidyl ester of QSY9 (9-[2-[[4-[[(2,5-dioxo-1-pyrrolidinyl)oxy]carbonyl]-1-piperidinyl]sulfonyl]phenyl]-3,6-bis(para-methylphenylamino sulfonic acid)-xanthylium chloride, Molecular Probes Invitrogen, CA, USA) to 5 equivalents Ni-NTA-lysine in 50 mM $NaHCO_3$, pH 9.0. After 12 hours incubation, the product was purified as for QSY7-NTA-Ni at the exception that a second TLC run eluted with acetonitrile/H_2O 2:1 was required (R_f = 0.68). The product was then extracted with H_2O.

QSY21-NTA-Ni — The succinimidyl ester of QSY21 (Molecular Probes Invitrogen, CA, USA) and 5 equivalents Ni-NTA-lysine were dissolved in 50 mM $NaHCO_3$, pH 9.0, containing 50% acetonitrile and incubated 12 hours. The product was purified by TLC eluted with $CHCl_3/CH_3OH/H_2O$ 65:24:4 (R_f = 0.19). The product was extracted with acetonitrile/H_2O 1:1.

Cy3-NTA-Ni — Cy3-NTA-Ni was produced by coupling the succinimidyl ester of Cy3 (Amersham Biosciences, NJ, USA) in DMF to 5 equivalents Ni-NTA-lysine in 50 mM $NaHCO_3$, pH 9.0 and incubated overnight. The product was purified by TLC with two subsequent elutions, $CHCl_3/CH_3OH/H_2O$ 64:33:4 (long elution, R_f = 0.05) and acetonitrile/H_2O 2:1 (short elution, R_f = 0.4). The product was extracted with acetonitrile/H_2O 1:1.

Cy3-bis-NTA-Ni — The bis-succinimidyl ester of Cy3 (Toronto Research Chemical, Toronto, Canada) was mixed to 10 equivalents Ni-NTA-lysine as for Cy3-NTA-Ni. The product was purified by TLC with two subsequent elutions, $CHCl_3/CH_3OH/H_2O$ 35:65:2 (long elution, R_f = 0.02) and acetonitrile/H_2O 2:1 (short elution, R_f = 0.5). The product was extracted with acetonitrile/H_2O 1:1.

Cy5-NTA-Ni — The succinimidyl ester of Cy5 (Amersham Biosciences) was mixed with 5 equivalents Ni-NTA-lysine in 50 mM $NaHCO_3$, pH 9.0 and incubated overnight. The product was purified as for Cy3-NTA-Ni with R_f equal to 0.05 and 0.9 for the first and second elution, respectively. The product was extracted with H_2O.

Rho-NTA-Ni — Rhodamine-NTA-Ni was produced by coupling rhodamine B in form of tetraethylrhodamine isothiocyanate (Fluka) to Ni-NTA-lysine as described for QSY7-NTA-Ni.

TexasRed-NTA-Ni — The succinimidyl ester of Texas Red-X "single isomer" (Molecular Probes Invitrogen) was coupled to 5 equivalents Ni-NTA-lysine in DMSO.

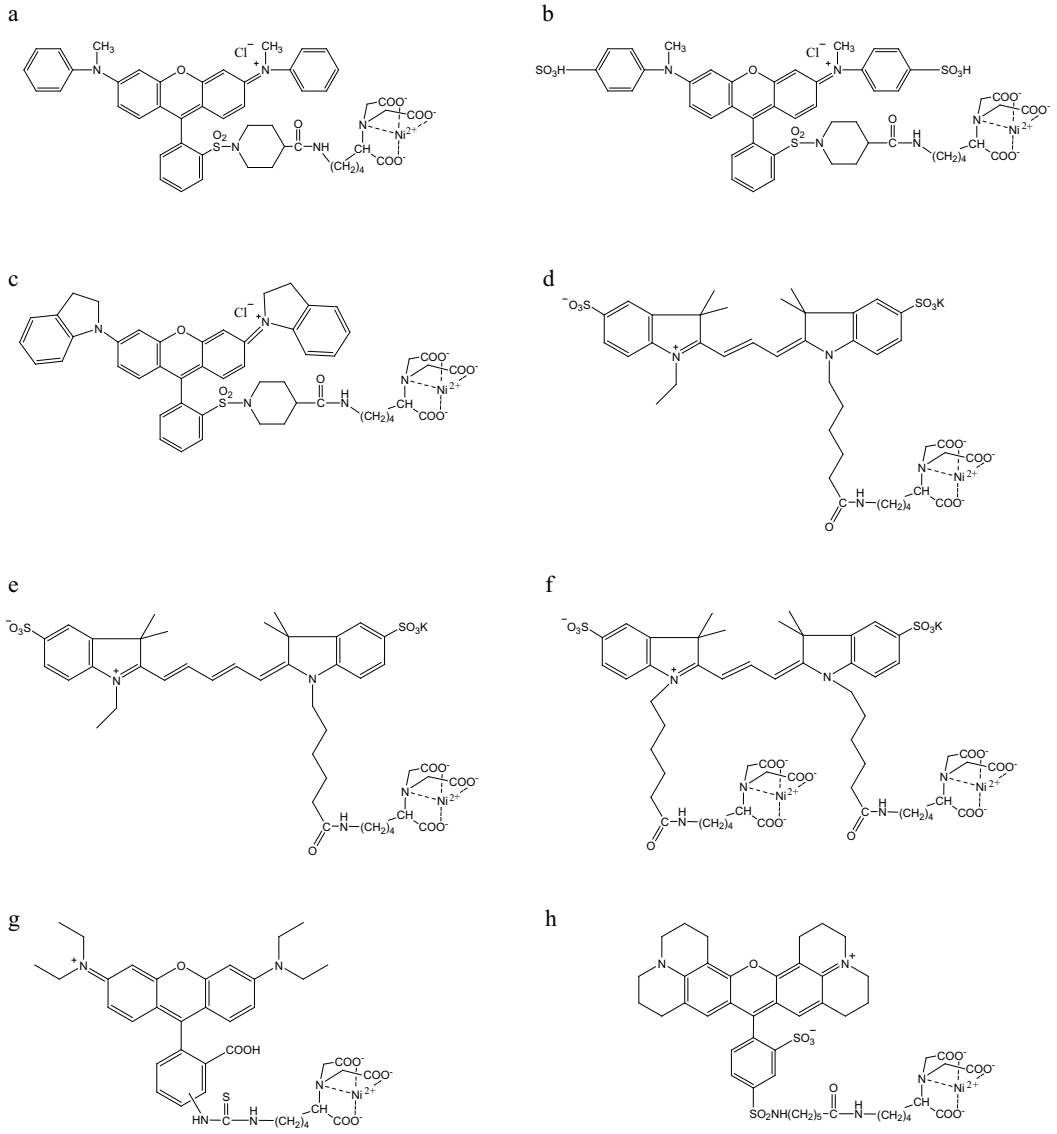

Figure 2.3: Structures of the synthesized NTA-probes. *(a) QSY7-NTA-Ni, QSY9-NTA-Ni (b), QSY21-NTA-Ni (c), Cy3-NTA-Ni (d), Cy5-NTA-Ni (e), Cy3-bis-NTA-Ni (f), Rho-NTA-Ni (g) and TexasRed-NTA-Ni (h). For QSY7-NTA-Co and QSY7-NTA-Cu, the structure is similar to (a), only the complexed transition metal ions are changed.*

The product was purified by TLC eluted with $CHCl_3/CH_3OH/H_2O$ 64:33:4 (R_f = 0.14). The product was extracted with DMSO.

2.3.2 Molecular and cellular biology

GFP-His$_6$ — This protein was expressed in *Escherichia coli* DH5α cells, transfected with the p6xHis-GFP IMAC control vector (Clontech, California, USA) encoding wild-type GFP from *Aequorea victoria* with a N-terminal His_6 extension (NCBI accession code U89936). DNA sequence contains two single restriction sites, EcoR V and EcoR I at the N- and C-terminus, respectively. Bacteria were cultured at 37°C in 200 ml of 2YT medium until OD reached 0.7 under ampicillin selection. Protein expression was induced with 1 mM IPTG at 30°C for 2 days. Bacteria were harvested and disrupted by sonication. The protein was purified from the 50'000 x g supernatant using the TALON metal affinity resin (Clontech, California, USA) with buffer A (50 mM NaH_2PO_4, 300 mM NaCl, pH 8.0) for equilibration and buffer B (50 mM NaH_2PO_4, 300 mM NaCl, 100 mM EDTA, pH 8.0) for elution. Dialysis against buffer A yielded a solution of 5.0 μM GFP-His_6 (ε_{395nm} = 26 $\pm$ 3 $mM^{-1}cm^{-1}$) with a purity of about 50% as evidence by SDS-PAGE.

GFP-His$_{10}$ — The GFP-His_{10} was constructed by adding His_4 to the N-terminal of GFP-His_6 using the QuickChange^{TM} site-directed mutagenesis kit (Stratagene, California, USA) with the conditions required by the provider in the presence of 4% DMSO for the reaction. The used oligonucleotides contain a BamH I restriction site followed by the coding sequence of His_4 (p10xHis-wtGFP*for* and p10xHis-wtGFP*rev*, see appendix A.1). The nucleotide sequence was verified and confirmed by restriction analysis and sequencing. Expression, purification and dialysis conditions were the same as for GFP-His_6, yielded a solution of 3.0 μM GFP-His_6 (ε_{395nm} = 26000 $\pm$ 3000 $M^{-1}cm^{-1}$) with a purity of about 50% as evidence by SDS-PAGE.

5-HT$_{3A}$ receptor sequences — These sequences were based on the short splicing version of the murine 5-HT_3R, corresponding to the SwissProt entry p23979 lacking the residues 360-365 (mature sequence numbering). Wild-type 5-HT_3R was transiently expressed in human embryonic kidney (HEK)-293 cells using the plasmid pcDNA3.1 (Invitrogen) and transfection using the modified calcium-phosphate method [142]. Experiments were performed 2 days after transfection. 5-HT_3R-N-His_6, containing Ser-His_6 between Thr6 and Gln7, was transiently expressed in HEK-293 cells using pCMVβ (Clontech) upon transfection using Effectene (Qiagen, Hilden, Germany) with 1.0 μg plasmid per 3.5 cm well. His_6 was introduced be-

tween Ser359 and Ala360 to give 5-HT_3R-Loop-His_6, which was stably expressed in HEK-293 cells using pEAK8 expression vector (Edge Biosystems, Maryland, USA) and puromycin selection. 5-HT_3R-C-His_6, a 5-HT_{3A} receptor containing a C-terminal Gly-His_6 extension, was stably expressed in HEK-293EBNA cells (HEK-293 cells constitutively expressing the Epstein Barr Virus Nuclear Antigen-1) using the pCEP4 expression vector (Invitrogen) and hygromycin B selection. 5-HT_3R-C-His_{10} was constructed by adding His_4 to the 5-HT_3R-C-His_6 and stably expressed in HEK-293 cells using pEAK8. Nucleotide sequences of all receptors were verified by restriction analysis and sequencing. Expressed proteins featured ligand binding and serotonin-activated current like the wild-type receptor.

GFP-NK1R-His_{10} — This sequence was composed of the signal sequence of the mouse 5-HT_3 receptor followed by a sequence encoding the enhanced GFP (Clontech) link to the human NK1R having a His_{10} sequence attached to the C-terminus. Stably expressing cells were obtained using pCEP4 as an expression vector. Functionality of the construct was demonstrated by ligand binding and Ca^{2+}-flux assays. Correct plasma membrane localization of GFP-NK1R-His_{10} was confirmed by prominent GFP fluorescence located at the plasma membrane using confocal microscopy [143].

2.3.3 Experimental methods

Monitoring *in vitro* labelling of His_6-GFP and His_{10}-GFP — Fluorescence measurements were done on a Spex Fluorolog II (Instrument S.A.) at 1.9 nm excitation and 2.3 nm emission band passes. Samples in 0.5 x 0.5 x 5 cm^3 quartz cuvettes (Hellma GmBH & Co, Müllheim, Germany) were excited at 395 nm; emission was recorded from 450-570 nm at 22°C. NTA-probes were titrated into 400 μl 25 nM GFP-His_6 or GFP-His_{10} in buffer A containing 800 μM $C_{12}E_9$ (Anatrace, Ohio, USA). Emission spectra were recorded 15 min after each addition. GFP-His tagged labelling was reversed by the addition of 1 μl EDTA, pH 8.0 to the corresponding sample.

The kinetics of NTA-probe binding to 2.5 nM GFP-His tagged in buffer A was monitored at 510 nm upon excitation at 395 nm with 1.9 nm and 3.6 nm for excitation and emission band passes.

Monitoring *in vivo* labelling of 5-HT_3R — HEK-293 cells, expressing either histidine-tagged or wild-type 5-HT_3Rs, were cultured on 0.18 mm thick glass coverslips in 6-well plates in Dulbecco's modified Eagle medium (DMEM) supplemented

with 2.2% of fetal calf serum under humidified 5% CO_2 atmosphere at 37°C. The coverslips were then transferred to a sample holder, and the cells covered 400 μl PBS containing 15 nM GR-flu (1,2,3,9 tetrahydro-3-[(5-methyl-1H-imidazol-4-yl)methyl]-9-(3-amino-(N-fluorescein-thiocarbamoyl)-propyl)4H-carbazol-4-one, Glaxo, Switzerland). Fluorescence images were recorded using a LSM 510 confocal microscope (Zeiss, Jena, Germany) equipped with appropriate excitation and emission filters for fluorescein, rhodamine and Cy5. Subsequently NTA-probes were added to the concentrations indicated. Receptor binding of NTA-probes was reversed by adding EDTA, pH 8.0, to give a final concentration of 5 mM. Nonspecific binding of GR-flu to cells, measured in the presence of 1 μM quipazin, was negligible.

***In vivo* labelling of GFP-NK1R-His** — GFP-NK1R-His_{10} was labelled with NTA-probes as described for 5-HT_3R.

2.3.4 Data treatment

Förster distance calculations — The Förster distance R_0 (nm) was calculated from equation 2.2, where $\kappa^2 = 2/3$ for the orientation factor assuming isotropic distribution of the transition dipoles of the donor and acceptor and $n = 1.4$ for the refractive index of the membrane. The overlap integral J ($M^{-1}{\cdot}cm^3$) was calculated using equation 2.4. The acceptor molar excitation coefficient $\varepsilon_A(\lambda)$ and the wavelength λ were in $M^{-1}cm^{-1}$ and cm respectively. Errors where calculated using the Gauss propagation method assuming 2% error for ε and emission spectra of GFP.

Affinity of NTA-probes to GFP-His tagged — All measurements were corrected for the contribution of the buffer and for inner filter effects, which is given by equation 2.9. F_{cor} and F_{obs} are the corrected and observed fluorescence intensities; OD_{ex} and OD_{em}, the optical density at the excitation and emission wavelength.

$$F_{corr} = F_{obs} \cdot 10^{((OD_{ex}+OD_{em})/2)} \tag{2.9}$$

Fluorescence intensity of GFP at 510 nm reported versus NTA-probes concentration was fitted with the Hill equation (2.10). F and F_0 are GFP fluorescence intensities with and without NTA-probes, c the concentration of NTA-probes (M), K_d the dissociation constant (M), E the energy transfer efficiency determined by equation 2.7 and h the Hill coefficient. The distance r separating the GFP emission dipole and NTA-probes absorbtion dipole was determined from equation 2.6 using the transfer efficiency E value obtained from the fit. Errors for E and K_d are obtained by the fit.

$$F = F_0 - E\frac{1}{1+\left(\frac{K_\mathrm{d}}{c}\right)^h} \tag{2.10}$$

Association and dissociation rate constants of NTA-probes to GFP-His tagged — Fluorescence intensity was corrected for the contribution of the buffer and for inner filter effects (equation 2.9). The effective rate constant k_obs ($\mathrm{M{\cdot}s^{-1}}$) was determined by fitting the decrease fluorescent intensity of GFP due to the addition of different concentrations of NTA-probes using equation 2.11. F_t and F_0 are the fluorescence intensities at time t (s) and $t = 0$ respectively. For the case of a reaction P + Q $\rightleftharpoons$ PQ, where the concentration of P (protein) stays constant, k_obs is linearly dependant with the concentration of Q (quencher) as described by equation 2.12 [144]. The association (k_on in $\mathrm{M^{-1}{\cdot}s^{-1}}$) and dissociation ($k_\mathrm{off}$ in $\mathrm{s^{-1}}$) rate constants are given by the slope and the intersection with the y axis. c is the concentration of NTA-probes (M).

$$F_\mathrm{t} = F_0 \cdot \exp\left(-k_\mathrm{obs} \cdot t\right) \tag{2.11}$$

$$k_\mathrm{obs} = k_\mathrm{off} + k_\mathrm{on} \cdot c \tag{2.12}$$

Kinetic dissociation induced by EDTA was studied using "Berkeley Madonna" software, which allows modelling and analyzing dynamic systems by numerical iteration. The model reaction presented in figure 2.6 is described by the following equations where P stands for protein (GFP), Q for quencher (NTA-Ni probes) and Q* for the quencher without the metal (NTA-probes) and PQ for the quencher bound to the protein. Using the Rosenbrock convergence method, values for the kinetic constants k_1 and k_2; k_on and k_off were obtained from association equation 2.12. Details are presented in section 2.4.2.

$$\frac{d\left[Q\right]}{dt} = -k_\mathrm{on}\left[P\right]\left[Q\right] + k_\mathrm{off}\left[PQ\right] - k_1\left[Q\right]\left[EDTA\right] \tag{2.13}$$

$$\frac{d\left[PQ\right]}{dt} = k_\mathrm{on}\left[P\right]\left[Q\right] - k_\mathrm{off}\left[PQ\right] - k_2\left[PQ\right]\left[EDTA\right] \tag{2.14}$$

$$\frac{d\left[P\right]}{dt} = -k_\mathrm{on}\left[P\right]\left[Q\right] + k_\mathrm{off}\left[PQ\right] + k_2\left[PQ\right]\left[EDTA\right] \tag{2.15}$$

$$\frac{d\left[Q^*\right]}{dt} = k_1\left[Q\right]\left[EDTA\right] + k_2\left[PQ\right]\left[EDTA\right] \tag{2.16}$$

Affinities of NTA-probes to 5-HT$_3$R *in vivo* — Affinities of NTA-probes to the 5-HT$_3$R were determined as for His-tagged GFP. No correction for inner filter were required since the experiments were performed in a confocal microscope. Fluorescence intensities were quantified using the LSM 510 software (Zeiss, Jena, Germany).

Evaluation of *in vivo* FRET data for the structure of 5-HT$_3$R — Fluorescence intensities were quantified from a region of interest using the LSM 510 software (Zeiss, Jena, Germany). FRET data for the 5-HT$_3$R was evaluated considering the following (for a detail treatment of FRET see [140]). (i) The 5-HT$_3$ is schematically depicted as a cylinder with overall dimensions of the highly homologous nicotinic acetylcholine receptor [107, 108]: 15 nm long, a radius of 4 nm and protruding 7 nm from the extracellular side of the membrane. (ii) The oligohistidine sequences are located on the surface of the receptor and not buried within the membrane, as all mutant receptors can be purified by Ni^{2+}-NTA chromatography. (iii) Each homopentameric receptor carries five equivalent hexahistidine sequences related by fivefold symmetry around the central axis of the receptor protein; in consequence, the five bound NTA chromophores are symmetrically distributed on a circle around the central axis. (iv) Each receptor binds only one GR-flu [145], which is located at 4.9 ± 0.9 nm above the center of the membrane [146] on the surface of the extracellular domain of the receptor [147]. (v) The efficiency of FRET is described by equation 2.17, which is a modified version of equation 2.6.

$$E_{\mathrm{sat}} = \sum_i \frac{\left(\frac{R_0}{r_i}\right)^6}{1 + \sum_i \left(\frac{R_0}{r_i}\right)^6} \tag{2.17}$$

For the pair GR-flu QSY7-NTA-Ni, $R_0 = 5.83 \pm 0.13$ nm. The orientation factor is set to $\kappa^2 = 2/3$, which is reasonable considering the low fluorescence anisotropy of the receptor-bound donor indicating high segmental motion of GR-flu. r_{i} is the distance between the chromophore of GR-flu and of the i^{th} NTA-probe for each of the the His_6 sequences, which are assumed to be independent and equivalent (identical R_0 and K_{d}). Distance reported is the axial height between GR-flu and the plane comprising the circle of the NTA-chromophores. E_{sat} is three to four times more sensitive to changes of height than to changes of radius; the radius was set to 4 nm, as variations of 0.5 nm yielded changes of E_{sat} within experimental errors. Changes in E_{sat} due to rotation of the positions of the NTA-probes around the central axis fall within the experimental error. Thus, only axial heights separating the

NTA-probes and GR-flu can be determined with significance.

2.4 Results and discussion

2.4.1 NTA-probes for *in vitro* labelling of proteins

Reversible labelling of proteins with NTA-probes was first characterized *in vitro* for a green fluorescent protein (wtGFP) containing an N-terminal hexahistidine (GFP-His_6). The probes QSY7-NTA-Ni and QSY9-NTA-Ni (figure 2.3) bind to GFP-His_6 within seconds (figure 2.4.a) and act as ideal acceptors for fluorescence resonance energy transfer (FRET) (figure 2.4.d), quenching the fluorescence of GFP almost entirely. The kinetics of the labelling reaction is linearly dependant on the concentration of the NTA-probes (figure 2.4.c), indicating that only one NTA-probe binds per GFP-His_6. Moreover, the dissociation constants obtained both at equilibrium and from binding kinetics are in good agreement. The nonunity of the Hill coefficients (figure 2.4.c) may be due to a slow structural reorganization (structural ripening) of the oligohistidine-NTA-Ni complex after the initial binding event. The distance between the fluorophore within GFP and the chromophore of the NTA-probe is estimated to be 3.3 nm, which is in agreement with the dimension of the interacting molecules (GFP measures approximately 3 x 4.5 nm, the NTA probes QSY7-NTA-Ni and QSY9-NTA-Ni about 1.8 x 1.5 nm). Labelling is fully reversed upon addition of EDTA (figure 2.4.a and b) indicating specific interaction of the NTA-probes with the polyhistidine sequence of GFP. This is confirmed by the absence of a decrease of GFP fluorescence upon addition of NTA-probes either without Ni^{2+} or in the presence of EDTA or imidazol.

The polyhistidine sequence peptide of GFP was then extended from His_6 to His_{10}. QSY7-NTA-Ni and QSY9-NTA-Ni probes label GFP-His_{10} within seconds and binding is fully reversible upon addition of EDTA showing the specificity of the interaction (figure 2.5.a). The extension of the tag size does not influence neither the FRET efficiency nor the stoichiometry between the NTA-probes and GFP-His_{10}, and has few effects on the Hill coefficient; rather it improves the affinity by a factor of three (table 2.1). Moreoever, the dissociation binding constant obtained at equilibrium and from binding kinetics are in agreement. A comparison between the kinetics binding of the probes to GFP-His_6 and GFP-His_{10} (table 2.3) shows that the extension of the polyhistidine sequence influences only the on rate of the binding resulting in a higher affinity. This supports the view of a freely diffusing NTA-probe that has more chance to meet and bind to a longer recognition peptide

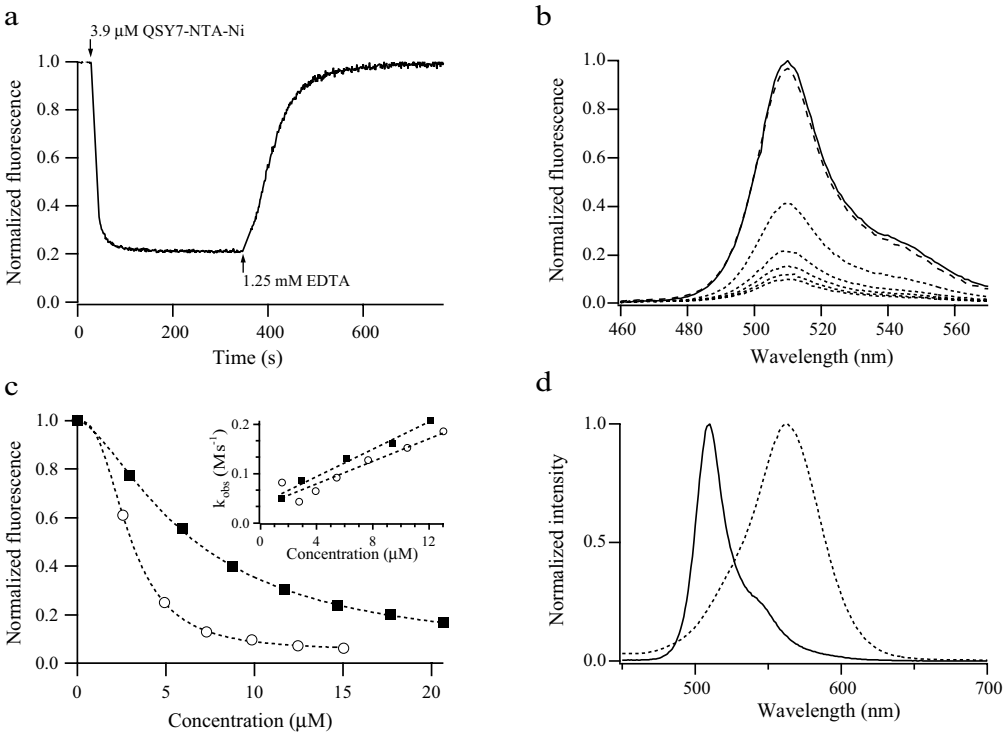

Figure 2.4: Labelling GFP-His$_6$ by QSY7-NTA-Ni and QSY9-NTA-Ni. *(a) Addition of 3.9 µM QSY7-NTA-Ni to 2.5 nM GFP-His$_6$ results in a rapid decrease of fluorescence intensity ($t_{1/2} \approx 5$ s), which is completely reversed by 1.25 mM EDTA ($t_{1/2} \approx 60$ s). (b) GFP-His$_6$ emission spectra intensity (continuous line, excitation at 395 nm, 25 nM) subsequently decreases by each addition of QSY7-NTA-Ni (dotted lines) reaching a saturable state. 1.25 mM EDTA completely reversed the binding (−− line) (c) Affinity of QSY7-NTA-Ni and QSY9-NTA-Ni for GFP-His$_6$. Normalized fluorescence intensity at equilibrium of GFP-His$_6$ incubated with the indicated concentration of QSY7-NTA-Ni (○) and QSY9-NTA-Ni (■). Dotted lines are fits using a Hill equation (Eq. 2.10) yielding dissociation constants $K_d = 3.0 \pm 0.2$ µM and 6.4 ± 0.2 µM, Hill coefficients $h = 1.6 \pm 0.2$ and 2.6 ± 0.2, and FRET efficiencies $E = 0.95 \pm 0.01$ and 0.96 ± 0.01 for QSY7-NTA-Ni and QSY9-NTA-Ni respectively. The distance between the chromophores of GFP-His$_6$ and the NTA-probes was calculated to be $r = 3.3 \pm 0.4$ nm (Eq. 2.6, table 2.1). Insert: the effective rate constants (k_{obs}) of the binding of QSY7-NTA-Ni (○) and QSY9-NTA-Ni (■) to GFP-His$_6$ is linear with the concentration indicating a one to one stoichiometry. Quantitative evaluation using relation 2.12 yielded rate constants for binding k_{on} of 11.4 ± 4.6 and 7.9 ± 1.9 $mM^{-1}s^{-1}$, and for dissociation k_{off} of 0.034 ± 0.034 and 0.061 ± 0.015 s^{-1} resulting in dissociation constants $K_d = k_{off}/k_{on}$ of 3.0 ± 3.2 and 7.7 ± 2.6 µM, respectively, for QSY7- and QSY9-NTA-Ni. (d) Normalized emission spectrum of GFP-His$_6$ (continuous line, excitation at 395 nm) and absorption spectrum of QSY7-NTA-Ni and QSY9-NTA-Ni (identical normalized absorption spectrum). $R_0 = 5.65 \pm 0.13$ nm for these pairs (table 2.2).*

than a shorter one.

Designing probes with two NTA-Ni moieties also improves the affinity towards polyhistidine sequences. For instance a Cy3 fluorescent probe with two NTA-Ni arms (figure 2.3.f) titrated to GFP-His_6 and GFP-His_{10} improves the affinity thirty fold (table 2.1) compared to its mono-NTA-Ni analogue (figure 2.3.d). The combination of an extended His_{10} polyhistidine peptide sequence with Cy3-bis-NTA-Ni probe containing two NTA-Ni moieties reaches dissociation constants in the order of 10 nM (table 2.1 and figure 2.5.a); this corresponds to a 100-fold increase in affinity compared to GFP-His_6 with Cy3-NTA-Ni. This led to the idea of synthesizing other probes containing several NTA-Ni moieties. For this purpose, we tried to couple the amino group of glutamate, containing two NTA-Ni bound to its carboxylic groups, to the succinimidyl ester of different probes. Unfortunately, the succinimidyl ester moiety was not reactive towards the amino group of glutamate. Therefore, probes containing two NTA-Ni arms are limited to commercially available probes doubly activated.

The effect of the metal ion upon the binding was also investigated. Ni^{2+} was replaced by Co^{2+} and Cu^{2+} in QSY7-NTA-Ni. The resulting probes bind to GFP-His_6 within seconds with micromolar dissociation constants (figure 2.5.b) that are shifted to higher and lower affinity for copper and cobalt, respectively, compared to the QSY7-NTA-Ni analogue (table 2.1). The increase of affinity in the order Cu^{2+} > Ni^{2+} > Co^{2+} was already observed for IMAC chromatography [148]. Addition of EDTA or imidazol in high amounts did not completely recover the original fluorescence intensity of GFP (table 2.1) resulting in a less specific interaction compared to Ni^{2+}. In the case of QSY7-NTA-Co, the recovery of only 50% fluorescence after addition of EDTA may be due to the oxydation of Co(II) to Co(III) resulting in an irreversible binding of the probe to polyhistidine sequence [148]. This explanation has not been proved; addition of 2% H_2O_2 as oxidative agent to the QSY7-NTA-Co GFP-His_6 adduct did not modified the binding (EDTA recovers 50% of the GFP fluorescence, as it was the case in the absence of H_2O_2). Therefore, exchange of the chelated metal ion has a direct effect on both affinity and specificity and does not confer any advantage compared to nickel since specificity and reversibility of the binding are of prime importance for the present application. Hence, nickel is used as the chelated metal ion in NTA-probes.

Other fluorescent probes like Cy5-, TexasRed-, Rho-NTA-Ni and nonfluorescent like QSY21-NTA-Ni were characterized upon binding on GFP-His_6 and GFP-His_{10}; dissociation constants and FRET efficiencies are reported in table 2.1. Their bindings are specific as EDTA completely recovers the fluorescence intensity of GFP.

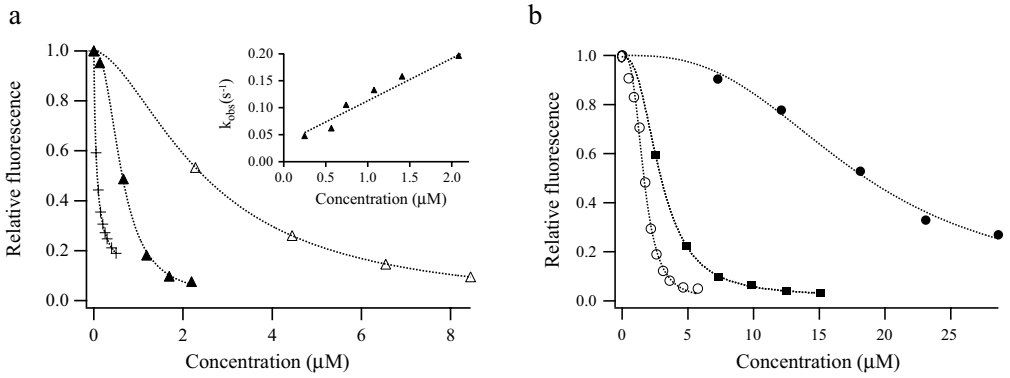

Figure 2.5: Improving the affinity binding of NTA-probes. *(a) Affinity of NTA-probes for GFP-His$_{10}$. Normalized fluorescence intensity at equilibrium of GFP-His$_{10}$ incubated with the indicated concentration of QSY7-NTA-Ni (▲), QSY9-NTA-Ni (△) and Cy3-bis-NTA-Ni (+) fitted with a Hill equation (Eq. 2.10) yielding dissociation constants K_d = 0.62 ± 0.03 µM, 2.4 ± 0.1 µM and 64 ± 5 nM, Hill coefficients h = 2.4 ± 0.3, 1.7 ± 0.1 and 1.0 ± 0.1 for QSY7-NTA-Ni, QSY9-NTA-Ni and Cy3-bis-NTA-Ni respectively. FRET efficiencies are presented in table 2.1. Addition of 1.25 mM EDTA totally reversed the binding. Insert: the effective rate constant (k_{obs}) of the binding of QSY7-NTA-Ni to 2.5 nM of GFP-His$_{10}$ (▲) is linearly dependant with the concentration of the former yielding k_{on} = 78.5 ± 30 $mM^{-1}s^{-1}$ and k_{off} = 0.034 ± 0.035 s^{-1}, resulting in a dissociation constant $K_d = k_{off}/k_{on}$ of 0.43 ± 0.48 µM. (b) Effect of the metal on the affinity of NTA-probes with GFP-His$_6$. Normalized fluorescence intensity at equilibrium of GFP-His$_6$ incubated with the indicated concentration of QSY7-NTA-Co (●), QSY7-NTA-Ni (■) and QSY7-NTA-Cu (○) fitted with a Hill equation (Eq. 2.10) yielding dissociation constants of K_d = 17 ± 1, 3.0 ± 0.2 and 1.6 ± 0.1 µM, Hill coefficients h = 3.5 ± 0.4, 1.6 ± 0.2 and 3.2 ± 0.2, respectively. Addition of 1.25 mM EDTA reversed completely the binding for QSY7-NTA-Ni; only 50% and 90% of the original fluorescence intensity of GFP-His$_6$ was recovered for QSY7-NTA-Co and QSY7-NTA-Cu respectively. Indeed, the kind of metal ion affects both the affinity and specificity.*

For all the spectrally different reporters (table 2.2), the distance separating the chromophores of GFP and bound NTA-Ni probes are identical in the errors limits for probes having comparing linker length; longer linkers between the metal moiety and the chromophore dipole results in longer distances. This is a supplementary proof of the specificity of the labelling and therefore shows the potential of the method for *in vitro* investigations of proteins containing a polyhistidine sequence.

Table 2.1: *In vitro* characteristics of the binding between NTA-probes and polyhistidine sequences His_6 and His_{10} of GFP: dissociation constants, energy transfer efficiencies and distances.

Probes	K_d (μM) **His_6**	K_d (μM) **His_{10}**	[1] E	[5] r (nm)
QSY7-NTA-Ni	3.0 ± 0.2	0.62 ± 0.03	0.95 ± 0.01	3.4 ± 0.4
QSY7-NTA-Cu	1.6 ± 0.1	-	[2]0.98 ± 0.01	[2]3.0 ± 0.6
QSY7-NTA-Co	17 ± 1	-	[3]0.97 ± 0.01	[3]3.2 ± 0.5
QSY9-NTA-Ni	6.4 ± 0.2	2.4 ± 0.1	0.96 ± 0.01	3.3 ± 0.4
QSY21-NTA-Ni	1.3 ± 0.5	0.6 ± 0.3	[4]0.89 ± 0.02	[4]3.2 ± 0.3
Cy3-NTA-Ni	6 ± 1	1.6 ± 0.2	0.89 ± 0.03	4.7 ± 0.5
Cy3-bis-NTA-Ni	0.2 ± 0.1	0.064 ± 0.005	0.92 ± 0.02	4.1 ± 0.5
Cy5-NTA-Ni	7.2 ± 0.7	6.7 ± 1.3	0.75 ± 0.05	3.9 ± 0.4
Rho-NTA-Ni	8 ± 1	-	0.85 ± 0.09	4.4 ± 1.4
TexasRed-NTA-Ni	0.2 ± 0.1	0.83 ± 0.02	0.88 ± 0.03	3.6 ± 0.5

[1] FRET efficiencies are the same for GFP-His_6 and GFP-His_{10} when measured.

[2,3,4] These value should be corrected for 10%, 50% and ∼14%, respectively, of unspecific binding respectively as revealed by EDTA.

[5] Calculated according to Eq. 2.6 with R_0 values from table 2.2. Indicated errors are 95% confidence.

2.4.2 *In vitro* competitive dissociation mechanisms of NTA probes with EDTA

To fully characterize the reversible labelling approach NTA probes, kinetics of the dissociation of the probes by competition with EDTA is investigated. Different amounts of QSY7-NTA-Ni are titrated to a solution of GFP-His_6, quenching the fluorescence of the latter though the formation of an adduct between the protein and the quencher (figure 2.6.a). Addition of a large excess of EDTA reverse the binding to a complete recovery of GFP fluorescence. However, the time course of the reversion (figure 2.6) does not correspond to a simple reaction where EDTA enters in competition by simply "removing" the nickel chelated to the free NTA-Ni probe (where $k_2 = 0$ according to figure 2.6.b insert), because its shape cannot be

Table 2.2: Förster distances for GFP and the different probes as well as their spectroscopic properties.

Probes	Abs (nm)	Em (nm)	ε ($M^{-1}cm^{-1}$)	$^2R_0$ (nm)
QSY7	564	[1]-	87'500	5.65 ± 0.13
QSY9	564	[1]-	87'500	5.65 ± 0.13
QSY21	660	[1]-	89'000	4.50 ± 0.11
Cy3	550	570	150'000	6.20 ± 0.15
Cy5	649	670	250'000	4.63 ± 0.11
Rho	543	569	105'000	5.90 ± 0.14
TexasRed	595	615	85'000	5.02 ± 0.12

[1] ϕ was determined to be $< 3{\cdot}10^{-4}$ and therefore the probes are assumed nonfluorescent.

[2] R_0 was determined (Eq. 2.2) using $n = 1.40 \pm 0.05$, $\phi_{\mathrm{wtGFP}} = 0.79$.

fitted with an exponential function. Therefore, it was suggested that EDTA can directly have an effect on the PQ adduct resulting in the reaction scheme presented in figure 2.6.b. This model has no analytical solution and a numerical approach is required for both approving the corresponding model and determining the different parameters k_1 and k_2. This analysis was used to determine the different kinetic constants for QSY7-NTA-Ni and QSY9-NTA-Ni on both GFP-His_6 and GFP-His_{10} (Table 2.3).

Interestingly, the nature of the probe as well as the length of histidine tagged sequence do not influence k_1 as it was expected by the model; this step of the reaction involves only the metal-bound to NTA and EDTA. Comparatively, k_2 seems to be influence by the length of the tag. This is not very clear since the errors are important. An explanation for these high errors on k_2 is the following. Since this factor has been introduced to explain the small "S" shape of the reversion kinetic (figure 2.6.b) during the first fifty seconds after the addition of EDTA , few points are available for the fits resulting in a high error. Nevertheless, the model proposed for the the interaction of EDTA during the reversion of the binding can be validated.

2.4.3 Structure of the 5-HT_{3A} receptor in living cells revealed with NTA chromophores

The NTA-probes were subsequently used in live cells to investigate the structure of the ionotropic serotonin 5-HT_3 receptor (5-HT_3R) [149] into which hexahistidine sequences were genetically engineered at any one of the three different positions (figure 2.7.a). FRET between receptor-bound GR-flu, a high affinity fluorescein labelled 5-HT_3R antagonist [150], and NTA-probe was used as indicator of the binding of

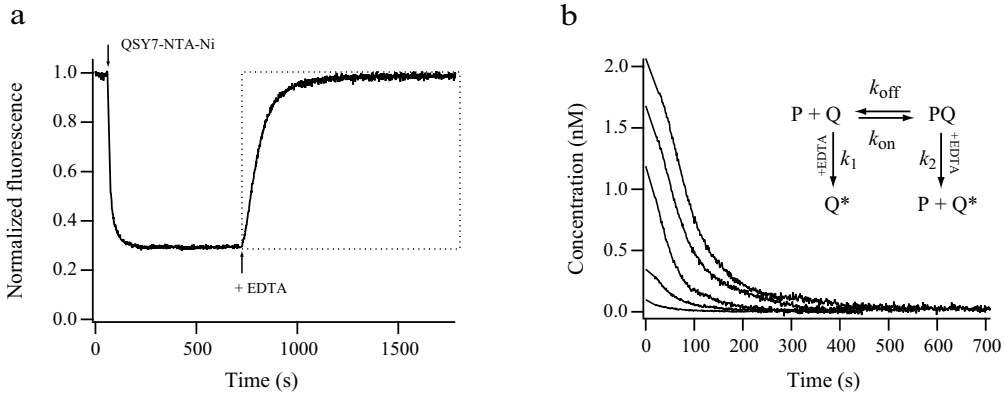

Figure 2.6: Kinetic model of the dissociation reaction induced by EDTA. *(a) Addition of 4.5 μM QSY7-NTA-Ni to 2.5 nM GFP-His$_{10}$ quenches the fluorescence of GFP, reaching a steady state that is reversed by EDTA in large excess (1 mM). The dotted box represents the region where the normalized fluorescence intensity is expressed in term of GFP-His$_6$-Ni-NTA-QSY7 concentration (PQ) that are reported in b. (b) The concentration of the adduct (PQ) between GFP-His$_6$ (P) and QSY7-NTA-Ni (Q) for different concentration of quencher versus time. Fitting using Eq.2.13, 2.14, 2.15 and 2.16 (as described in section 2.3.4) yielded k_1 = 33.4 $\pm$ 8.2 $M^{-1}s^{-1}$ and k_2 = 71 $\pm$ 180 $M^{-1}s^{-1}$. Insert: proposed model for the reversion of the binding by EDTA. P stands for protein, Q for quencher, PQ for the quencher-bound to the protein, and Q^* for the quencher without the metal. No equilibrium is assumed for the reaction involving EDTA due to its high affinity with divalent metals.*

Table 2.3: Kinetics constants.

	GFP-His$_6$		GFP-His$_{10}$
	QSY7-NTA-Ni	QSY9-NTA-Ni	QSY7-NTA-Ni
k_{on} ($mM^{-1}s^{-1}$)	11.4 $\pm$ 4.6	7.9 $\pm$ 1.9	78.5 $\pm$ 30
k_{off} (s^{-1})	0.034 $\pm$ 0.034	0.061 $\pm$ 0.015	0.034 $\pm$ 0.035
k_1 ($M^{-1}s^{-1}$)	33.4 $\pm$ 8.2	34.8 $\pm$ 7.1	45.2 $\pm$ 12
k_2 ($M^{-1}s^{-1}$)	71 $\pm$ 180	53 $\pm$ 51	270 $\pm$ 250

These constants refer to the proposed model (fig. 2.6.b).

the latter to the receptor, as well as to determine the distance between these compounds. The addition of QSY7-NTA-Ni to cells expressing 5-HT_3-C-His_6 resulted in a rapid (within 30 seconds) decrease of fluorescence intensity of receptor-bound GR-flu, which can be completely recovered within a few minutes upon the addition of EDTA (figure 2.7.b). The rapid binding of QSY7-NTA-Ni to 5-HT_3R allowed consecutive additions of the compound to the same cells in order to obtain a complete binding isotherm; addition of EDTA restored the initial fluorescence of receptor-bound GR-flu (figure 2.7.c).

Binding of QSY7-NTA-Ni to the three different His-tagged 5-HT_3Rs yielded similar dissociation binding constants ranging from 1-4 μM; however, the fluorescence intensity of GR-flu decreased to different extend (figure 2.8.a). As the FRET efficiency correspond to the observed decrease in normalized fluorescence, these data indicate that the distance between GR-flu and the NTA-probes decreases in the order 5-HT_3R-Loop-His_6 > 5-HT_3R-N-His_6 > 5-HT_3R-C-His_6. High concentration up to 6 μM of QSY7-NTA-Ni had no effect on the fluorescence of GR-flu bound to wild-type of 5-HT_3R, which contains no oligohistidine sequence (figure 2.8.a), showing that it is indeed the NTA-oligohistidine interaction that is the origin of the observed fluorescence decrease. QSY9-NTA-Ni showed effects similar to those of QSY7-NTA-Ni on the fluorescence intensity of GR-flu bound to 5-HT_3R-C-His_6 and 5-HT_3R-N-His_6, and at concentrations up to 12 μM, did not bind to wild-type 5-HT_3R. But in contrast to QSY7-NTA-Ni, it did not affect the fluorescence intensity of GR-flu bound to 5-HT_3R-Loop-His_6 (figure 2.8.b). These results indicate that (i) the His_6 sequence in the loop is located in the cytosol whereas the N- and C-terminal His_6-sequences are extracellular, confirming the proposed topology of the 5-HT_3R, (ii) FRET is dependant of the binding of QSY9-NTA-Ni to an oligohistidine sequence and (iii) the membrane is impermeable to QSY9-NTA-Ni, owing to its charged SO_3^- groups (figure 2.3.b). This view is supported by the inability of QSY9-NTA-Ni to interact with a cytosolic His-tag fused to the C-terminus of NK1R (see below). Thus, QSY7-NTA-Ni and QSY9-NTA-Ni can be used to determine the topology of membrane proteins in living cells without the need for fixation and, or, permeabilization of the cells.

The spatial positions of the polyhistidine sequences within the 5-HT_3R were evaluated from FRET upon QSY7-NTA-Ni binding (figure 2.9). Whereas the average distances between the donor-acceptor chromophores can be determined with a precision of about ± 0.3 nm, the binding site of the NTA on a hexahistidine sequence in the receptor is located within 1.5 nm from the position of a particular NTA chromophore; this uncertainty is given by the length of the fully extended

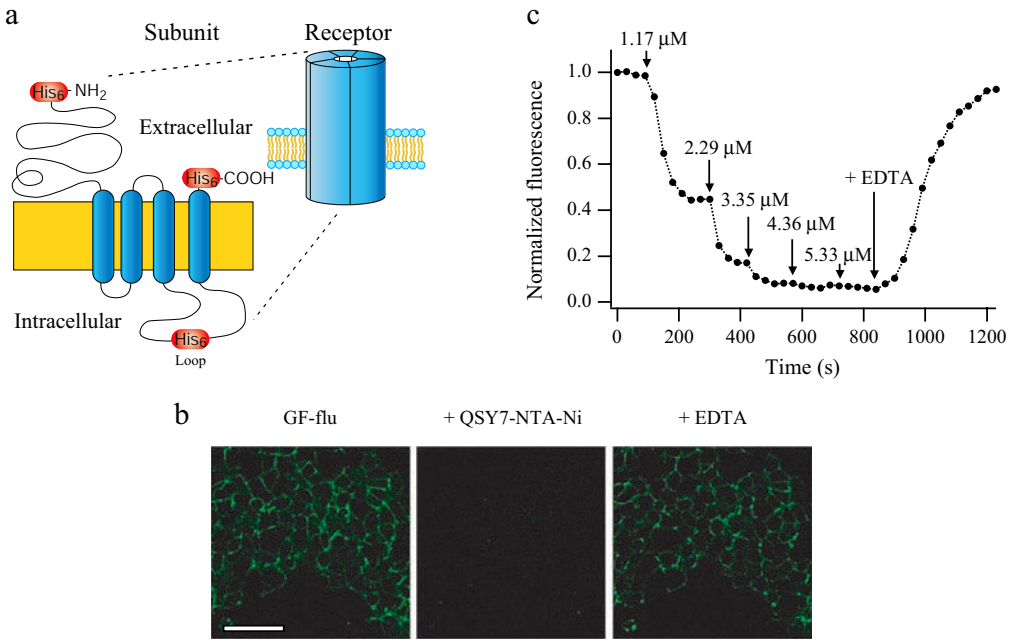

Figure 2.7: Reversible *in vivo* labelling of the 5-HT$_3$R. *(a) Topology of a subunit of the homopentameric 5-HT$_3$R showing the extracellular N-terminal ligand-binding region, the four predicted transmembrane segments, the large intracellular loop and the extracellular C-terminus [147]. Four different protein mutants were produced comprising an oligohistidine sequence either at the N-terminus (5-HT$_3$R-N-His$_6$), in the second intracellular loop (5-HT$_3$R-Loop-His$_6$) or at the C-terminus (5-HT−3R-C-His$_6$ or 5-HT−3R-C-His$_{10}$). The insert shows a cylindrical model of the homopentameric 5-HT$_3$R. (b) HEK-293 cells expressing the 5-HT$_3$R-C-His$_6$ were exposed for 15 min to 15 nM GR-flu, resulting in a selective staining of 5-HT$_3$R in the cellular membrane as observed by fluorescence confocal microscopy (left). Upon addition of QSY7-NTA-Ni at a final concentration of 5 µM, the fluorescence intensity of GR-flu dropped to 5% of the initial value (middle). Addition of 5 mM EDTA established the original fluorescence intensity (right). Scale bar is 50 µm. (c) QSY7-NTA-Ni was added consecutively at the concentration indicated to HEK-293 cells containing GR-flu bound to 5-HT$_3$R-C-His$_6$. On each addition, the fluorescence intensity of receptor-bound GR-flu decreased to reach a steady level within 1 min and, finally, saturation at 5% of its original fluorescence intensity. After about 13 min, 5 mM EDTA was added to restore the original GR-flu fluorescence intensity within 5 min.*

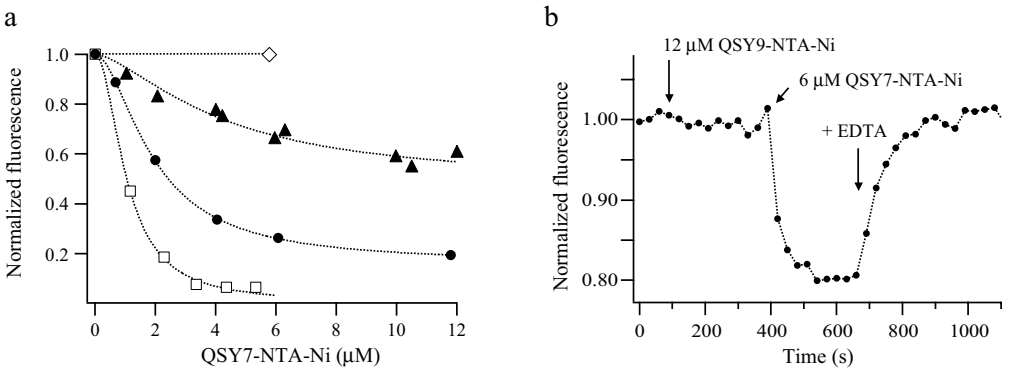

Figure 2.8: Structure of 5-HT$_3$R in live cells investigated by FRET using NTA-probes. *(a) Binding of increase amount of QSY7-NTA-Ni to the different hexahistidine-containing 5-HT$_3$Rs resulted in a saturable decrease of the fluorescence intensity of GR-flu. Apparent dissociation constants are K_d = 1.95 ± 0.03 µM, 4.2 ± 0.7 µM and 1.05 ± 0.07 µM and FRET efficiencies at saturation are E = 0.83 ± 0.01, 0.52 ± 0.06 and 1.00 ± 0.05 for 5-HT$_3$R-N-His$_6$ (●), 5-HT$_3$R-Loop-His$_6$ (▲) and for 5-HT−3R-C-His$_6$ (□), respectively. Addition of QSY7-NTA-Ni had no effect on the fluorescence intensity of GR-flu bound to wild-type 5-HT$_3$R (◇). QSY9-NTA-Ni exhibited apparent dissociation constants K_d = 12.7 ± 0.5 and 7.8 ± 2.4 µM, and FRET efficiencies at saturation E = 0.72 ± 0.06 and 0.78 ± 0.18 for 5-HT$_3$-C-His$_6$ and 5-HT$_3$-N-His$_6$, respectively and had no effect on the fluorescence of GR-flu bound to wild-type 5-HT$_3$R. In all cases, addition of 5 mM EDTA resulted in a recovery of 95-100%. (b) Addition of 12 µM QSY9-NTA-Ni did not affect the fluorescence intensity of GR-flu bound to 5-HT$_3$-Loop-His$_6$. Addition of 6 µM QSY7-NTA-Ni, however, reduced the fluorescence intensity of GR-flu by 20%. Addition of EDTA to 5 mM restored the original fluorescence intensity.*

spacer separating the NTA chromophore from the His-tag. The margin in the precision of localization might be reduced to about 0.7 nm by using a NTA-probe with a shorter spacer and a smaller chromophore. The N-terminal His_6 sequence seems to be located near the apex of the receptor protein, which is in agreement with a structural model of the 5-HT_3R [147]. The oligohistidine tags of 5-HT_3R-C-His_6 and 5-HT_3R-Loop-His_6 are located close to the surface or within the interface of the outer and inner leaflet of the membrane, respectively, because owing to their polarity, oligohistidine sequences are not expected to be in the hydrophobic membrane core [151]. The observed position of the C-terminal polyhistidine sequence is in agreement with the hydropathy analysis of the 5-HT_3R amino acid sequence [42], which predicts that only three amino acids at the C-terminus (plus in the case of 5-HT_3R-C-His_6, the His_6 sequence) protrude from the hydrophobic membrane core to the extracellular side of the membrane. The distance between the NTA-probes bound to extracellular (5-HT_3R-C-His_6) and intracellular (5-HT_3R-Loop-His_6) His_6 sequences is $\geqslant 2.8 \pm 0.5$ nm (difference between d and c in figure 2.9.f), which is comparable to the thickness of the hydrophobic membrane core (2.5-3 nm [151,152]) and to the distance of 3-3.5 nm between the two rings of charged amino acids on either side of the transmembrane domain of the highly homologous nicotinic acetylcholine receptor [108]. To my knowledge, this is the first report on localization of a sequence within the intracellular domain of a ligand-gated ion channel in living cells.

It has been demonstrated that nonfluorescent NTA probes in combination with fluorescently labelled protein can deliver important information about the structure of the protein and its molecular interactions. Molecular interactions between proteins in live cells are often investigated by FRET microscopy using proteins labelled with, for instance, two spectrally GFP-analogs [112]. In such cases, problems arise from variations in expression levels of the donor and acceptor proteins, which can be very different between experiments complicating, in addition to cross-talk, precise analysis of FRET [112, 139]. However, FRET can be determined accurately by, for example, acceptor bleaching or fluorescence lifetime imaging [139]. Reversible *in vivo* labelling with NTA-probes offers an alternative and simple one-color approach to measure FRET. One of the interacting proteins is labelled with a fluorescent FRET donor (*e.g.*, GFP), the partner protein contains an oligohistidine sequence. Then the latter protein is rapidly labelled with a nonfluorescent NTA-probe as FRET acceptor. The interaction between the two proteins is demonstrated unequivocally when the donor fluorescence intensity decreases upon addition of the acceptor. Specificity of the labelling can be checked by EDTA addition, which reverses NTA-probe

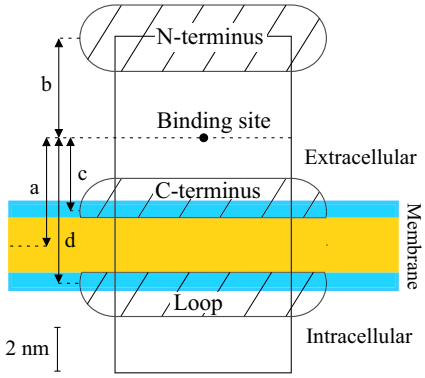

Figure 2.9: Model structure of the 5-HT$_3$R from FRET data using NTA-probes in live cells. *The location of the different His-tags within the 5-HT$_3$R were estimated using the topology information from figure 2.8.b and FRET data from figure 2.8.a as described in section 2.3.4. $R_0 = 5.83 \pm 0.13$ nm for GR-flu (donor) and QSY7-, QSY9-NTA-Ni (acceptors). In the absence of detailed structural information, the 5-HT$_3$R is modelled as a 15 nm long cylinder with a 4 nm radius, protruding 7 nm from the extracellular side of the membrane, corresponding to the dimensions of the highly homologous nAchR [107, 108]. The membrane comprises a hydrophobic core (yellow, 2.5 nm) and two polar interfacial regions (blue, 2 x 0.75 nm) [152]. GR-flu (•) is bound 4.9 ± 0.9 nm above the center of the membrane [145] on the surface of the extracellular part of the receptor [147] (arrow a). For each sort of His-tagged 5-HT$_3$R, the NTA-probes are distributed by 5-fold symmetry on a circle with a radius of 4 nm; their actual angular positions around the major symmetry axis with respect to the GR-flu could not be determined as FRET depends only weakly on this axial rotation. In the case of the 5-HT$_3$R-N-His$_6$, NTA-probes are located 4.5 ± 0.2 nm above GR-flu (arrow b), close to the apex of the receptor. QSY7-NTA-Ni probes bound to 5-HT$_3$R-C-His$_6$ and 5-HT$_3$R-Loop-His$_6$, respectively, are located at $\leqslant 3.5$ nm below GR-flu in the extracellular domain (arrow c), and 6.3 ± 0.3 nm below GR-flu in the intracellular domain (arrow d). The positions of the hexahistidine sequences of a particular 5-HT$_3$R are within about 1.5 nm of the corresponding NTA-probes, owing to the distance between the chromophore center and the Ni^{2+} ion (figure 2.3.a and b), and located with fivefold symmetry within a hemi-torus with torus and tube radii of 4 and 1.5 nm, respectively, around the receptor, excluding the hydrophobic core of the membrane owing to the polarity of histidine [151] (crosshatched regions).*

binding.

The fast reversibility of the binding of NTA-probes to oligohistidine sequences might improve FRET experiments considerably. The fluorescence of the FRET donor can be easily measured before and after a titration experiment delivering reliable reference values indispensable for the quantitative evaluation of FRET. Also, several FRET acceptors with different R_0 values can be applied consecutively to the same sample, as NTA probe can be removed by EDTA addition and medium exchange. This subsequently facilitates the optimization of precise distance measurements within proteins and protein complexes.

2.4.4 Fluorescent NTA probes label the 5-HT$_3$ receptor in live cells

Imaging nonfluorescent proteins within a living cell by labelling with NTA fluorophores might be hampered by the relatively low affinity of NTA to hexahistidine sequences. Because this would result in a considerable fluorescence background of unbound NTA fluorophores, the hexahistidine sequence was elongated, increasing the affinity of QSY7-NTA-Ni for 5-HT$_3$R-C-His$_{10}$ sixfold over its affinity for 5-HT$_3$-C-His$_6$ (figure 2.10.a). In turn, labelling the 5-HT$_3$R-C-His$_{10}$ with tetraethyl rhodamine-NTA-Ni (Rho-NTA-Ni) in live cells allowed imaging and localization of the receptor in the cell membrane by confocal microscopy (figure 2.10.b right). The specificity of labelling with Rho-NTA-Ni was demonstrated with bound GR-flu a fluorescein labelled antagonist of the 5-HT$_3$R (i) by colocalization of rhodamine and fluorescein fluorescence (figure 2.10.b left) and (ii) by observation of FRET between GR-flu and Rho-NTA-Ni (figure 2.10.b middle). This example shows that it is possible to measure simultaneously the binding of two different markers (Rho-NTA-Ni and GR-flu) to the receptor. Similarly, other fluorescent NTA-probes were used (table 2.4).

2.4.5 A G protein-coupled receptor investigated with NTA chromophores *in vivo*

The novel labelling procedure was also applied to the NK1 tachykinin receptor [153] (NK1R), a representative of the large G protein-couple receptor family [154]. A GFP and an oligonucleotide sequence were fused to the extracellular N-terminal and at the intracellular C terminus, respectively, yielding, GFP-NK1R-His$_{10}$ (figure 2.11.a). Binding of QSY7-NTA-Ni diminished the fluorescence of GFP-NK1R-His$_{10}$ in a saturable manner, whereas QSY9-NTA-Ni is indeed membrane impermeable, as previously shown (figure 2.11.b). Moreover, the affinity of QSY7-NTA-Ni

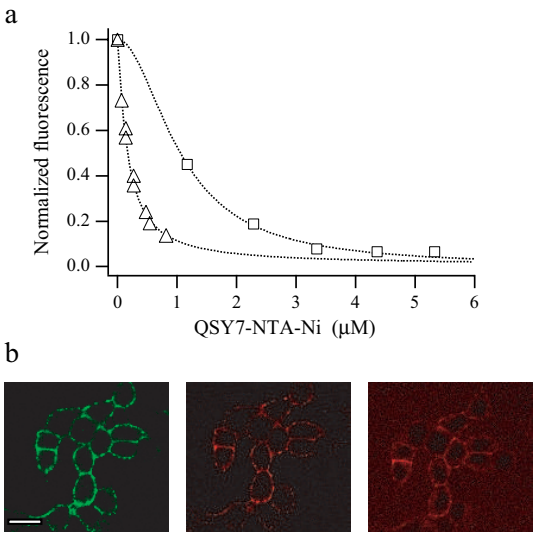

Figure 2.10: *In vivo* labelling of the 5-HT$_3$R-C-His$_{10}$. *(a) Extending the length of the hexahistidine sequence increases its affinity for NTA-probes. Sequential addition of QSY7-NTA-Ni to HEK-293 cells expressing the 5-HT$_3$R-C-His$_6$ (□) and 5-HT$_3$R-C-His$_{10}$ (△) resulted in a saturable decrease of the fluorescence intensity of receptor-bound GR-flu, yielding K_d = 1.05 ± 0.07 µM or 166 ± 7 nM, and maximal FRET efficiency E_{max} = 1.00 ± 0.05 or 0.99 ± 0.02, for the respective receptors. (b) Localization of 5-HT$_3$R-C-His$_{10}$. HEK-293 cells expressing 5-HT$_3$R-C-His$_{10}$ were incubated with 20 nM GR-flu for 20 minutes. Subsequently Rho-NTA-Ni was added to a final concentration of 0.5 µM, decreasing the GR-flu fluorescence intensity by 25%. Rho-NTA-Ni fluorescence (right: excitation 548 nm, emission filter LP580 nm) localized with GR-flu fluorescence (left: excitation 458 nm, emission filter BP505-530 nm). Upon excitation of GR-flu, Rho-NTA-Ni fluorescence was also observed because of FRET (middle: excitation 458 nm, emission filter LP580 nm). Scale bar is 20 µm.*

for the intracellular His-tag in the NK1 receptor is comparable to the one obtained for oligohistidine-labelled of GFP and 5-HT_3 receptor. The distance between the chromophore of GFP and QSY7-NTA-Ni in the case of GFP-NK1R-His_{10} is determined from FRET measurements as 5.7 nm, sufficient to span the membrane the hydrophobic core of the plasma membrane (2.5-3.0 nm) or the entire membrane (3.5-4.7 nm) [152]. This shows the potential of the method for studying protein-protein interactions within cellular signaling.

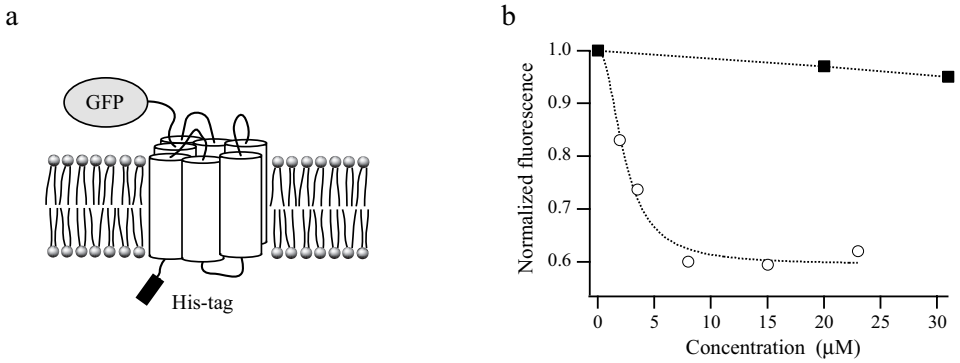

Figure 2.11: *In vivo* labelling of a G protein-coupled receptor. *(a) Seven transmembrane topology of the GFP-NK1R-His_{10} with the fluorescent protein at the extracellular N-terminal and the polyhistidine sequence at the intracellular C-terminal. (b) Addition of increasing concentration of QSY7-NTA-Ni to HEK-293 cells expressing GFP-NK1R-His_{10} in the plasma membrane results in a saturable decrease of GFP fluorescence (○), whereas QSY9-NTA-Ni has almost no effect (■), demonstrating the membrane impermeability of the latter probe. Evaluation of the binding isotherm of QSY7-NTA-Ni yielded a dissociation constant $K_d = 2.4 \pm 0.2$ μM and FRET efficiency at saturation $E = 0.41 \pm 0.02$. A distance of 5.7 nm between the chromophores of GFP and QSY7-NTA-Ni was obtained using $R_0 = 5.4 \pm 0.3$ nm, assuming $\kappa^2 = 2/3$ for enhanced GFP and QSY7-NTA-Ni.*

2.5 Conclusion

The present approach overcomes several limitations of existing labelling methods. It allows fast and reversible, site-specific, and *in vivo* labelling of proteins by small, nonperturbing molecular probes (table 2.5). It has been demonstrated that NTA-probes having a wide range of spectroscopic properties can be used to rapidly label molecules in a fully reversible manner. This generic method can be applied both *in vivo* and *in vitro* to investigate molecular interactions, to visualize His-tagged molecules and to elucidate the structure and topology of proteins. This methodology is nearly a ready for use labelling technique since polyhistidine sequences genetically

Table 2.4: K_d values (μM) for NTA-probes interacting with polyhistidine tagged receptors in live HEK-293 cells.

Receptors	**QSY7-NTA-Ni**	**QSY9-NTA-Ni**	**Rho-NTA-Ni**
5-HT_3R-C-His_6	1.05 ± 0.07	12.7 ± 0.5	1.70 ± 0.18
5-HT_3R-C-His_{10}	0.166 ± 0.007	2.6 ± 0.6	1.45 ± 1.13
5-HT_3R-Loop-His_6	4.2 ± 0.7	NB	1.5 ± 0.5
5-HT_3R-N-His_6	1.95 ± 0.03	7.8 ± 2.4	
GFP-NK1R-His_{10}	2.4 ± 0.2	NB	
Receptors	**TexRed-NTA-Ni**	**Cy3-bis-NTA-Ni**	**Cy5-NTA-Ni**
5-HT_3R-C-His_{10}	0.22 ± 0.05	0.55 ± 0.05	$\geq$ 2.5

NB for no binding, the cell plasma membrane is impermeable towards the probe.

fused to proteins are used for protein purification. Close to two thousand indexed proteins contain a His_6 recognition sequence peptide (BLAST using the SIB network sevice) that can be labelled by the present approach. Moreover, NTA probes are readily and economically produced from commercially available compounds. It will therefore facilitate the quantitative analysis of biochemical networks that control and maintain cellular function, which is a major goal of proteomics.

Table 2.5: Comparative table of different methodologies for labelling proteins with small-molecule probes and their relative attributes.

Methods	**Tag size**	**Partner size**	***In vivo***	**Reversability**	**Kinetics**
GFP	27 kDa	-	Yes	-	-
hAGT	20 kDa	$<$ 1 kDa	Yes	No	minutes
HaloTag	33 kDa	$<$ 1 kDa	Yes	No	min. to hours
DHFR	18 kDa	$<$ 1 kDa	Yes	No	min. to hours
ACP	7 kDa	$<$ 1 kDa	Yes	No	min. to hours
FKBP	12 kDa	$<$ 1 kDa	Yes	More or less	min. to hours
Epitope	5-30 aa	150 kDa	No	More or less	min. to hours
Biotin ligase	15 aa	$>$ 1kDa	No	More or less	min. to hours
FlAsH	6-10 aa	$<$ 1 kDa	Yes	More or less	min. to hours
NTA	6-10 aa	$<$ 1 kDa	Yes	Yes	seconds

Chapter 3

NTA-fluorophores for single-molecule microscopy of living cells: Diffusion of the 5-HT_{3A} receptor

Abstract — Techniques allowing selective detection of a few molecules, or even one molecule in living cells, offer novel ways to investigate the dynamics of cellular organization. So far, access to single-molecule properties was achieved by gold particles, latex beads, fluorescent quantum dots that are all rather big or small covalently-bound fluorescent labels that irreversibly photobleached. Here, the new fluorescence labelling method using NTA-fluorophores specifically and reversibly bound to engineered oligohistidine sequences, are used to probe the lateral diffusion of the ionotropic 5-HT_3 receptor in living cells. Particle tracking yielded heterogenous and complex trajectories of the receptor. Distribution of microscopic diffusion constants and fractions of mobile and immobile receptors revealed a significant decrease of the lateral mobility of the desensitized receptor after binding of serotonin. The present approach overcomes several limitations of conventional labelling methods. Reversibility of the binding allows successive tracking of single membrane proteins on the same cell under various conditions, yielding information on plasma membrane distribution, lateral mobility and modulation of these by stimuli.

3.1 Introduction

The advances in biology over the last half-century can best be summarized as understanding biology on a chemical basis. The genomes of many species, including humans, have now been sequenced, as well as high resolution structures of many macromolecular machineries have been obtained. So what are the new challenges of the post-genomic era? Well, there are many. But one challenge in particular is to study how molecular machineries work in real time, especially how they work individually or together in living cells. In order to reach this goal, technologies have to be developed which allow the detection of single molecules. Several technologies opened the door to single molecule detection but only one allows real time imaging of single molecules in a non-invasive way, suitable for life science; that is single-molecule imaging (SMI) and single molecule spectroscopy (SMS). Since few years, it is possible to detect photons emitted by a single fluorescent probe bound to the molecule of interest at room temperature and to image it over time. Single-molecule spectroscopy allows one to realize spectroscopic measurements and to monitor dynamic processes of a molecule. Single-molecule fluorescence spectroscopy provides a new and direct approach to investigate the molecular function of biochemical reactions. In contrast to ensemble measurements like fluorescence recovery after photobleaching (FRAP) or solution experiments, which yield information only on average molecular properties, single-molecule experiments provide information on individuals, such as distribution and time trajectories of properties that would otherwise be hidden. Whether each individual molecule has slightly different but constant properties or changes properties over time, cannot be answered correctly by averaging the observable. Therefore, SMS and SMI represent a versatile tool to observe the dynamics, the motion and folding of proteins or biomolecules in their native environment at the single-molecule level [155, 156].

Different probes have been used so far for the detection of single molecules. For instance, latex beads (∼500 nm in diameter) [157] and gold nanoparticles (∼40 nm in diameter) [158] attached to the protein of interest were widely used. Because these particles are extremely photostable, they allow long and fast measurements, but their large size is the main drawback; nevertheless, they are still often used. On the other hand, small fluorophores have been used for SMS on cells like organic dyes (*e.g.* Cy5, Alexa 647, Cy3, rhodamine...) covalently bound to the proteins of interest, fused fluorescent proteins (*e.g.* GFP, YFP), or coated semiconductor nanoparticles [128, 159]. Quantum dots have the advantage to be extremely photostable compared to other fluorescent reporters but are unfortunately also rather large (4-8 nm in

diameter), which might limit certain applications.

Since the development of single-molecule fluorescence spectroscopy at room temperature, the motion of several different biomolecules has been observed both *in vitro* and *in vivo*. The technique has been applied to directly observe the motions of linear and rotational molecular motors, enzymatic reactions, structural dynamics of proteins, DNA-protein interactions, single lipid molecules in a lipid bilayer and movements of single ion channels in a model membrane *in vitro* [160–164]. The first biological events observed at the single-molecule level *in vivo* were the reaction of ligand and receptor proteins [165] and the movement of lipid molecules [166] on the surface of living cells. Since then, ion channels [167], ligand-gated ion channels [159, 168], G protein-coupled receptors [169], cell-adhesion proteins [170], viral proteins [171], cooperative protein assembly [172] and components of the cytoskeleton [173] have been visualized as single molecule in live cells. The list of molecules that have been visualized is growing rapidly.

The interaction of ligand-gated ion channels, like the 5-HT_3 receptor, with cytoskeletal components and clustering proteins is a major determinant of the topology of these ionotropic receptors at the cell surface and of their trafficking through synthesis, recycling and degradation pathways. Neurotransmitter receptor movements into and out of synapses are one of the core mechanisms for rapidly changing the number of functional receptors during synaptic plasticity. The rapid gain and loss of receptors from synaptic sites are accounted by both endocytosis and exocytosis, as well as lateral diffusion of receptors in the plane of the cell membrane [174]. It has been suggested that endocytosis and exocytosis take place outside the synapse and that the receptors diffuse inside the synaptic cavity [175, 176]. The events are independent and are regulated by neuronal activity and interactions with scaffolding proteins [157]. At inhibitory synapses, glycine and $GABA_A$ receptor clusters are stabilized by the scaffolding protein gephyrin, which links to tubuline [159]. Certain scaffolding proteins have been identified that cluster AMPA and NMDA receptors at synapses [174]. In the case of the nAChRs, rapsyn is believed to form a cytoskeletal anchor [177]. Not much is known about the anchoring of the 5-HT_3 receptor. It was reported that both native and exogenous 5-HT_3 receptors form clusters associated with F-actin [178]. These clusters associated to the cytoskeletal network most probably play a key role in the physiological regulation of the receptor topology and dynamics, as is the case for other members of the ligand-gated ion channel family.

Here, a new generic method for *in vivo* membrane protein labelling is presented, which allows repetitive site-specific labelling with small fluorescent reporters for single-molecule spectroscopy. As presented in detail in chapter 2, the principle of

labelling relies on the specific interaction between a polyhistidine sequence as recognition element and a fluorescent NTA-probe. The genetically engineered tag can be introduced at a particular location where it does not disturb the protein structure and function in an extracellular accessible region since the probe employed here is not membrane permeable. The probe contains a metal-ion-chelating nitrilotriacetic (NTA) part covalently bound to a fluorescent moiety, which can have a wide range of properties. The site-specific interaction between the polyhistidine sequence and the small probe is reversible. The mean residence time of the probe on the recognition peptide sequence is in the order of some tens of seconds, which allows adequate data acquisition from single fluorescent particles before the probe dissociates. Therefore, irreversibly photobleached fluorophores can be replaced by fresh ones, which overcomes the limitation linked with conventional covalent labelling. The labelling procedure can be virtually indefinitely repeated on the same cell allowing single-molecule imaging of biological processes under variable conditions with small tags and small fluorescent probes.

Single-molecule spectroscopy of the 5-HT$_3$ serotonin receptor containing a polyhistidine tag was performed in live cells to first prove the feasibility of this labelling method and secondly to get information on the mobility of the receptor in native plasma membranes. The diffusion of the 5-HT$_3$R was investigated depending on its activation state revealing significative change in its mobility between the basal and the desensitized state. The mobility of the 5-HT$_3$R in the basal state was corroborated by measurements using a specific fluorescent antagonist of the receptor.

3.2 Properties of single fluorescent molecules

The signal to noise ratio is the most important factor in SMS since it sets the fundamental detection limit. Therefore, appropriate fluorescent probes have to be used. They have to exhibit a high extinction coefficient at the excitation wavelength, a high fluorescent quantum yield and a high photostability. Additionally, the ideal fluorophore should have a fairly short fluorescence lifetime so that it can go through the excitation and emission cycles at high frequency and should not show fluorescence intermittencies as a result of, for example, triplet transitions (dark state). The fluorescent molecule should also emit in the spectral range where the sensitivity of the detector is high [156]. In cell imaging, red fluorescent reporters are preferred since the fluorescence background of living cells in this spectral region is low.

An intrinsic property of all conventional organic fluorophores is that they

undergo irreversible photobleaching, which limits the number of photons that can be detected from a single fluorophore. Common dye molecules can emit up to 10^6 photons before photobleaching occurs. This single-step photobleaching is one of the signature of a single fluorescent molecule and is actually the criterion used in SMS cell imaging (figure 3.1) due to its direct access. Anti-bunching [179], defined dipole moments [180] and shape or size and intensity of the spot are the other criteria characterizing a single fluorescent molecule. Whereas the first three criteria are very strong, the latter two are very weak because the shape and intensity of the signal depends on the chemical structure of the fluorophore, its orientation relative to a support and its molecular environment.

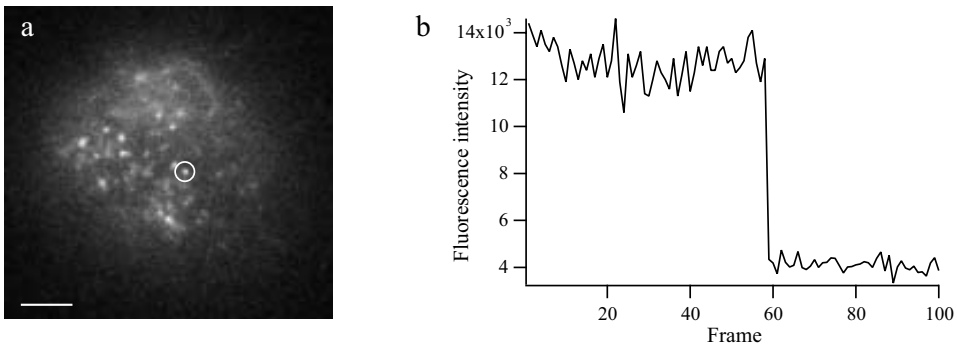

Figure 3.1: Single fluorescent molecule imaging. *(a) Fluorescence image of single 5-HT$_3$Rs labelled with Atto 647-NTA-Ni in HEK-293 cells. Scale bar represents 5 μm. (b) Irreversible single step photobleaching of an Atto 647-NTA-Ni bound to 5-HT$_3$R. The integrated light intensity inside the white circle in (a) was plotted versus a series of frames. The single-step photobleaching event is a proof that the encircled bright spot resulted from the emission of only one single fluorescent molecule.*

3.3 Materials and methods

3.3.1 Fluorescent probes

Atto 647-NTA-Ni — The succinimidyl ester of Atto 647 (Fluka, Buchs, Switzerland) dissolved in DMF was mixed to five equivalent Ni-NTA-lysine in 50 mM $NaHCO_3$ pH 8.0 (Atto 647 is less stable pH 9.0). The reaction was incubated overnight in the dark at 22°C. The product Atto 647-NTA-Ni was purified by thin layer chromatography on silica gel 60 plates 200 x 200 x 0.25 mm^3 (Merck, Darmstadt, Germany) eluted with $CHCl_3/CH_3OH/H_20$ 64:33:4 ($R_f = 0.14$). The yield of the reaction was ∼17% after extraction of the product with H_2O. The structure of

Atto 647 was not revealed by the provider.

GR-Cy5 — GR-H (1,2,3,9 tetrahydro-3-[(5-methyl-1H-imidazol-4-yl)methyl]-9-(3-amino-propyl)-4H-carbazol-4-one) (Glaxo Wellcome, Geneva, Switzerland) was labelled with the succinimidyl ester of Cy5 (Amersham Biosciences, NJ, USA) as described in [145].

3.3.2 Molecular and cellular biology

wt5-HT$_3$R — The sequence corresponds to the long splice variant of the murine 5-HT$_3$R, corresponding to the SwissProt entry p23979 containing two conflict regions, Glu8→Ala-Arg and Thr279→Thr-Ala (mature sequence numbering). The sequence was inserted into pcDNA 3.1(-) between Xho I and Not I restriction sites that are located before and after the coding region, respectively. The nucleotide sequence was verified by restriction analysis and sequencing (the first and last 400 nucleotides of the receptor sequence).

5-HT$_3$R-C-His$_{10}$ — The sequence corresponds to the short splice variant of the murine 5-HT$_3$R, corresponding to the SwissProt entry p23979 containing two conflict regions (Glu8→Ala-Arg and Thr279→Thr-Ala) and lacking the residues 360-365 (mature sequence numbering). A His$_{10}$ sequence was inserted at the C-terminal of the protein after Ser464. The construct was inserted in pEAK8 vector between Hind III and Not I restriction sites that are located just in front and behind the protein sequence respectively. The nucleotide sequence was verified by restriction analysis and sequencing of the whole coding region (see appendix A.2).

Cell culturing and transfection — HEK-293 cells were cultured with a density of 150'000 cells/ml on 0.18 mm thick glass coverslips in 6-well plates in Dulbecco's modified Eagle medium (DMEM) supplemented with 2.2% of fetal calf serum under humidified 5% CO_2 atmosphere at 37°C. Cells were transfected 14 to 18 hours after splitting using Effectene^{TM} (Qiagen, Hilden, Germany) according to the supplied protocol with 0.16 μg receptor plasmid DNA, 0.04 μg EGFP (enhanced green fluorescent protein) plasmid DNA (Clontech, Palo Alto, CA, USA), 1.6 μl enhancer, 2 μl effectene and 100 μl EC buffer per well (corresponding to 2 ml medium). Cell DMEM medium was replaced by DMEM supplemented with 10% of fetal calf serum, 6 to 12 hours after transfection.

3.3.3 Fluorescence imaging set-up

The setup is based on wide field laser illumination and detection using an intensified CCD camera sensitive enough to detect light emitted by single fluorescent molecules. A schematic view of the setup is shown in figure 3.2. Circularly polarized light from a HeNe laser (632.8 nm, 0.5 kW/cm^2) or a tunable single mode Ar^+ laser (457.9, 488, 514.5 nm) (both from Coherent, Auburn, CA, USA) was directed by a dichroic mirror into a microscope objective (C-Apochromat 63x W Korr, 1.2 NA, Zeiss, Jena, Germany) to illuminate a 22 μm diameter region of the sample. Fluorescence was collected by the same objective, passed through adequate filter and mirror (table 3.1) and imaged on an intensified CCD camera (I-Pentamax 512 EFT, Roper Scientific, USA). To minimize fluorescence bleaching of the sample, a shutter (LS3T2, Vincent Association, Rochester, USA) was used with tunable sampling frequencies and illumination times. Illuminated cells were continuously perfused with a VC-77SP fast step perfusion system (Warner Instruments Corp, Hamden, CT, USA).

Table 3.1: Excitation wavelength, dichroic mirrors and emission filters used for SMI.

Dye	Excitation (nm)	[1]Dichroic mirror	[1]Emission filter
Atto 647 / Cy5	632.8	Q645LP	HQ710/120
GFP	488	Q495LP	HQ525/50

[1] Filters and dichroic mirrors were from Chroma (Rockingham, VT, USA).

3.3.4 Experimental methods

Single-molecule imaging in living cells — The coverslips were transferred to a sample holder 48 hours after transfection and the cells were covered with 400 μl Dulbecco's phosphate-buffered saline (D-PBS) (Gibco Invitrogen, CA, USA) containing 0.9 mM $CaCl_2$, 0.5 mM $MgCl_2$, 2.7 mM KCl, 1.5 mM KH_2PO_4, 138.0 mM NaCl and 8.1 mM Na_2HPO_4 at pH 7.4. All ligands were dissolved in the D-PBS buffer and cells were continuously perfused during experiments. Single-molecule fluorescence images were recording at a frequency of 4 Hz with an exposition time of 50 ms for 100 frames (figure 3.2). Measurements were performed on the upper plasma membrane of cells preselected using the cotransfected cytosolic EGFP marker. Cells expressing the 5-HT_3R were incubated for 25-35 seconds with either 100 pM GR-Cy5, 500 pM Atto 647-NTA-Ni or 500 pM Atto 647-NTA-Ni with 2

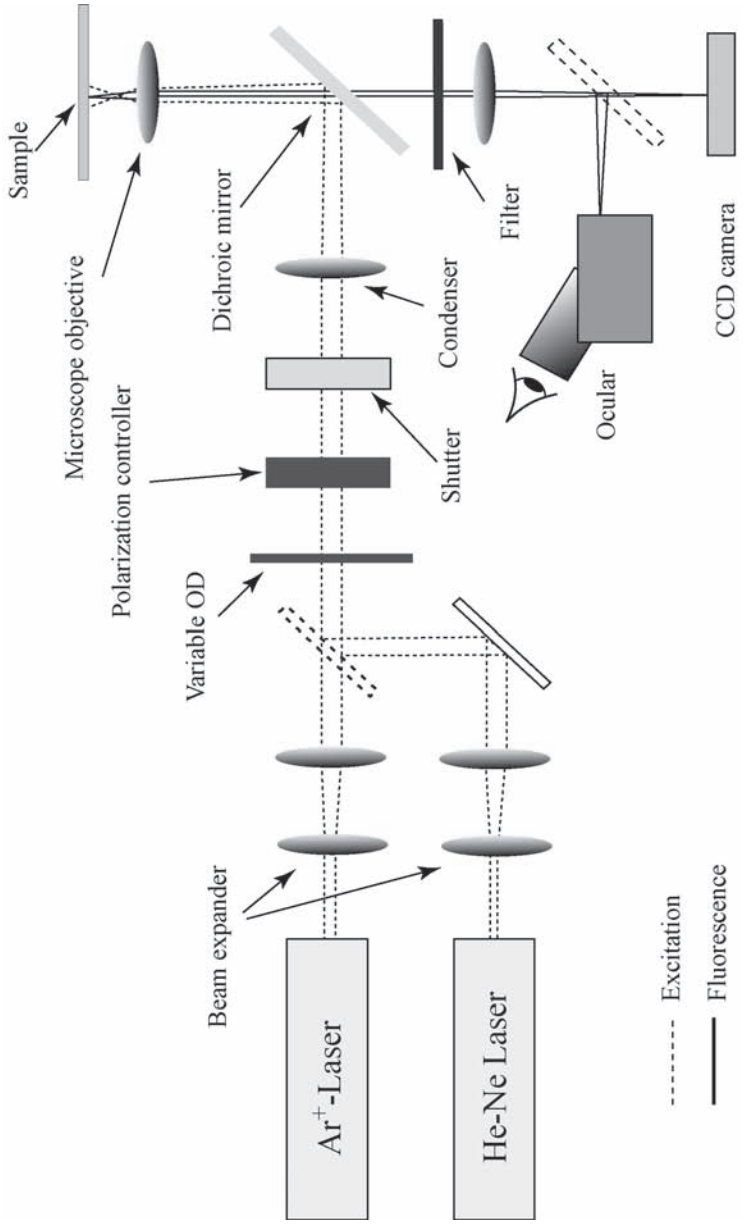

Figure 3.2: Schematic view of the single-molecule fluorescence imaging set-up. *HeNe laser generates light of 632.8 nm and the Ar^+ laser generates either 457.9, 488 or 514.5 nm wavelengths. Emission filters and dichroic mirrors are presented in table 3.1. The variable neutral density filer (OD) was used to tune the excitation laser intensity.*

μM serotonin (5-HT) (Fluka, Buchs, Switzerland) before washing with the buffer. Series of fluorescent images were recorded with a delay of 6-7 seconds after the start of washing to ensure that no free fluorescent ligand remained in solution. Before the first recording, the sample was continuously exposed to excitation light for 1 minute to decrease the autofluorescence of the cells. No significant unspecific binding of GR-Cy5 and Atto 647-NTA-Ni was observed on native HEK-293 cells or HEK-293 cells expressing the wt5-HT_3R.

Dissociation rate constant of Atto 647-NTA-Ni — Cells transiently expressing the 5-HT_3R-C-His_{10} were prepared as for single-molecule imaging (see above) in D-PBS buffer. Sequences of fluorescence images were performed at different frequencies (1, 2, 4, 6 , 8, 10 and 12 Hz) with an exposition time of 50 ms for 150 frames (figure 3.2). Cells were incubated for 40 seconds with 2.0-0.5 nM Atto 647-NTA-Ni and then continuously washed with D-PBS buffer. Series of fluorescent images were recorded with a delay of 6-7 seconds after start of washing to ensure that no free fluorescent ligand remained in solution. Recordings at the different sampling frequencies were all performed on the same cell and the experiment was repeated twice.

3.3.5 Data treatment

Dissociation rate constant — The dissociation rate constant of Atto 647-NTA-Ni from 5-HT_3-C-His_{10} was evaluated from the fluorescence intensity decay during washing. The decrease of fluorescence intensity is a superposition of the dissociation of the ligand and photobleaching of the fluorophore as described by equations 3.1 and 3.2.

$$\frac{dF}{dt} = -k_{\text{off}} \cdot F - k_{\text{bl}} \cdot \nu \cdot t_{\text{ex}} \cdot F \tag{3.1}$$

$$F = F_0 \cdot \exp\left(-\left(k_{\text{off}} + k_{\text{bl}} \cdot \nu \cdot t_{\text{ex}}\right) \cdot t\right) = F_0 \cdot \exp\left(-k_{\text{obs}} \cdot t\right) \tag{3.2}$$

F and F_0 are the fluorescent intensity at time t and $t = 0$ respectively, k_{off} the dissociation rate (s^{-1}), k_{bl} the photobleaching rate (s^{-1}), t_{ex} the exposition time per frame (s), ν the sampling frequency (Hz) and t the time (s). The dissociation rate constant is obtained from the intercept of a linear fit of the plot of the effective fluorescent decay rate constant k_{obs} versus the frequency using equation 3.3.

$$k_{\text{obs}} = k_{\text{off}} + k_{\text{bl}} \cdot t_{\text{ex}} \cdot \nu \tag{3.3}$$

Single molecule tracking — Single-molecule tracking was performed using a homemade computer program written in the Igor Pro software (WaveMetrics, Lake Oswego, OR, USA), which first localized single molecules and then tracked them in order to collect information about the mobility or diffusion constants. Image series of single fluorescent molecules were processed in six steps. (i) A Gaussian filter was applied to each image to remove background noise and then (ii) to localize all the local maxima of intensity. (iii) All the assigned maxima were then marked in the original image sequence and each of them was fitted (iv) according to a two-dimensional Gaussian fit. This step allowed us to discriminate single-molecules by assigning shape constraints on the peaks (*e.g.* width of the peaks in two dimensions and intensity). Signal caused by cosmic rays (too narrow), from vesicles or from the autofluorescence of the cell (too large) and from several fluorescent molecules within a single spot (elongated peak) were this way discriminated. A successful fit gave the position of the particle with an accuracy much higher that the actual size of the pixel (225 x 225 nm^2) mainly determined by the surrounding noise. (v) Trajectories of each selected single molecules were then determined by calculating for all images of the series the distance separating all fitted molecules in image i to all fitted molecules in image i+1. Closest molecules in image i and i+1 were considered to be the same as long as distance remained within a certain threshold fixed at 4 pixels (1 μm). The trajectories were occasionally interrupted by blinking, crossing of two molecules and unsuccessful fits. (vi) All trajectories were visually checked to both link interrupted traces and observe one-step photobleaching. Only traces fulfilling these seven criteria were used for further analysis.

Classification and characterization of trajectories — Square displacements r^2 were calculated between all points of a tracked trace and averaged for each corresponding time interval between two images (t_{lag}) yielding mean square displacements $MSD(t_{\mathrm{lag}})$. For each trajectory, the dependency of *MSD* versus t_{lag} is the signature of the diffusion properties of the receptor. For a free brownian diffusion in a plane, the *MSD* is linearly dependent on t_{lag} and can be fitted by equation 3.4 where D is the diffusion constant (in μm^{2}s^{-1}).

$$MSD(t_{\mathrm{lag}}) = 4{\cdot}D \cdot t_{\mathrm{lag}} \tag{3.4}$$

If the particle is confined within a certain domain, the diffusion inside the compartment will be free yielding a linear dependence for short t_{lag} corresponding to *MSD*s much smaller than the compartment dimension. At large t_{lag}, the *MSD* reach a constant value which is related to the dimensions L (μm) of the confinement

area. Such behavior can be fitted with equation 3.5. This relation can also be applied for Brownian diffusing particles with the difference that the value of L obtained is large, inconsistent with the observed phenomena.

$$MSD(t_{\mathrm{lag}}) = \frac{L^2}{3} \cdot \left(1 - \exp\left(-\frac{12 \cdot D \cdot t_{\mathrm{lag}}}{L^2}\right)\right) + noise \tag{3.5}$$

The traces of individual molecules were usually too short for the determination of $MSD(t_{\mathrm{lag}})$ with sufficient accuracy. Therefore, individual molecules were classified and grouped into two main different categories, immobile particles and mobile particles according to specific criteria determined from measurements of immobile molecules on a glass surface (figure 3.3); a distinction was made between mobile molecules that were confined and non-confined. The r^2 within the same category were combined and $MSD(t_{\mathrm{lag}})$ versus t_{lag} plots were fitted using equation 3.5 yielding diffusion coefficients D and size of the confined domain L. All errors indicated were calculated according to Gauss propagation method and are 95% confidence intervals.

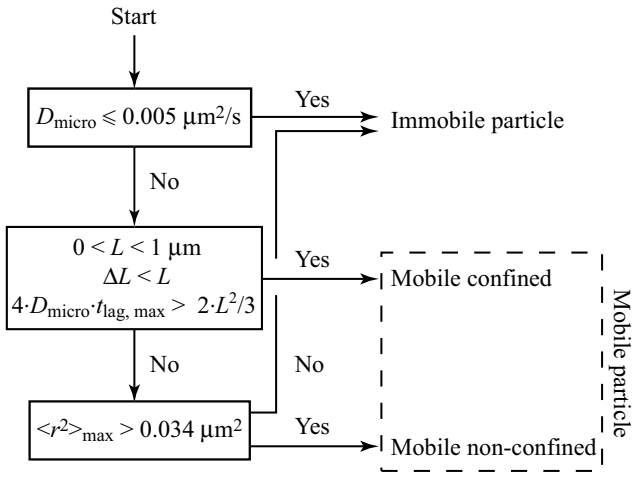

Figure 3.3: Schematic description of the algorithm used for particle classification. *Criteria presented in the boxes yield two classes of particles: the immobile and the mobile (confined and non-confined) particles.*

Classification of trajectories within two main categories, mobile and immobile particles, was performed using three criteria as presented in figure 3.3. The first criterium is the microscopic diffusion coefficient D_{micro} that corresponds to the diffusion coefficient obtained from a linear fit (equation 3.4) of the first four points of the $MSD(t_{\mathrm{lag}})$, as described by Kusumi *et al.* [158]. The second is the maximal mean r^2 and the third one is based on the results of a confined fit (equation 3.5). For a molecule to be considered as confined, the size of the domain L should be smaller

than 1 μm and its error ΔL should not exceed the dimensions of the confinement. Moreover, the trace of the particle should be long enough to "feel" the confinement: The final *MSD* of the particle, according to its D_{micro}, should be at least twice the *MSD* corresponding to L ($4{\cdot}D_{\text{micro}}{\cdot}t_{lag,max} > 2{\cdot}L^2/3$). The choice of the threshold value of 0.005 $\mu\text{m}^2\text{s}^{-1}$ for $D_{\text{micro,threshold}}$ and 0.034 μm^2 for $<r^2>_{\text{max,threshold}}$ are discussed in details in section 3.4.2, as well as the classification procedure. Particle classification according to this procedure was in agreement with visual inspection.

3.4 Results and discussion

3.4.1 Reversible labelling for single-molecule spectroscopy

Reversible labelling of proteins with a fluorescent NTA probe for single-molecule spectroscopy (SMS) was performed on living cells. The serotonin type 3A receptor containing an extracellular C-terminal decahistidine sequence (5-HT$_3$R-C-His$_{10}$) (figure 3.4.a) expressed in HEK-293 cells was labelled by incubating for 25 to 35 seconds with 500 pM Atto 647-NTA-Ni, a small organic fluorescent reporter. Under continuous washing with buffer, single 5-HT$_3$R-C-His$_{10}$ were imaged in the upper plasma membrane of living cells (figure 3.4.b) for several frames before the bound Atto 647-NTA-Ni irreversibly photobleached (figure 3.1.b) or dissociated from the receptor as a result of the non-covalent interaction. Particle tracking yielded traces that exceeded 15 frames for at least 50% of the particles (figure 3.4.c). In comparison with fluorescent proteins like YFP, for which not more than ten frames can be recorded before photobleaching occurs [181] in a wide field set-up, the NTA probes are much more stable and slower events can therefore be directly visualized. Furthermore, full freedom in the choice of the dye is provided, allowing to work in spectral region where the autofluorescence is low and to tune the properties of the fluorophore in applications like single-molecule FRET. Diffusion of the labelled receptor could be imaged up to 20 seconds, which corresponds to 80 frames recorded at a frequency of 4 Hz (figure 3.4.c).

Specificity of the labelling methodology was verified by incubating native HEK-293 cells and HEK-293 cells expressing wt5-HT$_3$R (containing no polyhistidine sequence) with 500 pM Atto 647-NTA-Ni for 30 seconds. After washing, no single fluorescent particles were observed on HEK-293 cell membrane, while few particles were detected on HEK-293 cells over expressing the wt5-HT$_3$R. All unspecifically bound probes moved very fast compared to specifically bound ones and were rapidly washed out during the first 10-15 frames of recording. Unspecific bound

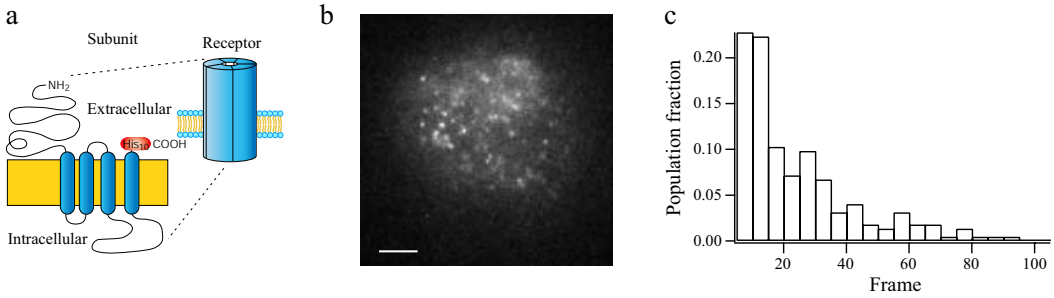

Figure 3.4: Single-molecule spectroscopy of the 5-HT$_3$R in a living cell. *(a) Topology of a subunit of the homopentameric 5-HT$_3$R showing the N-terminal ligand-binding region, the four predicted transmembrane segments, the large intracellular loop and the extracellular C-terminus where a His$_{10}$ sequence was genetically fused. The insert shows a cylindrical model of the 5-HT$_3$ receptor. (b) HEK-293 cells expressing the 5-HT$_3$R-C-His$_{10}$ were incubated for 30 seconds with 500 pM Atto 647-NTA-Ni and then continuously washed, labelling only a fraction of the receptor as revealed by single-molecule spectroscopy using 632.8 nm laser excitation (500 W/cm^2). Each bright spot corresponds to a single Atto 647-NTA-Ni bound to 5-HT$_3$R-C-His$_{10}$; all of them showed characteristic single-step photobleaching. Scale bar is 5 μm. (c) Distribution of the trace lengths obtained from particle tracking (see section 3.3.5) on a population of 222 traces of Atto 647-NTA-Ni bound to 5-HT$_3$R-C-His$_{10}$. The histogram revealed that 10% of the traces were longer than 50 frames.*

probes were assessed to be less than 5%. Interestingly, the molecular structure of the fluorophore played a role in the specificity of the probe. For instance, Cy5-NTA-Ni (figure 2.3) was not suited for single-particle labelling: Controls revealed significant unspecific labelling on the membrane of HEK-293 cells (Cy5 is known to be a membrane probe). Therefore, the Atto 647 dye is much more suited for this application compared to Cy5; it is not a membrane probe and is much more photostable.

Since the attachment of NTA-probes to polyhistidine sequences is reversible (figure 2.1), the probe can dissociate during washing and labelling can then be repeated many times as long as the illuminated cell remains alive. Photobleached fluorescent labels can thus be removed and replaced by new ones. Successive cycles of incubation, washing and recording were performed on the same cell (figure 3.5.a) and the relative fluorescence intensity reached after each association step was found to vary by less than 7% (figure 3.5.a left row). Each cycles lasted about one minute (25-35 seconds incubation, 6-7 seconds delay before recording and 100 frames at 4Hz recording) yielding up to 20 traces longer than 15 frames per recording. Therefore, acquisition of data could be performed very rapidly as 5 cycles ($\sim$5 minutes) could be easily performed on the same cell yielding around 100 traces per cell. Experiments on 10-20 cells yielded sufficient traces for good statistics of diffusion modes. Reversible site-specific labelling presents therefore several advantages for single-molecule spectroscopy compared to conventional labelling methods. From an experimental point of view, this labelling procedure is very convenient since the set-up can be adjusted and the focus can easily be set because probes bleached during adjustments can be replaced.

The dissociation rate constant of Atto 647-NTA-Ni was determined on a single cell with single-molecule sensitivity from the decay of the fluorescence intensity in an image series under continuous washing. To distinguish between fluorescence decrease due to the probe dissociation from the one resulting from fluorescence bleaching, measurements were repetitively recorded at different frequencies, as described in section 3.3.5 (figure 3.5.a). While photobleaching depended only on the exposure time, which remained constant for all the recordings since the number of frames recorded was identical, the dissociation of the probe increased with decreasing frequencies corresponding to longer total measurement times (figure 3.5.b). The resulting dissociation constant $k_{off} = 0.026 \pm 0.012$ s^{-1} was similar to the values obtained on the purified GFP-His$_{10}$ (table 2.3). According to the corresponding halftime $t_{1/2}$ = -1/k_{off}· ln(1/2), half of the probes dissociated from the tagged receptor within 27 seconds under continuous washing. The dissociation kinetics was therefore slow enough to record 100 frames at 4 Hz and fast enough for repeated

labelling on the same cell.

The association rate constant of the probe to the histidine tagged receptor could not be determined due to the relatively high value of the dissociation rate constant. The procedure to determine this factor is to incubate with the probe a single cell expressing the 5-HT$_3$R-C-His$_{10}$ for different time periods and then to record the fluorescence after a rapid wash allowing to remove all the unbound probes.

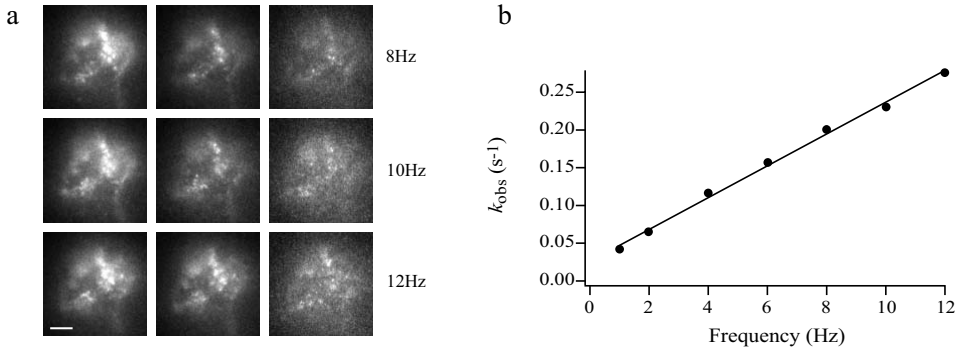

Figure 3.5: *In vivo* reversible labelling for single-molecule spectroscopy. *(a) Fluorescent images of a cell incubated for 30 seconds incubation with 2 nM Atto 647-NTA-Ni. After dissociation, Atto 647-NTA-Ni is replaced on the same cell and cycles are repeated (second and third line). Image sequences were acquired at different frequencies as indicated and images correspond to frame 0 (left), 50 (middle) and 100 (right). Scale bar is 5 µm. (b) The observed dissociation rate constant (k_{obs}) of Atto 647-NTA-Ni is linearly dependent on the sampling frequency. Quantitative evaluation using equation 3.3 yields k_{off} = 0.026 ± 0.012 s^{-1} and k_{bl} = 1.1 ± 0.1 ms^{-1}. Errors are within the points.*

3.4.2 Diffusion of the 5-HT$_3$R in living cells

The lateral mobility of the 5-HT$_3$R-C-His$_{10}$ was monitored in HEK-293 cells using repetitive labelling with Atto 647-NTA-Ni and quasi irreversible labelling with GR-Cy5 (k_{off} = 0.28· 10^{-3} s^{-1} corresponding to $t_{1/2} \approx$ 40 minutes [150]), a fluorescent antagonist of the receptor. Typical traces were 20 frames long, some being longer than 90 frames, yielding reliable trajectories of single receptors in the upper plasma membrane of living cells (figure 3.6). Trajectories were very heterogeneous and complex. Most particles were found either immobile (figure 3.6.a), mobile within a confined region (figure 3.6.b) or freely mobile (figure 3.6.c) as revealed by the dependency of the mean square displacement (*MSD*) versus the time lag (t_{lag}) (figure 3.7). Transitions between these diffusion modes could be observed in some trajectories: Some mobile molecules became immobile or confined (figure 3.6.d), or

inversely (figure 3.6.e). In addition to the three main modes, particles exhibiting hopping, directed or very slow diffusion were also observed (figure 3.6.f, g and h). This high diversity of diffusing particles impeded a clear classification of particles into distinct classes. For instance, the method proposed by Schütz and Schmidt [182] based on the cumulative distribution function did not yield meaningful results. It is also remarkable that it was not possible to make an homogeneous population of mobile molecules. This means that the diffusion is heterogeneous in nature with the 5-HT$_3$R being constantly hindered in his diffusion in a way depending on its local environment. Therefore, another procedure was implemented (see section 3.3.5).

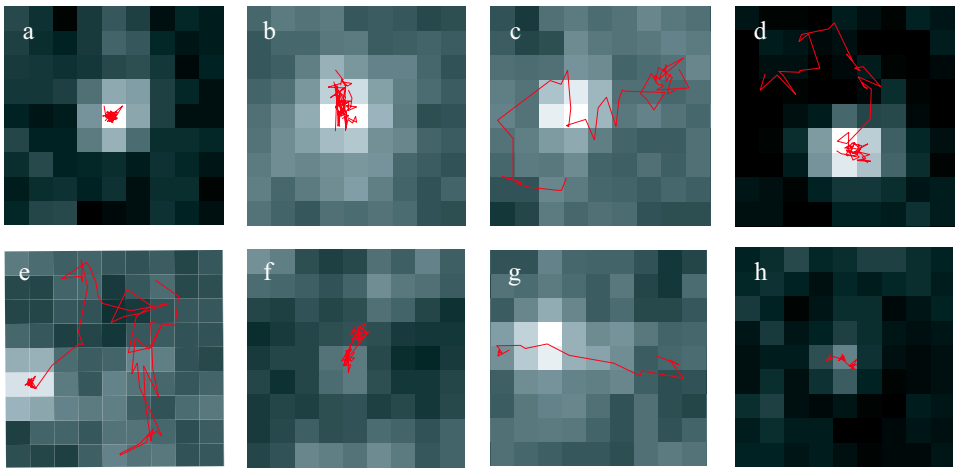

Figure 3.6: Heterogeneous diffusion of 5-HT$_3$Rs in HEK-293 cells. *The positions of single Atto 647-NTA-Ni probes bound to 5-HT$_3$R-C-His$_{10}$ were evaluated from 2D Gaussian fits on a series of frame recorded at 4 Hz, yielding trajectories (red line) of the receptor in the upper plasma membrane. Receptors exhibit three distinctive diffusing modes: (a) immobile, (b) mobile confined and (c) mobile non-confined. Their corresponding MSDs versus t_{lag} is presented in figure 3.7. Nevertheless, some trajectories present combined diffusion modes. The receptor can be mobile and then confined (d) or immobile and then mobile (e), hopping from one confined domain to another (f), or diffusing linearly (g), or slowly moving with short interruptions (h). The pixel size corresponds to 225 x 225 nm^2.*

Diffusing particles were classified into two main categories, immobile and mobile particles, according to the microscopic diffusion constant and the maximal recorded mean square displacement $<MSD>_{max}$ (section 3.3.5). Immobile receptors were defined as those whose D_{micro} is below 0.005 μm^2/s. This value corresponds to the resolution limit of our set-up as determined from measurements on fluorescent molecules immobilized on a glass surface. It should be noticed that this criterium does not necessarily mean that the molecules are effectively immobile since they

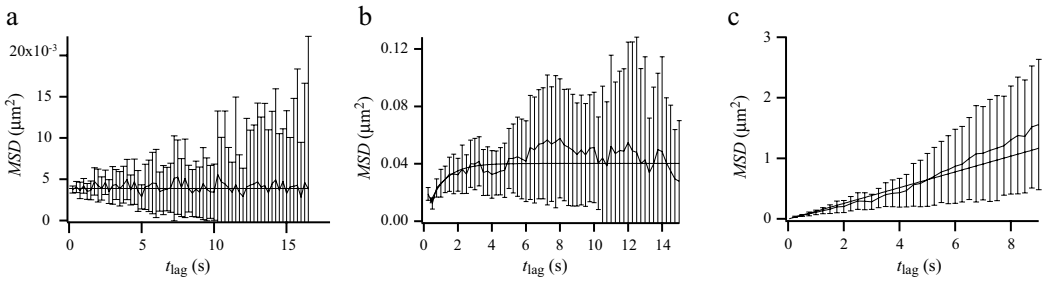

Figure 3.7: Diffusion of single receptors in the membrane of living cells. *Mean square displacement MSD versus time lag for an immobile (a), a mobile confined (b) and a mobile non-confined (c) 5-HT$_3$ receptor in HEK-293 cells labelled with Atto 647-NTA-Ni. (a) MSD of an immobile particle is constant versus time meaning that the particle does not move. The average <MSD> = 0.0038 ± 0.0005 μm^2 corresponds to the noise and sets the localization accuracy to 44 nm. (b) In the case of a confined particle, its MSD increases to reach a limiting value corresponding to the boundary of the confinement. Fitting with equation 3.5 yielded D = 0.010 ± 0.006 μm^{2}s^{-1} and L = 0.347 ± 0.012 μm. (c) In the case of a particle diffusing freely in the plasma membrane, MSD is linearly dependent on t_{lag}. Fitting with equation 3.4 yielded D = 0.033 ± 0.006 μm^{2}s^{-1}. Deviation of MSDs from the fit for large t_{lag} is due to a weak statistics. The MSD of (a), (b) and (c) corresponds to the trajectories presented in figure 3.6.a, b and c, respectively.*

could move very slowly. Indeed, for very long traces, a very small displacement could be detected for several molecules.

This criterium was however not sufficient for receptor classification. Several immobile receptors were wrongly classified because they were in noisy regions of the cell so that the measurements on the glass surface were not representative. The surrounding noise had a direct effect on the localization precision whose error had repercussions on the microscopic diffusion coefficient value. To account for this, we required that receptors moved at least over a certain distance corresponding to an $MSD_{\max} \geqslant 0.034$ μm^2 to consider them truly mobile. Some receptors seemed to diffuse within confinement region as shown in figure 3.6. We therefore investigated whether these receptors would diffuse within regions of precise dimensions. The regions were however found to widely vary. Thus, we considered this apparent confinement to be a manifestation of the heterogeneous diffusion and did not set a separate class for them. The classification of receptors according to the procedure described above was verified for each tracked molecule. Moreover the procedure was found to allow correct classification of other types of diffusing membrane proteins like nAChR or MHC (major histocompatibility complex) proteins.

The heterogeneous behavior of the receptor suggests that it interacts somehow with the cytoskeleton, probably in a reversible manner. Disruption of the cytoskeleton with latrunculin A, an actin-binding toxin, which inhibits actin polymerization, did not allow measurements. The plasma membranes of such treated cells were not flat anymore and moreover, cells did not tightly bind to the glass coverslips and dissociated under washing.

3.4.3 Mobility of the 5-HT_3R with and without bound ligand

The diffusion of the 5-HT_3R was then investigated in living HEK-293 cells depending on its state of activation. We used Atto 647-NTA-Ni with or without incubation with serotonin to determine the mobility of the receptor in its desensitized and in its basal state, respectively. We then compared and related the results with the mobility of the receptor revealed with the fluorescent antagonist GR-Cy5, which most probably stabilized the receptor in the basal state. GR-Cy5 site-specifically binds to the binding pocket of the 5-HT_3R in a quasi irreversible manner; only one GR-Cy5 binds per receptor [145].

Mobility of receptors obtained from GR-Cy5 and Atto 647-NTA-Ni in the presence and in the absence of serotonin were first compared via the distributions of the microscopic diffusion constants of the individual receptors. A comparison of the medians of the histograms (figure 3.8) revealed that the distribution of the microscopic diffusion coefficients of the receptors incubated with serotonin (median $= 0.0022\ \mu m^2/s$) was significantly different from the ones labelled with GR-Cy5 (median $= 0.0041\ \mu m^2/s$) or with the NTA-probe in the absence of serotonin (median $= 0.0038\ \mu m^2/s$) with 99.9% confidence (Mann-Whitney U-test, $P < 0.001$). In contrast, the populations of receptors measured via GR-Cy5 and Atto 647-NTA-Ni without incubation with serotonin were undistinguishable (Mann-Whitney U-test, $P \approx 0.4$). This analysis therefore shows that the receptor in its desensitized state was less mobile or that its mobility was slowed down compared to the basal state.

The difference of mobility of the receptor depending on the functional state was even clearer when considering the mobile and immobile fractions classified as mentioned above (figure 3.9, table 3.2). The desensitized receptor was significantly less mobile with 99% confidence compared to both receptors labelled with GR-Cy5 and or with the NTA-probe without serotonin. In contrast, no distinction could be made between the mobility of receptors reported by GR-Cy5 and Atto 647-NTA-Ni (χ^2 test, $P > 0.9$). This similarity is a strong indication that both the NTA-probes and the GR-Cy5 report on receptors in the basal or non-activated state.

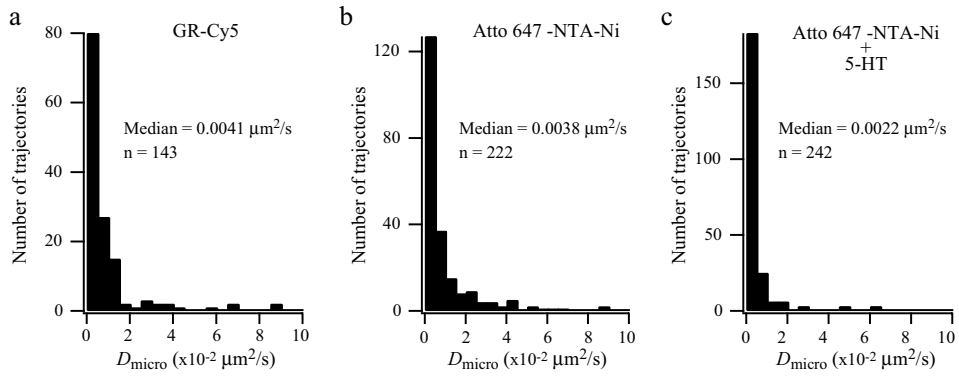

Figure 3.8: Lateral mobility of 5-HT$_3$R in live cells depends on the functional state of the receptor. *Histograms of microscopic diffusion constant of receptors labelled with the fluorescent antagonist GR-Cy5 (a), Atto 647-NTA-Ni without 5-HT (b) and Atto 647-NTA-Ni with 5-HT (c). Median values and number of reconstituted traces are indicated. Bin size corresponds to 0.005 μm^2/s. The histogram in the presence of serotonin is significantly different from the two other conditions demonstrating that the diffusion of the receptor diminished with 99.9% confidence (Mann-Whitney U-test, $P < 0.001$).*

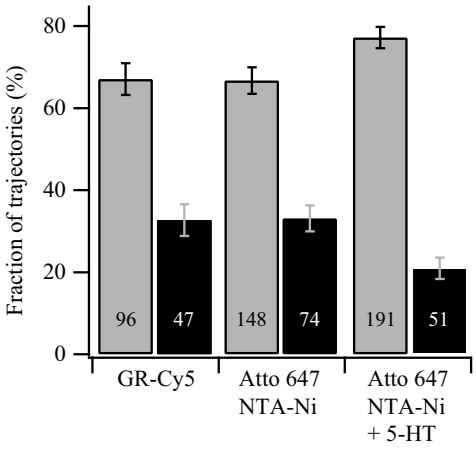

Figure 3.9: Fraction of immobile and mobile 5-HT$_3$ receptors. *The fractions of immobile (grey) and mobile (black) receptors as revealed by the antagonist GR-Cy5 and by Atto 647-NTA-Ni in absence of the serotonin were identical (χ^2 test, $P > 0.9$). The presence of serotonin significantly decreased the mobile fraction from 33% to 21% (χ^2 test, $P < 0.01$). The number of traces constituting the fractions are indicated in the bars and percentage values reported are indicated in table 3.2.*

While serotonin modulates the fraction of mobile and immobile receptors, it does not change the diffusion rate of the mobile receptors as judged from the calculated *MSD*s by combining all the mobile trajectories versus t_{lag} (figure 3.10 and table 3.2). The plots show a deviation at large *MSD*s from a straight line characteristic for Brownian diffusion. The origin of this deviation is unclear and might be due to the finite dimension of the membrane region that is flat and where diffusion can be monitored. In addition, the fraction of confined molecules and molecules changing their mode of diffusion, will also lower the observed *MSD* at high t_{lag}. The macroscopic diffusion constant obtained with the model describing a confined movement (equation 3.5) yielded diffusion constants that are identical for the three populations (figure 3.10). The values for D correspond within error to the diffusion constant obtained by fluorescence correlation spectroscopy (FCS) for the receptor labelled with GR-Cy5 in live cells ($D_{\mathrm{FCS}} = 0.027 \pm 0.013\ \mu\mathrm{m}^2/\mathrm{s}$) [183], as well as the lateral mobility of the glycine receptor, an other ligand-gated ion channel, revealed by SMS in the perisynaptic region of neurons [159]. Furthermore from the fits, we obtain the information that the receptors diffuse in confined region of about 1 μm.

We then further investigated whether the respective proportions of free and confined receptors vary depending on the functional receptor state. No significant differences were observed showing that the main influence of the serotonin was to shift a part of the mobile receptors to the immobile or slow moving particles.

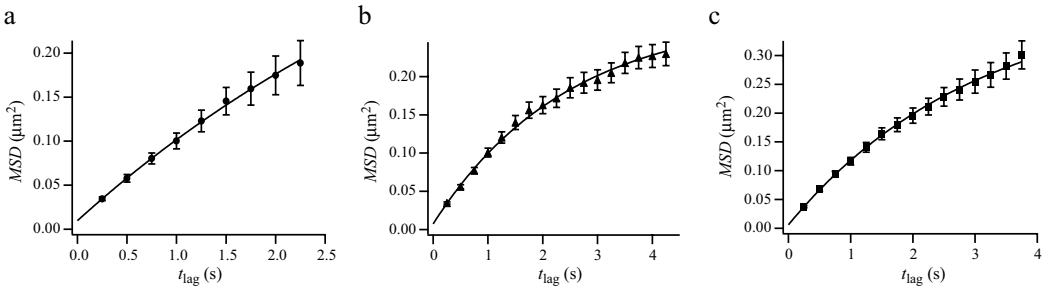

Figure 3.10: Diffusion coefficients of mobile 5-HT$_3$ receptors in living cells. *Mean square displacement (MSD) versus time lag (t_{lag}) of the mobile receptors revealed using (a) GR-Cy5, (b) Atto 647-NTA-Ni without and (c) with serotonin. Fit with equation 3.5 yields (a) D = 0.026 ± 0.012 μm^2/s and L = 1.2 ± 1.3 μm, (b) D = 0.028 ± 0.004 μm^2/s and L = 0.9 ± 0.6 μm, (c) D = 0.033 ± 0.006 μm^2/s and L = 1.1 ± 0.2 μm.*

What could be the reason for the mobility modulation observed upon addition of the agonist? Binding of the agonist might induce conformational changes

of the receptor, which in turn might tighten its interaction with the cytoskeleton or with other receptors or clusters. The fact that we observed an heterogeneous behavior points towards a modulated interaction with other cellular components. The decrease of the fraction of mobile receptors due to receptor internalization [184] appears rather improbable since the overall receptor number remained constant.

It is likely that this modulation of the mobility will have a profound biological importance. The decrease in mobility at certain locations when and where the serotonin is present will result in an increase of the effective concentration of 5-HT_3Rs, which might participate in the development of the synapse. More generally, such modulation of the mobility as shown for other receptors, like glycine, AMPA and NMDA receptors [159,168], to be the core mechanisms during synaptic plasticity as mentioned in the introduction of this chapter.

Table 3.2: Experimental information of the different conditions and their respective immobile and mobile fractions.

	GR-Cy5	**Atto 647-NTA-Ni**	**Atto 647-NTA-Ni + 5-HT**
Number of cells	10	9	9
Number of traces	143	222	242
Immobile fraction (%)	67.1 ± 7.8 (96)	66.7 ± 6.4 (148)	78.9 ± 5.2 (191)
Mobile fraction (%)	32.9 ± 7.8 (47)	33.3 ± 6.4 (74)	21.1 ± 5.2 (51)
D ($\mu m^2/s$)	0.026 ± 0.012	0.028 ± 0.004	0.033 ± 0.006

Number of trajectories constituting the fraction are indicated in brackets.

3.5 Conclusion

The present approach of reversible and repetitive labelling with Atto 647-NTA-Ni has been established here for single particle tracking of membrane receptors. It overcomes several limitations of existing labelling methods by allowing fast (few seconds incubation), reversible, site-specific, successive *in vivo* labelling of proteins by small, non-perturbing molecular probes. Polyhistidine tags are very versatile as small recognition sequence peptide and are already genetically fused to many proteins of interest as the tag is widely used for protein purification. This generic labelling method can be applied at the single particle level to elucidate the organization and lateral diffusion of membrane proteins that control signaling pathways in live cells. This new method allowed us to reveal the heterogeneous diffusion of the 5-HT_3R, which was found to be modulated by the presence of the agonist, leading to the increase immobilization of receptors. We infer that this phenomenon is in-

strumental in synapse development by increasing the local amount of receptor where serotonin is liberated by a neighbor cell. The fluorescent NTA-probes report the lateral mobility of the receptor yielding the same diffusing behavior as the fluorescent antagonist, showing the reliability of the methodology.

Chapter 4

Conformational dynamics of the 5-HT_{3A} receptor

Abstract — Neurotransmitter-gated ion channels, such as the 5-HT_3 serotonin receptor, are important for synaptic transmission between neurons. Using site-specific fluorescent labelling in living cells, agonist-mediated molecular rearrangements within the extracellular domain of the TM2 were investigated. For this to be feasible, single cysteine receptor mutants were engineered from position 13' to 30', each of them characterized for ligand binding, gating and accessibility of the cysteine side chain with thiol reactive fluorophores in living cells. Screening over the functional mutants under different functional states revealed that cysteines localized at position 17', 20' and 24' could be fluorescently labelled with rhodamine and Cy5 as revealed by the staining of the receptors in the cellular membrane. A rhodamine fluorophore tethered to the cysteine residue at the 20' position detected productive binding of agonist. During serotonin application, fluorescence decreased by ∼18%, indicating a change of the environment for the fluorophore. In contrast, mCBPG mediated an increase of fluorescence intensity revealing a potential different activation mechanism. These preliminary results demonstrate the potential of single-cysteine receptor mutants as a tool for probing conformational transition since multiple reporter probes can be site-specifically inserted to all accessible regions within the receptor.

4.1 Introduction

The activation of ion channels that are gated by neurotransmitters is initiated by the interaction of agonist and receptor. The signal generated under ligand binding at the agonist binding-site, which is located in the extracellular N-terminal domain, must be then propagated to the pore at a distant location. Although radioactive ligands and electrophysiological studies have provided valuable information about receptor structure and function, little is known about the structural dynamics underlying receptor activation and antagonism.

The first developed model of Cys-loop ligand-gated ion channel receptor activation is the one proposed by Unwin and coworkers. It is based on the atomic model of the acetylcholine receptor obtained by cryoelectron microscopy, the resolution of which has been extended to 4 Å by computational methods [108]. The model proposes an explanation of how the pore opens when acetylcholine binds to the receptor. The AChR receptor is viewed as build of two rings; an inner ring of five α-helices shaping the pore, which curve radially to create a tapering path for the ions, and an outer ring of fifteen α-helices, which coil around and each other and shield the inner ring from lipids. The gate is depicted as a constricted hydrophobic girdle at the middle of the lipid bilayer, formed by weak interactions between neighboring inner helices. When the acetylcholine enters the ligand-binding domain, it triggers rotations of the protein chains on opposite sides of the entrance to the pore. These rotations are communicated through the inner helices, and open the pore by breaking the girdle apart.

This view is not entirely supported by Taly *et al.* [185]. From normal mode analysis of the homopentameric α7 nAChR, they proposed that the opening of the channel is caused by a concerted symmetrical twist of the protein with opposing rotation of the extracellular and intracellular domains. This model does not involve any dramatic reorganization of the transmembrane domain compared to the original model of Unwin. Nevertheless, the question of how binding of an agonist leads to the channel opening and, which conformational rearrangements are involved remains unresolved because of the absence of high resolution structure of the open and closed channel state. In addition to the transmembrane segment TM2, which contains the receptor gate, also other receptor domains including the transmembrane segment TM4 move as a consequence of conformational changes induced by agonist-mediated receptor activation [186], which contradicts the model proposed by Unwin. Most evidence for this is provided by studies on the nicotinic acetylcholine receptor [187].

There are many experimental techniques to study changes in protein con-

formation during gating, but no global structural change is implicated by these observation. Thus, single-channel electrophysiology detects transition of the channel between open and closed states and allows perturbation analysis using rate-equilibrium free energy relationship [186]. Fluorescence resonance energy transfer provides distances between and sometimes rotations of chromophores. Selective accessibility to covalent modification, such as SCAM [188], disulfide trapping [189] and electrophysiology-coordinated mass spectrometry [190], indicates which side chains are accessible in functionally defined states. Conventional mutagenesis [191] and unnatural amino acid mutagenesis [129] allow to correlate functional measurements with the chemistry of side chains. Backbone mutagenesis can probe interactions, and conformational changes, of the backbone. Combining site-specific fluorescent labelling and simultaneous electrophysiological analysis identified conformational changes associated with the activation of receptors. Fluorescence allows sensitive and time-resolved observation of conformational changes due to the inherent sensitivity of fluorophores toward their local environment, *i.e.* polarity, pH and proximity of quenchers. If the environment of the fluorophore changes upon activation, a change in the intensity of fluorescence might be observed. This approach has been used successfully to identify conformational changes in the voltage sensor of Shaker potassium channels [192, 193] and to identify an intermediate state of the GABA transporter [194, 195].

Distinct structural changes have been revealed within the Cys-loop ligand-gated ion channel family. Fluorescent tags attached to cysteine residues in the region of the binding site of GABA receptor revealed significant fluorescence intensity changes induced by ligand binding and different conformational changes were detected [196]. Similarly, Lester and colleagues studied conformational transition of the muscle nicotinic acetylcholine receptor by tethering a rhodamine fluorophore to a cysteine side chain introduced at the β19' position in the TM2 region of the receptor [197]. During agonist activation, they detected a fluorescence increase interpreted as a movement of the fluorophore to a more hydrophobic environment. The conformational transitions observed were described as not tightly coupled to channel activation, suggesting that sequential rather than fully concerted transitions occur during receptor gating. Agonist-induced dynamic rearrangements within the intracellular side of the 5-HT_{3A} receptor have also been reported [198]. An enhanced green fluorescent protein was inserted into each cytoplasmic TM3-TM4 loop of all five subunits allowing the formation of ionotropic receptor with intrinsic fluorophores in a homopentameric organization and conformational changes induced by prolonged ligand incubation were sensed by homo-FRET for detergent solubilized

receptor proteins.

The model proposed by Unwin emphasizes the role of the TM2-TM3 linker region as a mechanical receiver for binding site conformational changes. Presumably, the force received by this linker region would then pull, push or torque the gate containing the TM2 helix. Functional changes have been observed as a result of the TM2-TM3 linker region mutations in the glycine receptor [199], nicotinic receptors [200], 5-HT_3 receptors [201] and $GABA_A$ receptors [202,203]. Some of these involved surface accessibility during agonist exposure [204]. An elegant study combines charge reversal, charge exchange and cysteine crosslinking approaches [202]. Other observations concern the effects of naturally occurring pathological mutations in the TM2-TM3 linker in the glycine receptor $\alpha 1$ [205] and the nACh receptor $\alpha 1$ subunit [206]. Assuming that TM2-TM3 linker region is the mechanical receiver of the binding event, two loops close to each other in the extracellular binding site (L2 and L7 in the structure of the AChBP [52]) are thought to be the mechanical actuator that engages the TM2-TM3 linker region. According to an experimentally based model, L2 and L7 bracket the TM2-TM3 loop, mechanically actuating both the opening and closing events [202].

Detailed SCAM analysis of TM2 residues exposed to water was performed by Karlin and coworkers [102]. Each residue in the TM2, both in the α- and β- subunits of the muscular nAChR was mutated to cysteine and the mutants were tested for reactivity towards small, charged sulphydryl-specific methanethiosulphonate reagents, such as methanethiosulphonate ethylammonium (MTSEA). Residues reacted with MTSEA over the entire length of the TM2 but with very different kinetics indicating helical nature of TM2 [207, 208]. At many positions in the TM2 segment, reactivity of substituted cysteines were different in the resting, desensitized and open states [207–209], due to accessibility changes, which is correlated to structural changes. Within the TM2 of the α-subunit of nAChR, the 9', 13' and 20' residues were reported to be in different environment in the resting, open and desensitized state [209]. SCAM was also used on the 5-HT_3R to identified the amino-acid residues in the TM2 domain lining the ion conduction pathway [210]. Cysteine was substituted for each residues, one at a time, from position -4' to the 20'.

In this chapter, residues within the upper part of the TM2 domain and the TM2-TM3 linker, corresponding to position 13' to 30', were substituted one at a time in the cysteine-less 5-HT_3R. Before 2003, the TM2 was thought to be up to 22', but since the Unwin's TM2 structure, its goes up to 28' where the channel is wider. Functionality of the mutants expressed in HEK-293 cells was verified and accessibility of the substituted cysteine residues was then determined by examin-

ing the ability of fluorescent MTSEA derivatives to couple to them under different functional states. Three single-cysteine mutants were site-specifically labelled. Conformational transitions at the 5-HT_3R was observed by tethering a rhodamine fluorophore to a substituted cysteine at the 20' position of TM2. Under agonist application, fluorescence changes were observed indicating a change of environment of the fluorophore.

4.2 Experimental techniques

As mentioned in the general introduction (chapter 1), ion channels are integrated in the cell membrane and mediate the ion flux across the membrane. Two experimental techniques applied in this chapter are widely used for their investigation and characterization. The most direct method to investigate ion channel activity is the observation of the electrical current caused by the ion flux through the open pores of channels in the cell plasma membrane, which is performed by whole cell patch-clamp. The indirect method is the observation of the depolarization or hyperpolarization, depending of the channel ion selectivity, of the plasma membrane resulting from the ion flux through the channels. Such variation of the cell membrane potential are reported by fluorescent molecules. While patch-clamp experiments are more sensitive and provide quantitative information of channel functions, fluorescent based assays can be performed faster and can easily be automated.

4.2.1 Whole cell patch-clamp

The patch-clamp technique was originally invented by Sakmann and Neher [211] in 1976 and since then it has been further developed as a standard tool for direct measurements of ion flux through ion channels embedded in cell membranes. In brief, a glass pipette with a micrometer-sized hole containing an Ag/AgCl wire connected to an amplifier headstage serves as measuring electrode, while a ground electrode is inserted into the surrounding electrolyte buffer. Both electrodes are connected to a feedback amplifier that maintains a constant voltage, usually around -60 mV, corresponding to the natural cellular transmembrane potential. Variation in the ion current from one electrode to the other caused by the opening of ion channels, are compensated by the feedback voltage, which is monitored and recorded over time.

In the whole cell patch clamp configuration, the pipette tip is first brought in contact with the cell surface to form first a tight electrical seal by suction (figure 4.1.a left) and then the membrane is perforated by successive suction. The electrode within the pipette is in electrical contact with the cytosol of the cell and therefore

macroscopic current over all ion channels in the cell membrane can be recorded. For more details, see [212].

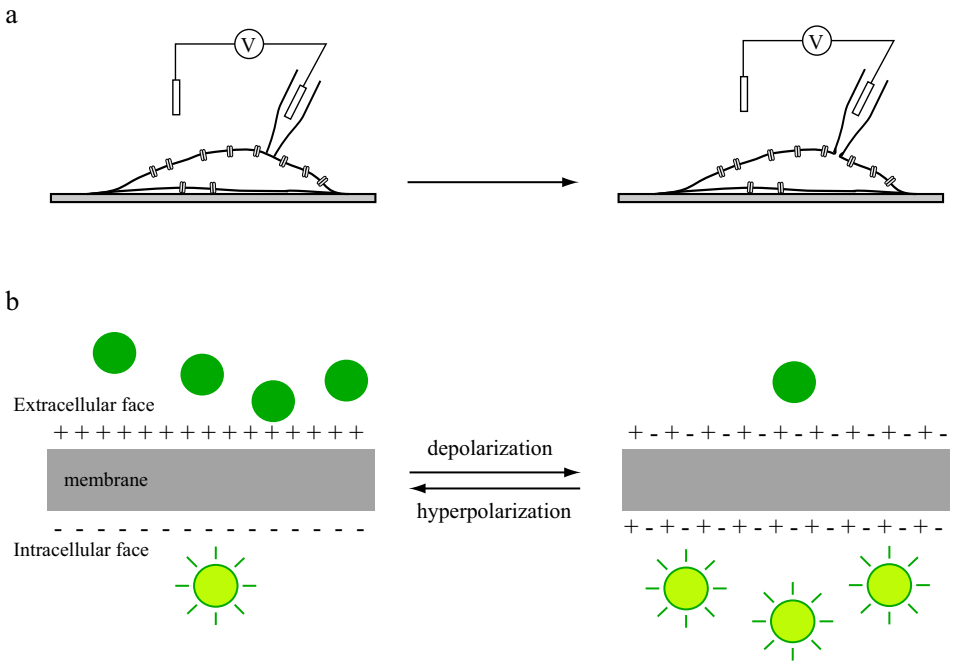

Figure 4.1: Whole cell patch-clamp and fluorescent based membrane potential assay: configuration and principle. *(a) A glass pipette containing an Ag/AgCl electrode is brought into contact with the cell membrane to form a tight electrical seal. The membrane inside the pipette is disrupted to measure the ensemble of ion channels embedded in the plasma membrane in the whole cell patch-clamp configuration. (b) Response mechanisms of membrane potential-sensitive probes. Lipophilic ion fluorescent probes are translocated across the membrane by an electrophoretic mechanism. Fluorescent changes associated with transmembrane redistribution results from the quenching of extracellular probes by membrane impermeable quenchers.*

4.2.2 Fluorescent based membrane potential assay

Potentiometric optical probes were developed in 1970s and were first used to determine the cell membrane potential [213]. These probes enable us to perform membrane potential measurements in organelles and in cells that are in general too small for microelectrodes. Moreover, in conjunction with imaging techniques, these probes can be employed to map variations in membrane potential across excitable cells, with spatial resolution [214].

Several types of probes with different response mechanisms exist. The membrane potential assay used here is based on probes that exhibit potential-dependent

changes in their transmembrane distribution. This relative distribution is accompanied by a fluorescence change that can be recorded in time as the fluorescence of the extracellular probes is quenched by non-permeable cell membrane quenchers.

4.3 Materials and methods

4.3.1 Fluorescent probes

MTS-probes — Cyanine 5 aminoethyl methanethiosulfonate (MTSEA) and sulforhodamine aminoethyl methanethiosulfonate were purchased from TRC (Toronto Research Chemicals, Toronto, Canada). Throughout this chapter, these probes are named as MTS-Cy5 and MTS-Rho respectively. Stock solutions of 2-5 mM MTS-probes in dry DMF were conserved at -80°C. Reactivity of the probes was checked by mixing the MTS probes to 5 equivalent L-cysteine (Fluka, Buchs, Switzerland) in water and incubating 12 hours in the dark. The products were analyzed by HPLC on a C_{18} reversed phase column (4.6 mm diameter, 25 cm length) (Vydac, Hesperia, CA, USA) eluted with 1 ml/min water/acetonitrile (linear gradient of 1%/min acetonitriline) in the presence of 0.1% trifluoroacetic acid. Chromatograms were compared to the corresponding hydrolyzed MTS probes as control. Elution times were of 46 min and 53.5 min for Rho-L-cysteine and hydrolyzed MTS-Rho and 37.2 min and 37.6 min for Cy5-L-cystein and hydrolysed MTS-Cy5 respectively.

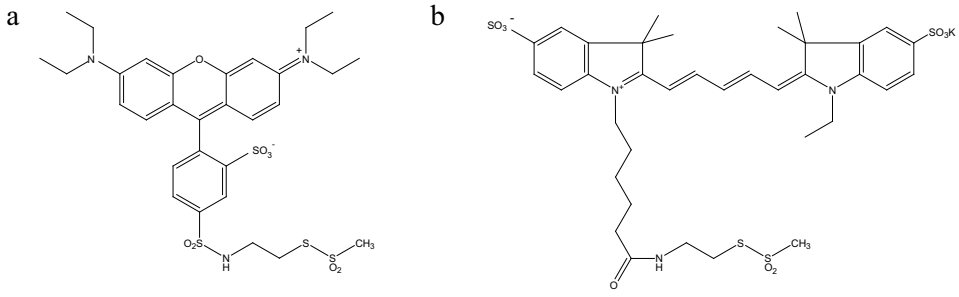

Figure 4.2: Methanethiosulfonate probes. *Chemical structure of (a) MTS-Rho and (b) MTS-Cy5.*

GR-flu — GR-H (1,2,3,9 tetrahydro-3-[(5-methyl-1H-imidazol-4-yl) methyl]-9-(3-amino-propyl)-4H-carbazol-4-one) (Glaxo Wellcome, Geneva, Switzerland) was labelled with fluorescein-5-isothiocynate (Molecular Probes Invitrogen, CA, USA) as

described in [105].

4.3.2 Molecular and cellular biology

5-HT_3R-ΔCys-His_{10} — The sequence of the cysteine-less mutant is based on the short splice variant of the murine 5-HT_3R, corresponding to the SwissProt entry p23979 containing two conflict regions, Glu31→Ala-Arg and Thr302→Thr-Ala (numbering corresponds to the precursor). All the cysteines were substituted with serine resulting in the following mutations, C269S, C315S, C359S, C381S and C394S at the exception of Cys161 and Cys175 because they form the disulphide bridge of the cys-loop (DNA was a kind gift from Nina Dixit). A His_{10} polyhistidine sequence was added at the C-terminus of the protein behind Ser487 by site-directed mutagenesis (QuickChange^{TM} mutagenesis kit, Stratagene, CA, USA) under the conditions required by the provider in the presence of 4% DMSO. Oligonucleotides 5HT3a-Δcys*for* and 5HT3a-Δcys*rev* were used (appendix A.1). The protein coding sequence was inserted in pcDNA3 vector (Invitrogen, CA, USA) between Hind III and Not I restriction sites that are located in front and behind the protein sequence respectively. The nucleotide sequence was verified by restriction analysis and sequencing of the whole coding region. The sequence of the construct is detailed in appendix A.3 and schematized in figure 4.3.a.

Single cysteine 5-HT_3R mutants — The sequences of the single substituted cysteine 5-HT_3R mutants were based on the cysteine-less 5-HT_3R-ΔCys-His_{10} sequence (see above and appendix A.3). TM2 containing coding sequence comprised between EcoR V and BamH I restriction sites (figure 4.3.a) was subcloned into pBluescript II SK (+) (Stratagene) and the resulting plasmid was used as template for all the site-directed mutagenesis (figure 4.3.c). Corresponding amino acids were mutated to cysteine using the QuickChange^{TM} site-directed mutagenesis kit (Stratagene) with the conditions required by the provider in the presence of 4% DMSO for the reaction. All oligonucleotides used are presented in appendix A1 (numbering corresponds to the amino acid mutated to cysteine of the unprocess precurssor of 5-HT_3R-ΔCys-His_{10}). The mutated nucleotide sequence was verified by restriction analysis and sequencing of the whole insert in pBluescript II SK (+) using the T7 primer; the sequencing was performed in one step. The mutated insert was then restricted, purified and ligated into the restricted EcoRV/BamH I pcDNA3 vector yielding 5-HT_3R constructs containing a single cysteine and a His_{10} C-terminal sequence (figure 4.3.d and e). Nucleotide sequences of all the single cysteine constructs were verified and confirmed by restriction analysis and sequencing.

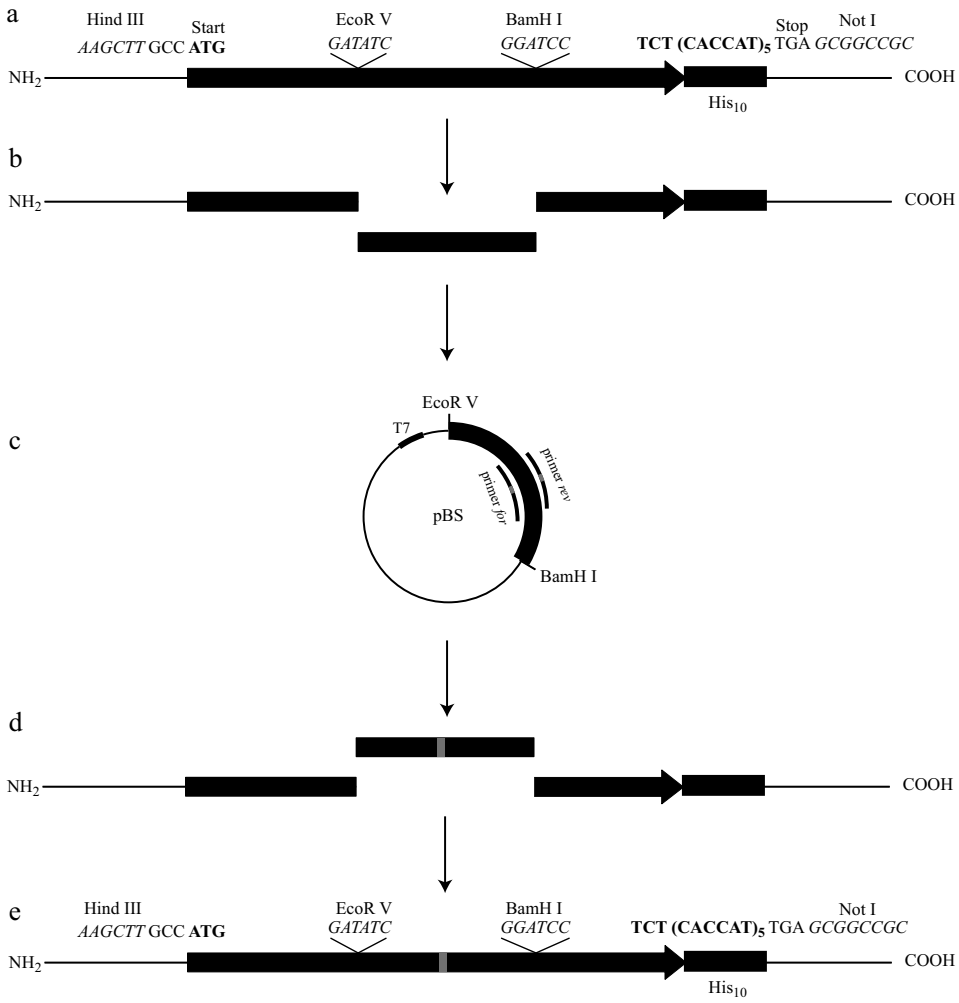

Figure 4.3: Cloning and mutagenesis procedure of the 5-HT$_3$R mutants containing a single cysteine. *(a) Schematic representation of the sequence of the 5-HT$_3$R-ΔCys-His$_{10}$ (between the start and the stop codon) made of the 5-HT$_3$R-ΔCys (black arrow) and comprising a His$_{10}$ at the C-terminal (black box). The constuct was cloned in pcDNA3. The sequence contains four unique restriction sites, Hind III, EcoR V, BamH I and Not I, whose sequence are in italics. For details, see appendix A.3.1. (b) 5-HT$_3$R-ΔCys-His$_{10}$ is restricted with EcoR V and BamH I and the fragment is ligated (c) into pBluescript II SK (+), which serves as template for the mutagenesis. Site-directed mutagenesis using the corresponding designed primers yielded mutated fragments of the receptor that were isolated with EcoR V and Hind III, purified and ligated in the EcoRV/BamH I cut pcDNA3 construct.*

Cell culturing and transfection — HEK-293 cells were cultured with a density of 150'000 cells/ml on 0.18 mm thick glass coverslips in 6-well plates (2 ml/well, for cell imaging), or 35 mm cell culture dishes (2 ml/dish, for eletrophysiology experiments), in Greiner 96-wells plates black clear bottom (0.2 ml/well, for membrane potential assays) or in 8-well chambered coverglass (0.4 ml/well, for cell imaging) in Dulbecco's modified Eagle medium (DMEM) supplemented with 2.2% of fetal calf serum under humidified 5% CO_2 atmosphere at 37°C. Cells were transfected 14 to 18 hours after splitting using Effectene^{TM} (Qiagen, Hilden, Germany) according to the supplied protocol with 0.2 μg DNA, 1.6 μl enhancer, 2 μl effectene and 100 μl EC buffer for 2 ml culture medium. DNA was either 100% receptor plasmid DNA or 80% receptor and 20% EGFP plasmid DNA (Clontech, Palo Alto, CA, USA). Cell DMEM medium was replaced by DMEM supplemented with 10% fetal calf serum, 6 to 12 hours after transfection for the labelling of the receptor with the MTS probes.

4.3.3 Experimental methods

Electrophysiology — Standard whole-cell patch-clamp experiments were performed on an inverted fluorescent microscope (Axiovert100, Zeiss, Jena, Germany) with an EPC-9 patch-clamp amplifier (HEKA Elektronik Dr. Schulze GmbH, Lambrecht, Germany). Acquisition and storage of data used the A/D converter of the EPC-9 and the PULSE 8.3 (HEKA) software. Borosilicate glass tubes GB150TF-8P 1.05 x 1.50 x 80 mm^3 (Science Products GmbH, Hofheim, Germany) were pulled with a pipette puller (P87, Sutter Instrument Comp, Novato, CA, USA) yielding pipettes of 5-10 MΩ resistance. Glass pipettes were filled with 140 mM NaCl, 10 mM EGTA, 10 mM HEPES, pH 7.4 buffer and the ground electrode was connected to the bath via a 1 M KCl agar bridge. 36-48 hours after transfection, DMEM culture medium was removed from HEK-293 cells expressing the receptor (in 35 mm cell culture dishes) and replaced by 2 ml buffer 2 mM $CaCl_2$, 147 mM NaCl, 12 mM glucose, 10 mM HEPES, 2 mM KCl, 1 mM $MgCl_2$, pH 7.4. The experiments were performed at room temperature with membrane potential kept at -60 mV. Serotonin (Fluka, Buchs, Switzerland) solutions and buffer were applied with a fast step RSC-200 perfusion system (Bio-Logic Science Instruments, Claix, France). For patching, cells were selected using the cotransfected EGFP fluorescent marker. All perfused solutions were made with the buffer used in the bath.

Membrane potential assays and imaging — Membrane potential fluorescent-based assay was performed using the FLIPR® membrane potential assay kit (Molecular Devices Corporation, Sunnyvale, CA, USA). Red loading buffer was dissolved

in 10 ml ready to use buffer component B according to the supplied protocol. HEK-293 cells expressing the receptor (in black clear bottom 96 well-plate, Greiner) were loaded with 50 μl/well loading buffer added to the 200 μl/well DMEM culture medium for 30-40 minutes at 37°C, 48 hours after transfection. Experiments were performed using a Flex Station (Molecular Devices Corporation) with 530 nm excitation and 565 nm emission wavelength with a 550 nm cut-off. Per well, 70 μl serotonin solutions in Dulbecco's phosphate-buffered saline (D-PBS: 0.901 mM $CaCl_2$, 0.493 mM $MgCl_2$, 2.67 mM KCl, 1.47 mM KH_2PO_4, 137.93 mM NaCl and 8.06 mM Na_2HPO_4) (Gibco Invitrogen, CA, USA) was added 20 seconds after the beginning of the recording with a relative velocity of 2. Recording was performed over 150 seconds with 1.5 seconds interval.

Membrane potential imaging was performed with a LSM 510 confocal microscope (Zeiss) equipped with appropriate excitation and emission filters. Coverslips were transferred to a sample holder and the cells covered with 200 μl D-PBS and 100 μl loading buffer. After 30-40 minutes incubation, fluorescent image sequences were then recorded and ligands serotonin was added by hand to a final concentration of 50 μM.

Protein labelling — HEK-293 cells expressing a single cysteine mutant of the 5-HT_3R in 8-well chambered coverglass or on glass coverslips in 6-well plates with 10% fetal calf serum supplemented DMEM medium were washed with standard PBS 48 hours after transfection. Cells were labelled with 5 μM MTS-probes in presence or absence of 100 μM serotonin in standard PBS for 45-60 seconds. Cells were then washed twice with D-PBS (Gibco Invitrogen, CA, USA) and then incubated for 20 minutes with 15-20 nM either GR-flu or GR-Cy5 in D-PBS before imaging.

Cell imaging — Cell imaging was performed using different set-ups: a LSM 510 confocal microscope (Zeiss) as described previously or a wide field fluorescence imaging microscope. Fluorescence changes were performed using either the set-up presented in chapter 3 (figure 3.2) or a wide-field imaging system described in the following. An inverted microscope (Axiovert 200M, Zeiss) was equipped with a wide-field 40x 1.3NA PlanNeoFluar oil immersion objective (Zeiss), a XBO 75 fluorescent lamp (Zeiss) whose light was directed to the sample by adequate filters and dichroic mirrors (Chroma, Rockingham, VT, USA)(table 4.1). Detection was performed by a sensitive iXon DV887 FI camera (Andor, Belfast, UK). To minimize fluorescence bleaching of the sample, a shutter was used with tunable illumination frequency and illumination times.

Table 4.1: Filter and dichroic mirrors used for wide field cell imaging.

Dye	Excitation filter (nm)	[1]Dichroic mirror	[1]Emission filter
GFP	S484/15	106361	54461
Cy5	S647/26	106361	54461
Rho	S555/25	106361	54461

[1] Filters and dichroic mirrors were from Chroma (Rockingham, VT, USA).

4.3.4 Data treatment

Dose response curves and EC_{50} values — Fluorescence dose response curves were recorded using membrane potential sensitive fluorescence dyes. The curves were analyzed using the software SOFTmax Pro 4.3 (Molecular Devices). The local maximal slopes S obtained within the 20 seconds after addition of the agonist were plotted versus the concentration of agonist c. The resulting dose response curve was fitted with the Hill equation (equation 4.1) where S and $S_{\max}$ are the slope and the maximal slope, respectively, EC_{50} the molar concentration of agonist, which produces 50% of the maximal response for that agonist and h the Hill coefficient. Current intensities obtained from whole-cell patch-clamp were reported versus the concentration of the agonist to be fitted with the Hill equation 4.2. I and $I_{\max}$ corresponds to the current and maximal current respectively. EC_{50} obtained form equations 4.1 and 4.2 are not identical (see section 4.4.2). All errors were calculated according to Gauss propagation method and corresponds to 95% confidence interval.

$$\frac{S}{S_{\max}} = \frac{1}{1 + \left(\frac{EC_{50}}{c}\right)^h} \tag{4.1}$$

$$\frac{I}{I_{\max}} = \frac{1}{1 + \left(\frac{EC_{50}}{c}\right)^h} \tag{4.2}$$

4.4 Results and discussion

4.4.1 Cloning and site-directed mutagenesis

Mutation of particular amino-acids to cysteine within the sequence of the 5-HT$_{3A}$ receptor was performed by site-directed mutagenesis according to the principle of cassettes. The receptor coding sequence cloned into the pcDNA3 mammalian plasmid vector has four distinctive restrictions sites, one to each end of the gene and two within the gene, yielding three fragments of similar size. Each fragment can be subcloned into an appropriated cloning vector for mutagenesis. The advantage of

this strategy is that the probability of introducing undesirable mutations is strongly reduced due to the small size of the insert and that the mutated fragment can be sequenced within one step, which is a substantial gain of time. Moreover, this cloning approach allows to mix different mutated fragments yielding rapidly many different mutants of the receptor.

4.4.2 Functionality and characterization of 5-HT_{3A} mutants

Functionality of all the different 5-HT_3 receptor mutants was investigated by fluorescent ligand binding experiments, and whole cell patch-clamp measurements and membrane potential assays in order to test which receptors would be candidates for MTS-labelling. HEK-293 cells expressing the 5-HT_3R mutants were selectively stained with GR-flu to localize, using fluorescence confocal microscopy, the receptor within the cellular membrane and estimate their expression level (figure 4.5.a). In order to image clearly a GR-flu stained cellular membrane, 100'000 receptors per cell were required. All the single cysteine mutants expressed in HEK-293 cells bound the fluorescent antagonist as revealed by cell imaging, at the exception of the receptor containing the V292C mutation (table 4.2). While the expression level was high enough to be detected, transfection efficiency (1-10%) was very low for nearly all the mutants. Nevertheless, binding of GR-flu to the receptors does not give information about the gating of the channel but rather demonstrated the presence of the 5-HT_3R embedded in the cellular membrane and the ability to bind ligands.

Activation of the 5-HT_3R mutants by its agonist serotonin was investigated by measuring variations of the cell membrane potential using a fluorescent-based assay and by recording the current going through the gated channel using whole cell patch-clamp measurements. Membrane potential responses were performed by fluorescence confocal imaging of HEK-293 cells transiently expressing the different mutant receptors (figure 4.5.b). It allowed a direct visualization of the fluorescence response of single cells with high sensitivity compared to fluorescence imaging plate readers where the response was recorded over an ensemble of cells. However, fluorescence imaging is not suited for quantitative evaluation of the response and effective concentration of serotonin (EC_{50}) were determined with the Flex Station plate reader. Maximal slope fluorescence responses after addition of serotonin (figure 4.5.c) were plotted versus the concentration of the agonist and fitted with a Hill equation (equation 4.1, figure 4.5.d) yielding EC_{50} values and Hill coefficients. EC_{50} values are reported for mutants whose expression level and transfection efficiency were high enough to detect a fluorescence response (table 4.2); Hill coefficients are

Table 4.2: Functional characterization of 5-HT$_{3A}$R mutants.

	Receptor	GR-flu binding	Membrane potential	Patch-clamp	
			EC_{50} (μM)	EC_{50} (μM)	h
	[1]5-HT$_{3A}$-C-His$_{10}$	Yes	0.24 ± 0.07	2.2 ± 0.2	2.0 ± 0.4
	5-HT$_{3A}$ΔCys	Yes	Yes	1.2 ± 0.4	1.5 ± 0.6
13'	V291C	Yes	0.04 ± 0.50	Yes	
14'	F292C	No	No	No	
15'	L293C	Yes	0.05 ± 0.16	Yes	
16'	I294C	Yes	0.02 ± 0.20	Yes	
17'	**I295C**	Yes	0.19 ± 0.44	Yes	
18'	V296C	Yes	0.05 ± 2	Yes	
19'	S297C	Yes	No	Yes	
20'	**D298C**	Yes	Yes	3.7 ± 0.7	1.2 ± 0.3
21'	T299C	Yes	Yes	Yes	
22'	L300C	Yes	No	Yes	
23'	P301C	Yes	No	Yes	
24'	**A302C**	Yes	0.1 ± 9	Yes	
25'	T303C	Yes	0.42 ± 0.07	Yes	
26'	A304C	Yes	No	No	
27'	I305C	Yes	No	Yes	
28'	G306C	Yes	0.50 ± 0.16	4.4 ± 0.8	1.6 ± 0.2
29'	T307C	Yes	Yes	Yes	
30'	P308C	Yes	0.24 ± 40	Yes	

[1]wt5-HT$_{3A}$ receptor containing a His$_{10}$ sequence at the C-terminus, see section 3.3.2.

Receptors indicated in bold were labelled with MTS-Rho and MTS-Cy5, see section 4.4.3.

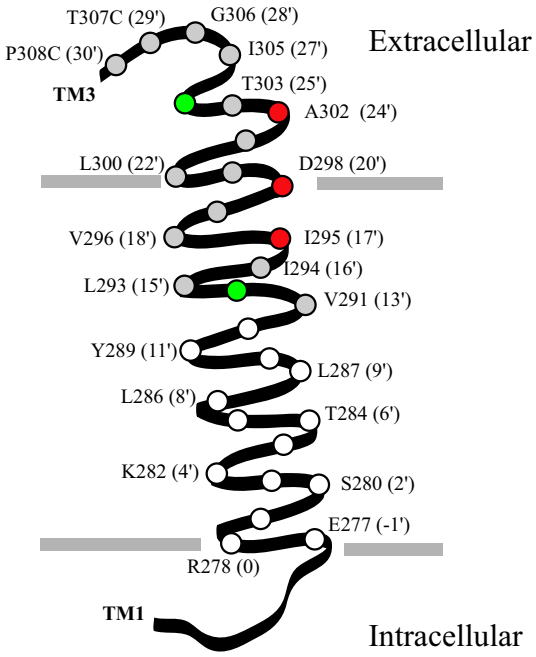

Figure 4.4: TM2 helix of the 5-HT$_{3A}$ receptor. *Schematic representation of the TM2 segment in α-helix conformation. The channel lumen is to the right of the helix; TM1 and TM3 (not shown) are to the left. Relative position of amino acids (◯) is based on SCAM data reported in [102, 210] and the structure from Unwin [108]. The grey lines indicate the boundary of the plasma membrane. The substituted cysteine residues are indicated in grey and the lethal mutations in green. Fluorescently labelled substituted cysteine side chains are in red.*

not indicated because they are no significance. Membrane potential fluorescence assays allowed a fast screening of receptor mutants functionality but required a transfection efficiency of at least 30%; Complete dose response curves were obtained for only nine of the receptor mutants.

Screening receptor activity by whole cell patch-clamp screening is more relevant than by membrane potential assays. Only cells expressing the receptors, as revealed by the coexpression with the fluorescent protein EGFP, were patched and current responses at 100 μM serotonin were recorded. Under these conditions, whole cell currents were obtained for all the receptor mutants with the exception of those containing a substituted cysteine at position F292C and A304C (table 4.2). For some, dose response curves were performed and fitted with a Hill equation (equation 4.2) yielding EC_{50} values and Hill coefficients (table 4.2).

Dose response curves obtained by membrane potential assays and electrophysiology were not identical; EC_{50} values obtained from membrane potential assays were shifted to smaller values (figure 4.5.d). This difference comes from the fact that the physical parameter observed upon the opening of the channel are fundamentally different. In whole cell patch-clamp experiments, EC_{50} values correspond to the concentration of agonist required to open 50% of the channels in a receptor population within the cellular membrane, whereas EC_{50} values from membrane potential assays represent the concentration of agonist depolarizing the cellular membrane half of its maximal value. Since maximal depolarization of the membrane requires less open channels and therefore less amount of agonist, compared to maximal whole cell current, EC_{50} values are different by about one order of magnitude (table 4.2). Membrane potential assays are physiologically and pharmacologically more relevant since they report the depolarization of the membrane, which is indeed the signalling principle of ion channels within neurons and nerves for instance.

The characterization of the different receptor mutants is by far not complete but is sufficient to determine those receptors which are functional. The cysteine-less receptor mutant as well as single cysteine receptor mutants ranging from V291C to P308C are activated by serotonin at the exception of the F292C and A304C mutants. Mutation F292C has already been reported to be lethal [210].

4.4.3 Fluorescence labelling of 5-HT_{3A} receptor

The accessibility of the different cysteine residues inserted within the TM2 helix and TM2-TM3 loop of the cysteine-less 5-HT_3 receptor was investigated in living cells. HEK-293 cells expressing the functional receptor mutants (table 4.6) were exposed

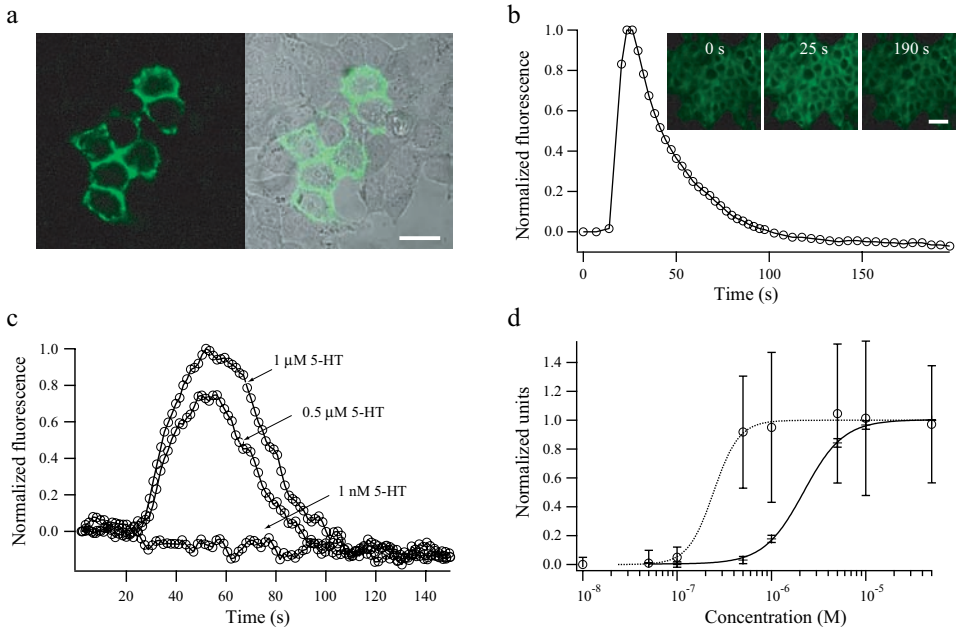

Figure 4.5: Functional characterization of 5-HT$_3$R mutants in living cells. *(a) HEK-293 cells transiently expressing 5-HT$_3$R were incubated for 15 min with 15 nM GR-flu, resulting in a selective staining of 5-HT$_3$R in the cellular membrane as revealed by the fluorescence confocal microscopy (scale bar is 15 µm). (b) Fluorescence intensity changes of membrane-potential sensitive probes after addition of 50 µM serotonin as observed by fluorescence confocal microscopy. Insert: 5-HT$_3$R expressing HEK-293 cells loaded with membrane potential sensitive fluorescent probes at the indicated time points of the response. (c) Fluorescence intensity changes of membrane potential sensitive probes in HEK-293 cells expressing the 5-HT$_3$-C-His$_{10}$ as observed in the Flex Station. Addition of serotonin at t = 22 s resulted in a transient increase of fluorescence intensity response. (d) 5-HT$_3$-C-His$_{10}$ normalized dose response curve obtained from membrane potential assays (∘) and whole cell patch-clamp measurements (+). Fits using the Hill equation (Eq. 4.1 and Eq 4.2) yielded EC$_{50}$ = 0.24 ±0.07 µM and 2.2 ± 0.2 µM, and h = 3.2 ± 1.6 and 2.0 ± 0.4, respectively.*

to thiol-reactive fluorophores, MTS-Rho and MTS-Cy5, in the presence or absence of serotonin. Accessible cysteine residues within the different functional states of the receptors were labelled resulting in a selective staining of the receptors in the cellular membrane (figure 4.6.a). Specificity of the labelling was confirmed by the colocalization with GR-flu, a highly specific fluorescent antagonist of the 5-HT$_3$R (figure 4.6.b). No labelling was observed on non-transfected cells (figure 4.6.c), as well as cells expressing the 5-HT$_{3A}\Delta$Cys receptor. An important factor for the labelling was the composition of cell culture medium. Strong specific labelling was observed with DMEM medium supplemented with 10% fetal calf serum, whereas with 2.2% fetal calf serum hardly any fluorescence was observed.

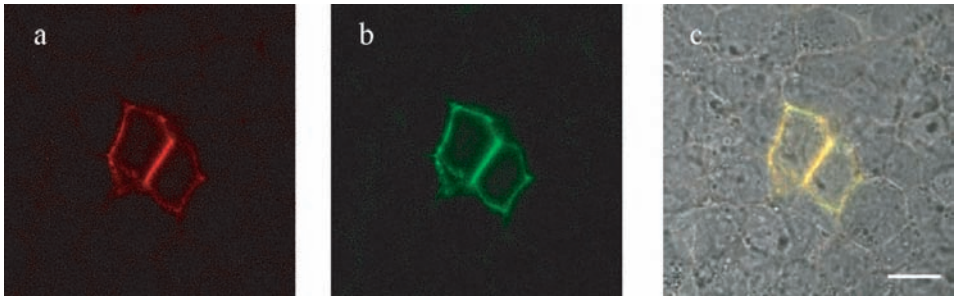

Figure 4.6: ***Labelling of a single cysteine mutant of the 5-HT$_3$R with fluorescent MTS in live cells.*** *Confocal images of HEK-293 cells transiently expressing the 5-HT$_3$R-D298C mutant. Cells were exposed to 5 μM MTS-Rho and 100 μM serotonin for 45 s, then washed and incubated 15 min with 15 nM GR-flu. Staining of the membrane was observed for both (a) MTS-Rho and (b) GR-flu. (c) Superposition of (a) and (b) showed the perfect colocalization of the GR-flu and MTS-Rho labelling. Transfected cells showed a 10-15 fold higher fluorescence than untransfected cells.*

Screening all the functional single cysteine 5-HT$_3$R mutants revealed that only three could be site-specifically labelled: The 5-HT$_3$R-I295C, D298C and A302C with their accessible cysteines at the 17', 20' and 24' position, respectively (figures 4.6 and 4.7). The labelling efficiency of these receptors was different and decreased in the order 5-HT$_3$R-D298C > A302C > I295C, as revealed by the comparison between GR-flu and MTS-probes fluorescent intensities (figure 4.7). However, no significant changes of the labelling efficiencies were observed when the reaction was performed in the resting (labelling without serotonin or after preincubation with a fluorescent antagonist) or desensitized state (labelling in the presence of serotonin), at the exception of the 5-HT$_3$R-D298C, where the presence of serotonin slightly increased the labelling efficiency, indicating a structural change within the upper region of TM2. No kinetic experiments were performed and reaction efficiencies were based

on observations at a single time point.

Blocking of endogenous surface sulfhydryl groups with small methanethiosulfonate to site-specifically label substituted cysteines with fluorescent MTS-probes as performed on the nAChR [197] would not have been possible or specific on the 5-HT_3R since their accessibility was not influenced by the state of the receptor, requiring therefore the cysteine-less receptor.

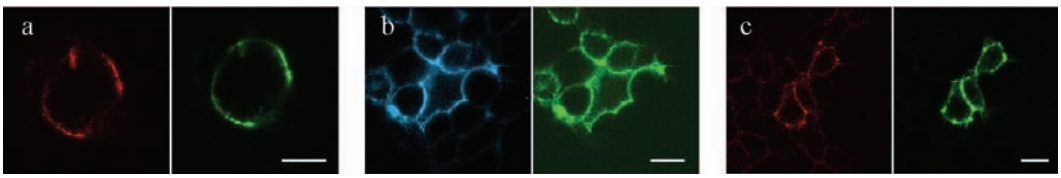

Figure 4.7: Labelling of a single cysteine mutants of the 5-HT_3R with fluorescent MTS probes in living cells. *Confocal images of HEK-293 cells transiently expressing the (a) 5-HT_3-I295C, (b) 5-HT_3R-D298C and (c) 5-HT_3R-A302C mutants. Cells were exposed to 5 μM MTS-Rho (red) or MTS-Cy5 (blue) and 100 μM serotonin for 45 s, then washed and incubated 15 min with 15 nM GR-flu (green) resulting in a colocalized staining of the receptors in the cellular membrane. Scale bars are 20 μm.*

The accessibility of the cysteine residues of the 5-HT_3R at positions 17' and 20' by fluorescent MTS probes shown here is consistent with SCAM data obtained using small methanethiosulfonate reagents like MTSEA, MTSET and MTSES on the TM2 segment of the 5-HT_3R [210,215] and α subunit of the muscle type nAChR [209]; no SCAM data have been reported for the 24' position. Here, labelling was restricted to the residues positioned towards the channel in the upper part of the TM2 whereas small MTS can probe down to 2' in the closed state and -5' in the open state. The accessibility of the fluorescent MTS probes was limited by their dimension and length of the linker. A longer linker would certainly have allowed to probe residues deeper in the channel.

The number of bound MTS-fluorophores per receptor was not investigated. Since the 5-HT_3R is homopentameric, single cysteine receptor mutants involved five cysteine residues and each of them can react, thus yielding up to five bound fluorophores per receptor. According the low resolution structure of the nAChR (figure 1.5), two relative positions can be assumed for these probes. First, the fluorophore moiety of the probes points inside the pore of the receptor directly into the extracellular funnel. Secondly, the fluorophore is inserted between the subunits just above the membrane or between the transmembrane helices pointing therefore outwards. The former position will allow the presence of only one fluorescent mole-

cule for sterical reasons whereas the latter will allow up to five MTS-fluorophores to react and bind to the substituted cysteines.

4.4.4 Conformational changes of 5-HT$_{3A}$ receptor

Rhodamine covalently bound to the extracellular end of the TM2 of the 5-HT$_3$ receptor was used as a fluorescent reporter of conformational changes occuring during receptor activation and desensitization. The 5-HT$_3$R-D298C mutant expressed in HEK-293 cells was labelled with MTS-Rho as described in section 4.4.3. This single-cysteine receptor mutant was selected over the other potential candidates due to the high accessibility and reactivity of the substituted cysteine at position 20'. Addition of serotonin resulted in a ∼18% decrease of fluorescence intensity (figure 4.8), indicating a change of the fluorophore's environment due to conformational changes upon receptor activation. The decrease of fluorescence induced by the binding of serotonin as well as its recovery seems to be biphasic as already reported by similar measurements on the nAChR [197]. No fluorescence dose response was measured. On control cells devoid of 5-HT$_3$ receptor, a 2-4% decrease of the fluorescence intensity was observed as result of serotonin application.

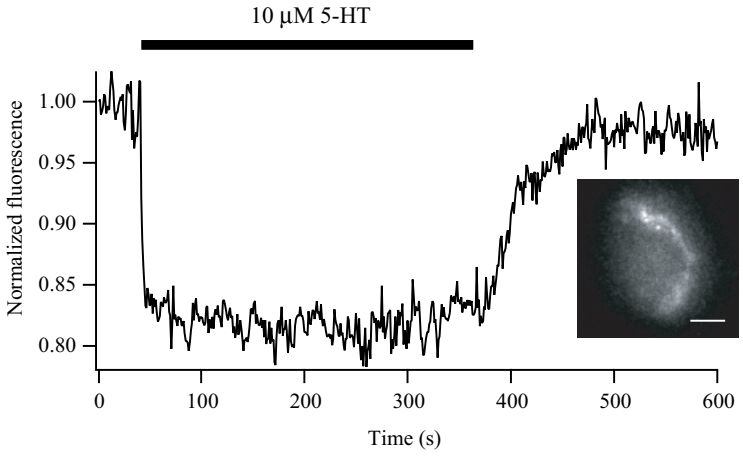

Figure 4.8: Conformational changes in 5-HT$_3$R induced by the binding of serotonin and observed by fluorescent probes. *Normalized fluorescence intensity of rhodamine bound to the 20' cysteine residue of the 5-HT$_3$R-D298C is depicted versus time. Application of the agonist serotonin to HEK-293 cells expressing the receptor resulted in a fluorescence intensity decrease of ∼18%, which was reversed upon washing. Insert: Fluorescence image of a HEK-293 cell expressing the 5-HT$_3$R-D298C labelled with MTS-Rho. Scale bar is 5 µm.*

Application of 10 μM mCPBG, another agonist of the 5-HT$_3$R, to the rhodamine labelled receptor induced an increase of ∼5% fluorescence intensity (data

not shown). After washing, fluorescence intensity reached again its initial value. No intensity changes were observed on control cells. Fluorescence intensity increase reported conformational changes within the surrounding region of the extracellular end of TM2. However, activation mechanism of the channel by mCPBG was different compared to serotonin since the fluorescence intensity changes were opposite. These phenomena were observed on different cells and on different days with high reproducibility. Nevertheless, these results are preliminary but might present interesting insights within the activation mechanism and conformational changes initiated by the interaction of agonist and receptor.

4.5 Conclusion

The cysteine-less receptor mutant of the 5-HT_3R has been revealed to be fully functional in terms of gating and ligand binding. It allowed therefore to substitute cysteine within its sequence whose accessibility can be then probe by multiple thiol-reactive compounds in order to yield structural features, opening therefore the door to decipher the gating mechanism. Cysteine residues within the outer half TM2 have been stained selectively with fluorescent thiol-reactive compounds. Preliminary results indicate that the fluorescence intensity is modulated by the interaction of the agonist with the binding site of the receptor, and that these changes depend on the nature of the agonist suggesting a potentially different gating mechanism. Simultaneous measurements of electrical current and fluorescence intensity would give insights to the dynamics of gating as well as comparison between fluorescent and current dose-response. In conjunction with structural studies, such knowledge will enhance our understanding of the structural transitions occurring during allosterically controlled channel gating.

Chapter 5

Effect of ligand binding on single 5-HT_{3A} receptor ion current

Abstract — Current through single 5-HT_{3A} mutant receptor-gated ion channels was recorded. Replacement of three arginine residues in the cytoplasmic loop of the cysteine-less 5-HT_3 receptor increased its conductance 70-fold compared to the wild-type receptor. Five conductance levels were determined ranging from 11 to 52 pS and their probability of occurrence was modulated by the amount of serotonin. These different current amplitudes were assumed to represent distinctive molecular entities probably modulated by the phosphorylation of the subunits. Amplitudes of open-channel ionic currents were increased in the presence of serotonin, which might result from structural fluctuations within the receptor. Noise analysis of current fluctuations revealed a $1/f^{\alpha}$ dependence with $\alpha < 1$. Moreover, this protein dynamics was related to a fractional Gaussian noise. A model based on continuous current changes proposed that charged amino-acids play a role in the structural fluctuations. This high conductive 5-HT_3 receptor mutant will be a building block for the investigation of the dynamics of the receptor in combination with fluorescently labelled single-cysteine receptors.

5.1 Introduction

Single-channel patch-clamp is a well suited and a widely used technique for the investigation and characterization of ion channels. It resolves in time ion flux through single channel yielding information on the kinetics and thermodynamics of channel gating. Nevertheless, only few experimental data of single-channel electrophysiology were reported on the 5-HT$_3$ receptor mainly due to its low conductance compared to other members of the ligand-gated ion channel family.

The first recording of current through single heteromeric 5-HT$_3$ receptors was reported in the late eighties by Derkach and colleagues [216]. They observed unitary currents of 15 pS and 9 pS in excised membrane patches from neurons of the guinea pig; the probability of occurrence of the high conductance channel decreased in time. Later, in N1E-115 neuroblastoma cells, discrete 5-HT$_3$ receptor-gated channels with a conductance of 6 pS were resolved in excised membrane patches when the driving force for Na^+ was enhanced [217]. Using the same cells but in cell-attached patches, distinctive conductive levels of 27, 18, 11 and 6 pS were observed [218]. Inhibition of protein kinase activity or patch excision increased the probability of occurrence of the 6 pS level and decrease that of the 27 pS level. Conversely, patch cramming and stimulation of protein kinase activity enhanced the probability of occurrence of the 27 pS level and decreased that of low conductance levels. These findings indicated for the first time that phosphorylation controls the conductance of the 5-HT$_3$ receptor. Other experiments reported the potential role of phosphorylation on the current mediated by the 5-HT$_3$ receptor. Substance P, an agonist of the NK1 tachykinin receptor has been reported to potentiate the 5-HT$_3$ receptor-mediated current in ganglion neurons through the activation of the protein kinase C [219].

Although single-channel currents of native 5-HT$_3$ receptors have been resolved since more than fifteen years, current through single cloned homopentameric 5-HT$_{3A}$ receptors have been reported only few years ago [220]. The low conductance value of the 5-HT$_{3A}$ receptor of less than 1 pS did not allow single-channel recording; instead fluctuation analysis on macroscopic currents was used [221]. However, in Ca^{2+}- and Mg^{2+}- free solutions, single channel current events were resolved yielding a unique conductance of 48 pS. These divalent cations were reported to decrease the channel conductance [94, 222]

The single-channel conductance of the 5-HT$_3$ receptor assembled as homomers of 5-HT$_{3A}$ subunits, or heteromers of 5-HT$_{3A}$ and 5-HT$_{3B}$ subunits, are markedly different, being <1 pS and 16 pS [75], respectively. Where does this difference come from? Paradoxically, the channel-lining of TM2 domain of the 5-HT$_{3A}$ subunit would

be predicted to promote cation conductance, whereas that of the 5-HT_{3B} would not [75]. A large cytosolic loop was reported to be responsible for the observed single-channel conductance values [223]. Replacement of three arginine residues, only present in this region of the 5-HT_{3A} subunit, by the corresponding sequences of the 5-HT_{3B} subunit increased single-channel conductance of the homopentameric 5-HT_{3A}R mutant 28-fold. According to the refined structure of the nAChR [109], these arginine residues are localized in the narrowest region of the membrane pore, forming lateral windows in the intracellular vestibule and thus determine the conductance of the channel.

Here, these three arginine residues unique to the 5-HT_{3A} were replaced by the corresponding 5-HT_{3B} sequences in the cysteine-less 5-HT_{3A} receptor. Single-channel current were recorded and multiple conductance levels were observed whose probability of occurrence was modulated by the amount of serotonin present. Unexpectedly, high current fluctuations were observed in the open state when the receptor was activated with serotonin. Noise analysis of the current in the open-state was performed for the first time on the 5-HT_3 receptor suggesting that charged residues are involved in the fluctuating domains.

5.2 Experimental techniques

As introduced in section 4.2, electrophysiology is well suited and extremely sensitive for investigating the function of ion channels embedded in membranes. Usually, two major methods are used to record ion currents passing a single channel in real time: the black lipid membrane (BLM) and the single-channel patch clamp techniques. In BLM experiments [224], channel proteins have to be reconstituted in an artificial planar lipid bilayer, which covers a hole in a teflon septum. In contrast, the patch-clamp technique allows to measure directly on living cells or on native membrane fragments and therefore to investigate channels in their native environment. In these two techniques, two electrodes are placed on the opposite sides of the membrane and connected to a feedback amplifier to record electrical currents.

5.2.1 Single-channel patch-clamp

The principle of a single-channel patch-clamp experiment is similar to that of a whole cell patch-clamp experiment; the differences concern the sensitivity and the patch configurations. Several configurations exist to resolve single channel currents, but only two of them are described. In the so-called cell-attached configuration, the pipette tip is brought into contact with the cell surface yielding a tight electrical seal

by gentle suction (figure 5.1.a). Channels within the pipette tip are activated by ligand dissolved in the pipette buffer. In this configuration, the potential difference across the channel within the pipette tip corresponds to the applied potential plus the cellular membrane potential.

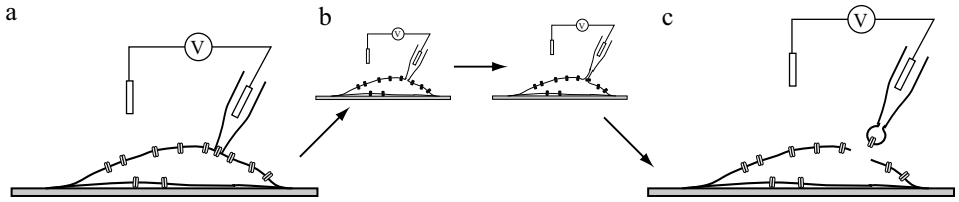

Figure 5.1: Single-channel patch-clamp configurations. *(a) Cell-attached, (b) whole-cell and (c) outside-out configurations.*

From the cell-attached configuration, the membrane in the patch pipette can be broken (whole-cell configuration) and then, by gently pulling the pipette away from the cell, a part of the membrane can be extracted. This manipulation yields the so-called outside-out configuration where the extracellular side of the membrane faces the bath. Here, the potential difference across the membrane corresponds to the applied potential.

5.3 Materials and methods

5.3.1 Molecular and cellular biology

5-HT$_3$R-QDA — The sequence is based on the 5-HT$_3$R-ΔCys-His$_{10}$ (see section 4.3.2 and appendix A.3) with three mutations: R441Q, R445D and R449A (numbering corresponds to the unprocessed precursor). Coding sequence comprised between BamH I and Not I (figure 4.3.a) was subcloned into pBluescript II SK (+) (Stratagene, California, USA), and the resulting plasmid was used as template for site-directed mutagenesis. Arg441, Arg445 and Arg449 were mutated using the QuickChange^{TM} site-directed mutagenesis kit (Stratagene) and oligonucleotides 5HT3aQDA*for* and 5HT3aQDA*rev* (appendix A.1) with the conditions required by the provider in the presence of 4% DMSO. The mutated nucleotide sequence was verified by restriction analysis and sequencing of the whole insert in pBluescript II SK (+) using the T7 primer; the sequencing was performed in one step. The mutated insert was then restricted, purified and ligated into the original pcDNA3 vector yielding 5-HT$_3$R-QDA construct.

Cell culturing and transfection — HEK-293 cells were cultured with a density of 150'000 cells/ml in 35 mm culture dishes (2 ml/dish) in Dulbecco's modified Eagle medium (DMEM) supplemented with 2.2% of fetal calf serum under humidified 5% CO_2 atmosphere at 37°C. Cells were transfected 14 to 18 hours after splitting using Effectene^{TM} (Qiagen, Hilden, Germany) according to the supplied protocol with 0.16 μg receptor DNA, 0.04 μg EGFP plasmid DNA (Clontech, Palo Alto, CA, USA), 1.6 μl enhancer, 2 μl effectene and 100 μl EC buffer for 2 ml culture medium.

5.3.2 Experimental methods

Electrophysiology — Standard whole cell patch-clamp experiments were performed as described in section 4.3.3. For single channel patch-clamp, borosilicate glass tubes GB150F-8P 1.05 x 1.50 x 80 mm^3 (Science Products GmbH, Hofheim, Germany) and an Ag/AgCl ground electrode were used. Data were recorded at 10 kHz and filtered at 2.9 kHz.

5.3.3 Data treatment

Dose response curves and EC_{50} values — Current intensities obtained from whole cell patch-clamp were treated as already described in section 4.3.4 and fitted with equation 4.2 yielding EC_{50} and Hill coefficient h. All errors were calculated according to Gauss propagation method and are 95% confidence intervals.

Determination of the conductance — Single-step amplitude of ionic current were measured using the Igor Pro software (WaveMetrics, Lake Oswego, OR, USA) and reported versus the holding potential. Fit using the modified Ohm's law (equation 5.1) yielded the single-channel conductance g and cellular membrane potential ϕ. V is the holding potential and I the current. All errors were calculated according to Gauss propagation method and are 95% confidence intervals.

$$I = g \cdot (V + \phi) \tag{5.1}$$

Intrinsic Johnson and shot noise — Johnson current noise σ_{th} is an equilibrium thermal noise and is defined by equation 5.2 where k_{B} is the Boltzmann's constant, T the absolute temperature, g the single-channel conductance and f_{B} the bandwidth [225].

$$\sigma_{\mathrm{th}} = \sqrt{4k_{\mathrm{B}} \cdot T \cdot g \cdot f_{\mathrm{B}}} \tag{5.2}$$

The shot noise σ_{sh} arises from the discrete nature of ionic flow through the channel and is defined by equation 5.3 where Δi is the average single-channel current and e the elementary charge [226].

$$\sigma_{sh} = \sqrt{2 \cdot \Delta i \cdot e \cdot f_B} \tag{5.3}$$

Power spectral density — Power spectral densities were computed using the Igor Pro software (WaveMetrics). The analysis were performed on segments of 51.2 ms sampled at 10 kHz with a bandwidth of 2.9 kHz.

5.4 Results and discussion

In order to resolve single channel events underlying the 5-HT_3R ion current, three arginine residues within the cytosolic loop of each subunit were substituted by glutamine, aspartic acid and alanine increasing the conductance of the ion channel as reported by Kelley *et al.* [223]. The sequence of the receptor investigated here is based on the cysteine-less receptor presented and characterized in chapter 4 with the three corresponding mutations yielding the 5-HT_3R-QDA. The cloning strategy as described in section 5.3.1 allows to insert the mutated region coding for the intracellular domain of the receptor, within the eighteen single cysteine receptor constructs presented in table 4.2. This would provide mutants for simultaneously recording single channel currents and conformational changes reported by a site-specifically bound fluorescent MTS-probe. The 5-HT_{3A}R mutant is functional in terms of gating (see below) and fluorescent antagonist binding (data not shown).

5.4.1 Whole cell patch-clamp characterization

Whole cell patch-clamp recorded inward currents of HEK-293 cells expressing the 5-HT_3R-QDA. The channels opened within tens of milliseconds after binding of the agonist reaching up to nanoampere currents, and then desensitized extremely slowly compared to the wt-5HT_{3A} receptor (figure 5.2.a). Dose response curves were fitted with a Hill equation yielded $EC_{50} = 0.2 \pm 0.1$ μM and $h = 0.9 \pm 0.3$ (figure 5.2.b), which are significantly different compared to the wt5-HT_3R (table 4.2); the affinity of the 5-HT_3R-QDA for serotonin was increased 10-fold. The unity value of the Hill coefficient supposes that only one ligand was required for the opening of the receptor mutant. These differences of behavior seem to be mainly due to the three mutations within the intracellular loop as the cysteine-less mutant featured similar EC_{50} and h values compared to the wild type receptor (table 4.2). No direct comparison can

be made with the mutant reported by Kelley *et al.* [223] since only its conductance was reported. Amplitude of the recording currents were in the same range as for the wild-type receptor expressed in HEK-293 cells, showing that indeed the expression level of the mutant receptor is significantly lower as its conductance was enhanced by about 70-fold (see section 5.4.2).

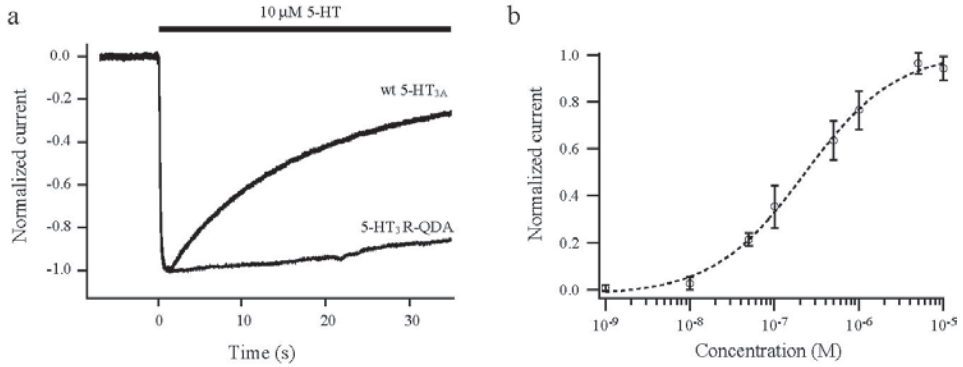

Figure 5.2: Whole-cell current characterization of the 5-HT$_3$R-QDA mutant. *(a) Whole-cell inward current response of HEK-293 cells expressing wt5-HT$_3$R and 5-HT$_3$R-QDA under continuous flow of serotonin. (b) Normalized dose response curve of the 5-HT$_3$R-QDA for serotonin. Fit using a Hill equation (Eq. 4.2) yielded $EC_{50} = 0.2 \pm 0.1$ µM and $h = 0.9 \pm 0.3$.*

5.4.2 Single channel current events

Ionic currents of single 5-HT$_3$R-QDA were recorded using two patch-clamp configurations, the cell-attached and the outside-out configuration. The signal to noise ratio of the former was higher compared to the later allowing the resolution of the opening of small conductances, and moreover the recording of events for several minutes since the stability of the seal is high. Nevertheless, determination of the conductance in this configuration required to record events at different holding potentials to account for the cell membrane potential, which is not required in the outside-out configuration. However, data obtained in both configurations are compared for a better reliability of the determined conductances of the channel.

Opening events were easily resolved and multiple conductances were observed in every recorded trace (figure 5.3.a). Five different conductances were determined from the slope of the current-potential plots, ranging from 11 pS to 52 pS (figure 5.3.b), which corresponds to a 70-fold increase of the conductance compared to the wild-type receptor [94, 223]. The activity of the unliganded receptor was relatively high since all the different conductance levels were observed (figure 5.3.a).

At 10 μM serotonin, the channel activity increased, but also the distribution of the different conductances (figure 5.4). Unliganded receptors showed two main conductances of 52 pS and 19 pS, whereas the presence of agonist increased the probability of occurrence of the higher conductance states at the expense of the lower.

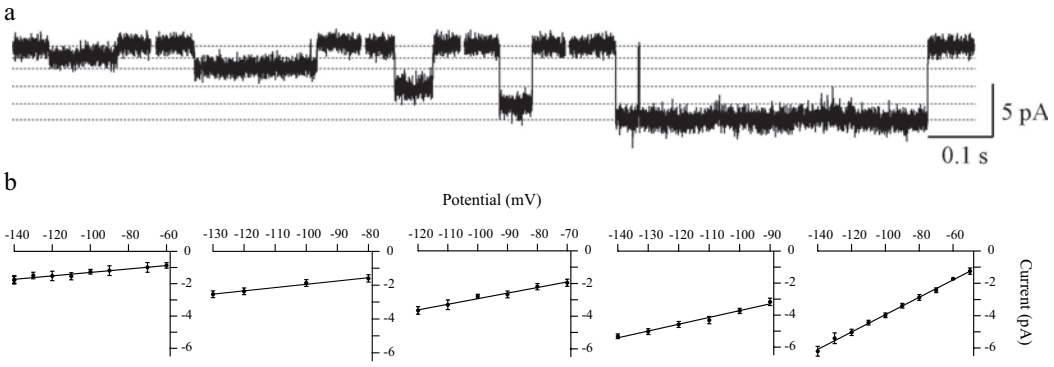

Figure 5.3: Multiple conductances of the 5-HT_3-QDA mutant receptor. *(a) Single channel events of the unliganded 5-HT_3R-QDA expressed in HEK-293 cells recorded at 10 kHz and filtered at 2.9 kHz with a holding potential of -100 mV in the cell-attached configuration. The membrane potential ϕ was estimated to be -32 mV. Five different amplitudes of single step events were observed, each of them corresponds to a different conductance. All the events reported originated from the same patch. (b) Current-potential plots of the five different open amplitudes shown in (a). Mean slope of the linear fits yielded conductances of 11 $\pm$ 2, 19 $\pm$ 3, 34 $\pm$ 4, 42 $\pm$ 5 and 52 $\pm$ 2 pS from the left to the right, respectively.*

We did not control whether antagonists blocked or decreased the activity of the receptor. Since the activity of the unliganded receptor is relatively important, antagonist binding should result in a decrease of the whole-cell current in a whole-cell patch.

All the current transitions opened and closed within one step (figure 5.3.a) at the exception of a few of them (0.5-1%) where intermediate levels corresponding to one of the conductances of the mutant receptor appeared either in the opening or closing of the channel (figure 5.5). We cannot conclude that the different conductances observed correspond to intermediate gating states since they were rarely observed. It rather seems that the different conductive channels are independent and that they correspond to distinctive molecular properties like phosphorylated or non-phosphorylated subunits [218]. These modifications are relatively slow and take place mostly in the closed state.

Within a burst, almost no flickering between closed and open states were observed in both the presence and absence of serotonin. This corresponds to a

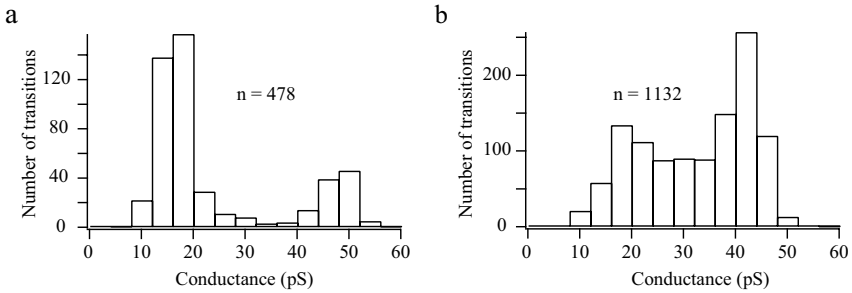

Figure 5.4: Distribution of conductances of the 5-HT$_3$R-QDA in living cells. *Histograms of all the conductances of the receptor recorded in the outside-out configuration at -100 mV for (a) the unliganded receptor and (b) in the presence of 10 μM of serotonin. Bin size is 4 pS. Experiments shown in (a) and (b) were performed on two different cells and number of events measured are indicated.*

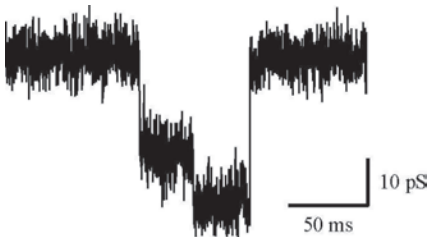

Figure 5.5: Intermediate open states of the 5-HT$_3$R-QDA. *Single-channel current of the unliganded receptor in the cell-attached configuration with an holding potential of -100 mV. The channel opened within two steps and closed within one step. The opening amplitudes corresponded to conductances of 19 $\pm$ 2 pS and 11 $\pm$ 2 pS, and the closing amplitude to a conductance of 34 $\pm$ 4 pS, respectively.*

gating equilibrium constant Θ estimated to be $\sim$300. The large value of Θ and the long open times explain the very slow desensitization of the receptor observed in whole-cell experiments (figure 5.2.a).

The multiple conductances of the 5-HT_3-QDA receptor mutant stem most probably from the substituted cysteines residues, since only one conductance was reported for the high conductive human 5-HT_{3A} receptor mutant [223]. However, multiple conductances were already measured for the heteropentameric 5-HT_3R in N1E-115 neuroblastoma cells [216, 218]. It has been reported that phosphorylation modulated the probability of occurrence of particular conductances [218].

5.4.3 Noise analysis of single activated 5-HT_3R

The amplitude of the ionic current in the open-channel state was larger when the 5-HT_3 receptor mutant was activated by 0.2 μM serotonin compared to the unliganded receptor indicating that the serotonin binding site is at the origin of a structural fluctuation somewhere within the channel lumen or any regions lining the ion flow (figure 5.6). The excess noise of an open-channel σ_{ex} was determined by subtracting the standard deviation of the current of the closed state from that of the open states. The contribution of the Johnson thermal noise and the shot noise originating from the ionic flow through the channel were determined according to equations 5.2 and 5.3, respectively. These two contributions were normalized by the current Δi in order to take into account all the opening transitions ranging from 11 pS to 52 pS. It resulted in a theoretical excess standard deviation defined as $({\sigma_{\mathrm{th}}}^2 + {\sigma_{\mathrm{sh}}}^2)/\Delta i$ equal to $1.3{\cdot}10^{-3}$ pA at an holding potential of -100 mV and bandwidth of 2.9 kHz in the case where the Johnson and shot noise are the only contribution of the excess of noise. In comparison, experimental normalized standard deviation of the open channel ionic current ${\sigma_{\mathrm{ex}}}^2/\Delta i$ determined over thirty events were of $1.4 \pm 1.2{\cdot}10^{-3}$ pA for the unliganded receptor mutant and of $7.7 \pm 2.0{\cdot}10^{-2}$ pA for the activated receptor mutant. These values showed that the modest excess noise of the unliganded receptor mutant arose mainly from the intrinsic thermal and shot noise whereas the large current fluctuations of the activated receptor have another origin.

The ionic current fluctuations were analyzed using the power spectral density (defined as the Fourrier transform of the autocorrelation function $<i(t)\ i(t')>$), which represents the frequency distribution of signal energy. The true spectrum of the channel current fluctuations $S_{\mathrm{i}}(f)$ corresponding to the open-channel noise excess, was obtained by subtracting the averaged spectrum of the background (*i.e.* closed state) from the opened channel spectrum. To minimize the influence of any

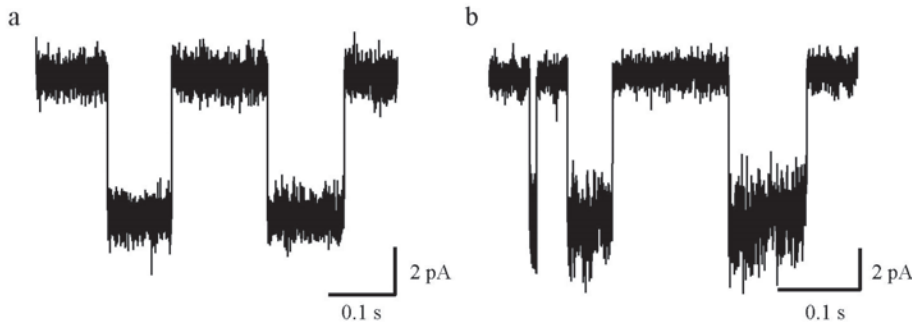

Figure 5.6: Amplitude of open-channel ion currents. *Typical current traces of 5-HT$_3$R in (a) the absence and (b) presence of 0.2 μM serotonin. Recording were obtained at 2.9 kHz bandwidth and -100 mV applied voltage in the cell-attached configuration.*

changes in the fluctuations of the baseline, background spectra were accumulated from segments adjacent to the single channel events [227].

The power spectral density, which characterizes the open channel state, was clearly different from the background and could be fitted by a power law function S_{i} $\propto 1/f^{\alpha}$ yielding $\alpha = 0.43 \pm 0.02$ (figure 5.7). The value of α suggests that memory effects are involved in the protein dynamics and that the open-channel spectrum is related to a fractional Gaussian noise. To our knowledge, this is the first time that such a behavior is observed for a single ion channel.

However, $1/f$ noise ($\alpha = 1$) was observed on different bacterial channels reconstituted into planar lipid bilayer [228–230]. The mechanism involved in the creation of $1/f$ noise is not very clear. For instance, in the case of the maltoporin channel it was observed that in single channel open states, switches between substates of slightly different conductances occurred [230] indicating that the $1/f$ dependence of the noise might originate from slow opening and closing events of the channel related to conformational flexibility of structural constituents. This hypothesis was confirmed on nanofabricated synthetic pores where this noise was related to the underlying motions of channel wall constituents [231].

Interestingly, the histogram of current fluctuation amplitudes of open activated 5-HT$_3$ receptors was perfectly fitted using a single Gaussian distribution, which was two times broader compared to the unliganded receptor mutant (figure 5.8.a). This excess of Gaussian noise is likely to arise from continuous current changes and not from discrete current transitions between conductance states [227]. The most probable origin of this continuous current changes is to consider that spontaneous thermal fluctuations arise within structural protein domains modulat-

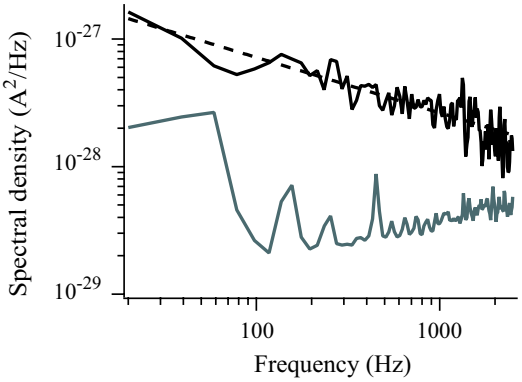

Figure 5.7: Spectral density analysis of ionic current fluctuations of the 5-HT_3 mutant receptor. *Averaged power spectral densities of current fluctuations in the closed state (grey) and open state after background substraction (black) of single 5-HT_3R channels activated by 0.2 μM serotonin. Dotted line is a fit using $S_i(f) \propto 1/f^{\alpha}$ yielding $\alpha = 0.43 \pm 0.02$.*

ing the size of the ion conductive pathway and therefore its conductance [232, 233]. The regions of the receptor that control channel conductance are the transmembrane pore as well as the proposed filter located in the intracellular loop [109, 223]. According to the homopentameric symmetry of the receptor, we can consider that conformational oscillations of elastic protein domains occur in a concerted normal mode and that the radius x of the pore is a normal coordinate. In this model, the current fluctuations δi were related to the variation of the radius $\delta x = x$ - x_{eq} around the equilibrium radius x_{eq}, the conductance g and the potential V resulting in equation 5.4.

$$\delta i = V \cdot \left(\frac{\delta g}{\delta x}\right)_{x_{\mathrm{eq}}} \delta x \tag{5.4}$$

The potential of the mean force was calculated using $U(\delta x) = -k_{\mathrm{B}}T \cdot \ln(P(\delta x))$, where $P(\delta x)$ is the probability density distribution of the radial motions derived from $P(\delta i)$ (figure 5.8.b). For a Gaussian distribution, $U(\delta x)$ corresponds to a harmonic potential described by equation 5.5 where $<x^2>$ is the mean square displacement and was used to fit $U(\delta x)$ (figure 5.8.b).

$$U(\delta x) = \frac{k_{\mathrm{B}}T\delta x^2}{2 < x^2 >} \tag{5.5}$$

The potential $U(\delta x)$ determined from the probability density function $P(\delta i)$ assuming $(\delta g/\delta x)_{x_{\mathrm{eq}}} = 10$ pS/nm was not relevant. It assumed a variation of the pore radius inconsistent with the structure of the receptor; the minimum radial distance from the central axis of the nAChR was reported to be 3 Å [108]. Thus, values for

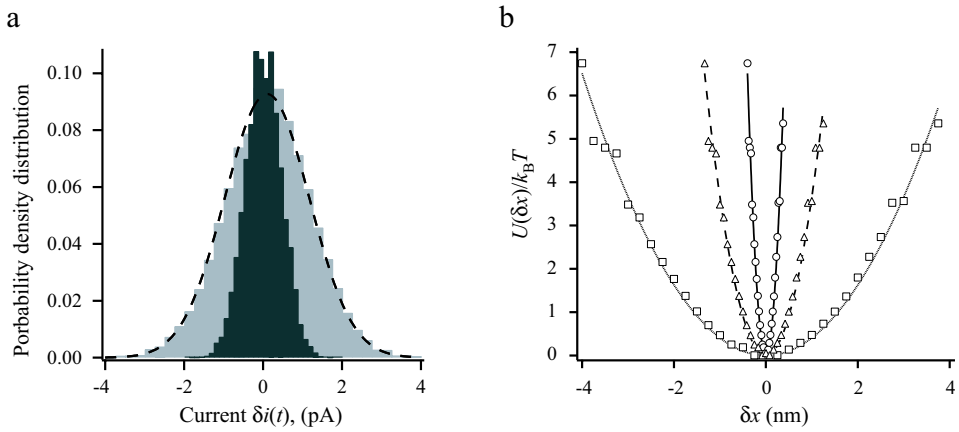

Figure 5.8: Gaussian current fluctuations and harmonic potential. *(a) Probability density distribution of the current fluctuations in the background (black) and in the open state (grey), both in the presence of 0.2 μM serotonin. The dashed line is the fit according to a Gaussian distribution. (b) Mean force potential represented in the domain coordinates using ($\delta g/\delta x$) = 10 pS/nm (□), 30 pS/nm (△) and 100 pS/nm (◯), and V = -100 mV. Fits using equation 5.5 yielded values of the root mean square displacements $\sqrt{< x^2 >}$ of 1.12 nm, 0.37 nm and 0.11 nm, respectively.*

$(\delta g/\delta x)_{x_{\mathrm{eq}}}$ in the range of 30-100 pS/nm have to be assumed suggesting that the oscillating domains in the 5-HT_3 receptor mutant contain charged amino acids. In comparison, $(\delta g/\delta x)_{x_{\mathrm{eq}}} \approx$ 5-10 pS/nm were reported for the nAChR [232]. The proposed model can be further developed using the Langevin equation to characterize the dynamics of the oscillations as it was already reported for the nAChR [232]. The mathematical development (not presented here) suggests that the current fluctuations correspond to a fractional Gaussian noise.

Thermodynamic investigations revealed that agonist binding is entropy-driven for the 5-HT_3 receptor [234] which corroborate the proposed model of oscillating domain in the activated state. Note that in the case of the nAChR, agonist binding is enthalpy and entropy driven [235].

5.5 Conclusion

The three mutated amino acids within the intracellular domain of the 5-HT_3 receptor subunits greatly enhanced its conductance and drastically decreased its desensitization rate. Single-channel openings and closings were resolved and five different conductance levels ranging from 11 to 52 pS were determined. We infer that the different conductances correspond to distinctive molecular states rather than inter-

mediate open states of the receptor; experimental evidence of multiple step opening and closing were rare. The origin of the excess noise in the open state of the liganded receptor is unclear. This might be caused by different mechanisms of the gating for 5-HT$_3$ activated and spontaneous openings, or by a cytosolic factor like phosphorylation [218]. According to our proposed model, current fluctuations observed in the open-states are related to an oscillating domain composed of charged amino-acids. Noise analysis show that the fluctuations were not random and non-correlated, and are assimilated to a fraction Gaussian noise.

Insertion of these cytoplasmic mutations within the 5-HT$_3$-D298C receptor mutant (table 4.2) will allow to simultaneous record conformational changes reported by a tethered cysteine reactive fluorophore and single-channel electrophysiology.

Chapter 6

General conclusions and outlook

The dynamics of both the 5-HT_{3A} receptor and 5-HT_{3A} receptor within cells was studied using fluorescence techniques and patch-clamp electrophysiology. This work provided new tools, a labelling method and receptor mutants, for the investigation of the distribution of receptors, receptor-ligand interactions, lateral mobility, conformational changes and gating of the receptor in living cells.

The method for protein labelling, based on small nickel-chelating nitrilotriacetic probes, represents an attractive alternative over current labelling approaches for studying molecular interactions and structural properties of proteins. These NTA-probes bind within seconds specifically and reversibly to short recognition peptides of six to ten histidines that can be genetically encoded to the C- or N-terminus or inserted within accessible loops of the target protein. Moreover, they are readily and economically produced from commercially available compounds. Applied to the 5-HT_3 receptor in live cells, we succeeded in determining plasma membrane distribution, receptor-ligand interactions and structural information on a ensemble of receptors. This new labelling method was further used to detect single receptors in the cell membrane and yielded information on their lateral mobility in different functional states. These NTA-probes represent a significant advantage over conventional methods (*i.e.* covalent labelling) for single molecule microscopy. They allow the successive labelling of receptors and therefore to record several movies on the same cell reducing significantly the time needed to obtain sufficient trajectories for a statistical evaluation. Moreover, this new method overcomes the irreversible photobleaching of organic fluorophores as well as the large size of *e.g.* quantum dots or antibodies. These small reporters should allow to access confined regions, like synapses, and to report on the organization and dynamics of their constituents.

Single-molecule microscopy revealed a surprising modulation of the receptor's

lateral mobility by the agonist serotonin. Desensitized 5-HT_3 receptors were significantly less mobile then receptors in the resting state. Receptors might accumulate where and when serotonin is released by a neighbor neuron resulting in the formation a synapse. Thus serotonin might be instrumental in serotonergic synapse development. Nevertheless, the mechanism involved in this decrease of lateral mobility is unclear. This could arise from an increased interaction of the receptor with the cellular membrane or the cytoskeletal network due to structural changes within the transmembrane domain or the intracellular domain, respectively. The mobility of the receptor in its open state was not investigated. Nevertheless this would be accessed using a slow desensitizing mutant receptor like the one presented in chapter 5 for instance.

The receptor mutants developed are powerful tools. The receptor containing no cysteine has shown to be fully functional. Therefore, cysteine residues can be inserted within the whole receptor sequence where they do not interfere with the functionality of the receptor allowing thus the insertion of multiple reporter probes. We demonstrated that a rhodamine fluorophore tethered to a cysteine residue could report conformational transitions of the receptor upon activation. However, other fluorescent reporters would have been even more sensitive towards environment changes like electrostatic sensitive [236] or environment sensitive dyes [237].

The high conductive receptor mutant, where three arginine residues in the cytosolic loop where replaced, allowed to resolve multiple conductive levels. In single-channel patch-clamp experiments, the activity of the unliganded receptor was relatively high indicating that the receptor mutants in the resting state might be opened or partially opened. In a whole-cell patch-clamp experiment, channel blockers or antagonists should result in a decrease of the current according to the hypothesis. This would give an explanation to the low currents observed in whole-cell patches.

This work is not at its end but valuable tools were developed to decipher the dynamics of the 5-HT_{3A} receptor. More insights of the gating mechanism of the 5-HT_3 receptor will be obtained using a high conductance receptor mutant containing a single cysteine that can be fluorescently labelled. Using single molecule microscopy and single-channel patch-clamp, conformational changes and electrical current will be simultaneously measured. The ionic current could be even more resolved using adequate buffers.

Abbreviations

5-HT	serotonin, 5-hydroxytryptamine
5-HT_3R	serotonin type 3 receptor
AChBP	acetylcholine binding protein
ACP	acyl carrier protein
Ala	alanine
AMPA	α-amino-3-hydroxy-5-methyl-4-isoxazole propionic acid
ATP	adenosine triphosphate
BirA	biotin ligase
BLM	black lipid membrane
BS	binding site
cAMP	cyclic adenosine diphosphate
CHO	Chinese hamster ovary
Cys	cysteine
D	diffusion coefficient
DA	dopamine
DHFR	dihydrofolate reductase
DMEM	Dubelcco's modified Eagle medium
DMF	dimethylformamide
DMSO	dimethylsulfoxide
DNA	deoxyribonucleic acid
D-PBS	Dulbecco's phosphate-buffered saline
EC_{50}	half maximal effective concentration
EDT	ethanedithiol
EDTA	ethylenediaminetetraacetic acid
EGFP	enhanced green fluorescent protein
EGTA	ethylene glycol-bis(2-aminoethylether)-N,N,N',N'-tetraacetic acid
ER	endoplasmic reticulum

FCS	fluorescence correlation spectroscopy
FKBP	FK506 binding protein
FlAsH	fluorescein arsenical helix binder
FRAP	fluorescence recovery after photobleaching
FRET	fluorescence resonance energy transfer
GABA	γ-aminobutyric acid
GFP	green fluorescent protein
Gln	glutamine
GluR	glutamate receptor
Gly	glycine
GPCR	G protein-coupled receptor
GR	1,2,3,9 tetrahydro-3-[(5-methyl-1H-imidazol-4-yl)methyl]-9-(3-amino-propyl)-4H-carbazol-4-one
GR-flu	1,2,3,9 tetrahydro-3-[(5-methyl-1H-imidazol-4-yl)methyl]-9-(3-amino-(N-fluorescein-thiocarbamoyl)-propyl)-4H-carbazol-4-one
hAGT	O^6-alkylguanine-DNA-alkyltransferase
HEPES	4-(2-hydroxyethyl)-1-piperazine-1-ethanesulfonic acid
HEK-293	human embryonic kidney cell
His	histidine
HPLC	high pressure liquid chromatography
IC_{50}	half maximal inhibitory concentration
IP_3	inositol trisphosphate
IPTG	isopropyl thiogalactoside
IUPHAR	international union of pharmacology
k_{on}	association rate constant
k_{off}	dissociation rate constant
K_a	association constant
K_d	dissociation constant
l	liter
LGIC	ligand-gated ion channel
M	molar (mol/l)
mCPBG	*m*-chlorophenylbiguanide
MHC	major histocompatibility complex
mol	mole
MSD	mean square displacement
MTS	methanethiosulfonate
MTSEA	2-aminoethyl-methanethiosulfonate or methanethiosulphonate ethylammonium

MTSES	2-sulfonatoethyl-methanthiosulfonate
MTSET	2-trimethylammonioethyl-methanethiosulfonate
MW	molecular weight
NCBI	national center for biotechnology information http://www.ncbi.nlm.nih.gov
NMDA	N-methyl-D-aspartic acid
NTA	nitrilotriacetic acid
NTA-lysine	N-(5-amino-1-carboxypentyl)iminodiacetic acid
OD	optical density
P_{2x}	purinergic receptor
PBS	phosphate-buffered saline
PLP	pyridoxal-5'-phosphate
PPTase	phosphopantetheine transferase
Pro	proline
SCAM	substituted-cysteine accessibility method
Ser	serine
SDS-PAGE	sodium dodecylsulfate polyacrylamide gel electrophoresis
SMI	single molecule imaging
SMS	single molecule spectroscopy
Thr	threonine
TLC	thin layer chromatography
TM	transmembrane domain
tRNA	transfer ribonucleic acid
wt	wild-type
YFP	yellow fluorescent protein
ZAC	zinc activated channel

Appendices

A.1 Oligonucleotides for site-directed mutagenesis

Oligonucleotide sequences used for site-directed mutagenesis. Mutated or inserted nucleic acids are underlined. The numbering in the primer names (from 291 to 308) corresponds to the target sequence of 5-HT_3R-ΔCys-His_{10} whose sequence is presented in appendix A.3.

p10xHis-wtGFP*for*	5'-G GAG GAA TAA ACC ATG GGG GGA TCC CAT CAC CAT CAC CAT CAT CAT CAT CAT GG-3'
p10xHis-wtGFP*rev*	5'-CC ATG ATG ATG ATG ATG ATG GTG ATG GTG ATG GGA TCC CCC CAT GGT TTA TTC CTC C-3'
5HT3a-Δcys*for*	5'-C ACA TCT GGG AAG CTT GCC ATG CGG-3'
5HT3a-Δcys*rev*	5'-A TAG TTT AGC GGC CGC TCA ATG GTG ATG GTG ATG GTG ATG GTG ATG GTG AGA ATA ATG CCA AAT GGA CCA G-3'
5HT3aV291C*for*	5'-CTT CTG GGA TAC TCA TGC TTC CTG ATC ATC GTG TCA GA-3'
5HT3aV291C*rev*	5'-TCT GAC ACG ATG ATC AGG AAG CAT GAG TAT CCC AGA AG-3'
5HT3aF292C*for*	5'-GGG ATA CTC AGT CTG CCT CAT CAT CGT GTC AG-3'
5HT3aF292C*rev*	5'-CTG ACA CGA TGA TGA GGC AGA CTG AGT ATC CC-3'

5HT3aL293C*for*	5'-GAT ACT CAG TCT TCT GCA TCA TCG TGT CAG ACA-3'
5HT3aL293C*rev*	5'-TGT CTG ACA CGA TGA TGC AGA AGA CTG AGT ATC-3'
5HT3aI294C*for*	5'-GGG ATA CTC AGT CTT CCT CTG CAT CGT GTC AGA C-3'
5HT3aI294C*rev*	5'-GTC TGA CAC GAT GCA GAG GAA GAC TGA GTA TCC C-3'
5HT3aI295C*for*	5'-CAG TCT TCC TCA TCT GCG TGT CAG ACA CAC TGC C-3'
5HT3aI295C*rev*	5'-GGC AGT GTG TCT GAC ACG CAG ATG AGG AAG ACT G-3'
5HT3aV296C*for*	5'-GTC TTC CTA ATC ATC TGC TCA GAC ACA CTG CCG-3'
5HT3aV296C*rev*	5'-CGG CAG TGT GTC TGA GCA GAT GAT GAG GAA GAC-3'
5HT3aS297C*for*	5'-CTT CCT CAT CAT CGT GTG TGA CAC ACT GCC GGC-3'
5HT3aS297C*rev*	5'-GCC GGC AGT GTG TCA CAC ACG ATG ATG AGG AAG-3'
5HT3aD298C*for*	5'-CCT CAT CAT CGT GTC ATG CAC ACT GCC GGC-3'
5HT3aD298C*rev*	5'-GCC GGC AGT GTG CAT GAC ACG ATG ATG AGG-3'
5HT3aT299C*for*	5'-CAT CAT CGT GTC AGA CTG TCT GCC GGC AAC GG-3'
5HT3aT299C*rev*	5'-CCG TTG CCG GCA GAC AGT CTG ACA CGA TGA TG-3'
5HT3aL300C*for*	5'-CAT CGT GTC AGA CAC ATG TCC GGC AAC GGC CAT CG-3'
5HT3aL300C*rev*	5'-CGA TGG CCG TTG CCG GAC ATG TGT CTG ACA CGA TG-3'
5HT3aP301C*for*	5'-CGT GTC AGA CAC ACT GTG CGC AAC GGC CAT CG-3'
5HT3aP301C*rev*	5'-CGA TGG CCG TTG CGC ACA GTG TGT CTG ACA CG-3'
5HT3aA302C*for*	5'-CGT GTC AGA CAC ACT GCC GTG TAC GGC CAT CGG TAC C-3'
5HT3aA302C*rev*	5'-GGT ACC GAT GGC CGT ACA CGG CAG TGT GTC TGA CAC G-3'

5HT3aT303C*for* 5'-GAC ACA CTG CCG GCA TGT GCC ATC GGT ACC C-3'

5HT3aT303C*rev* 5'-GGG TAC CGA TGG CAC ATG CCG GCA GTG TGT C-3'

5HT3aA304C*for* 5'-CAC ACT GCC GGC AAC GTG CAT CGG TAC CCC-3'

5HT3aA304C*rev* 5'-GGG GTA CCG ATG CAC GTT GCC GGC AGT GTG-3'

5HT3aI305C*for* 5'-GGC AAC GGC CTG CGG TAC CCC C-3'

5HT3aI305C*rev* 5'-GGG GGT ACC GCA GGC CGT TGC C-3'

5HT3aG306C*for* 5'-GCA ACG GCC ATC TGT ACC CCC CTC-3'

5HT3aG306C*rev* 5'-GAG GGG GGT ACA GAT GGC CGT TGC-3'

5HT3aT307C*for* 5'-GCA ACG GCC ATC GGT TGC CCC CTC ATT GGT GTC-3'

5HT3aT307C*rev* 5'-GAC ACC AAT GAG GGG GCA ACC GAT GGC CGT TGC-3'

5HT3aP308C*for* 5'-CGG CCA TCG GTA CCT GCC TCA TTG GTG TCT AC-3'

5HT3aP308C*for* 5'-GTA GAC ACC AAT GAG GCA GGT ACC GAT GGC CG-3'

5HT3aQDA*for* 5'-C CAC TTC CTG GAG AAG CAG GAT GAG ATG GAT GAG GTG GCA GCG GAC TGG CTG CGG GTG G-3'

5HT3aQDA*rev* 5'-C CAC CCG CAG CCA GTC CGC TGC CAC CTC ATC CAT CTC ATC CTG CTT CTC CAG GAA GTG G-3'

A.2 Sequence of the 5-HT$_3$R-C-His$_{10}$

A.2.1 Nucleotide sequence

1 AAA GCT TAC TCC ACC *atg CGG CTC TGC ATC CCG CAG GTG CTG TTG*
11 *GCC TTG TTC CTT TCC ATG CTG ACA GCG CCG GGA GAA GGC* AGC CGG
26 AGG AGG GCC ACC CAG GCC CGA GAT ACC ACC CAG CCT GCT CTA CTA
41 AGG CTG TCA GAC CAC CTC CTG GCT AAC TAC AAG AAG GGG GTG CGG
56 CCT GTG CGG GAC TGG AGG AAG CCT ACT ACT GTC TCC ATT GAT GTC
71 ATC ATG TAT GCC ATC CTC AAC GTG GAT GAG AAG AAC CAG GTT CTG
86 ACC ACC TAC ATA TGG TAC CGG CAG TAC TGG ACT GAT GAG TTT CTG
101 CAG TGG ACT CCT GAG GAC TTC GAC AAT GTC ACC AAA TTG TCC ATC
116 CCC ACA GAC AGC ATC TGG GTC CCT GAC ATT CTC ATC AAT GAG TTT
131 GTG GAC GTG GGG AAG TCT CCG AAC ATT CCT TAT GTG TAC GTG CAT
146 CAT CGA GGT GAA GTT CAG AAC TAC AAG CCC TTG CAA TTG GTG ACC
161 GCC TGT AGC CTT GAC ATC TAC AAC TTC CCC TTT GAT GTG CAG AAC
176 TGT TCT CTG ACT TTC ACC AGC TGG CTG CAC ACC ATC CAG GAC ATC
191 AAC ATT ACT CTG TGG CGA TCA CCG GAA GAA GTG AGG TCT GAC AAG
206 AGC ATC TTC ATA AAT CAG GGC GAG TGG GAG CTG CTG GAG GTG TTC
221 CCC CAG TTC AAG GAG TTC AGC ATA GAT ATC AGT AAC AGC TAT GCA
236 GAA ATG AAG TTC TAC GTG ATC ATC CGC CGG AGG CCT TTA TTC TAT
251 GCA GTC AGC CTC TTG CTG CCC AGT ATC TTC CTC ATG GTC GTG GAC
266 ATT GTG GGC TTT TGC CTG CCC CCG GAC AGT GGT GAG AGA GTC TCT
281 TTT AAG ATC ACA CTC CTT CTG GGA TAC TCA GTC TTC CTC ATC ATC
296 GTG TCA GAC ACA CTG CCG GCA ACG GCC ATC GGT ACC CCC CTC ATT
311 GGT GTC TAC TTT GTG GTG TGC ATG GCT CTG CTA GTG ATA AGC CTC
326 GCT GAG ACC ATC TTC ATT GTG CGG CTG GTG CAT AAG CAG GAC CTA
341 CAG CGG CCA GTA CCT GAC TGG CTG AGG CAC CTG GTC CTA GAC AGA
356 ATA GCC TGG ATA CTC TGC CTA GGG GAG CAG CCT ATG GCC CAT AGA
371 CCC CCA GCC ACC TTC CAA GCC AAC AAG ACT GAT GAC TGC TCA GCC
386 ATG GGA AAC CAC TGC AGC CAT GTT GGA GGA CCT CAG GAC TTG GAG
401 AAG ACC CCA AGG GGC AGA GGT AGC CCT CTT CCA CCA CCA AGG GAG
416 GCC TCA CTG GCT GTG CGT GGT CTC TTG CAA GAG CTA TCC TCC ATC
431 CGC CAC TTC CTG GAG AAG CGG GAT GAG ATG CGG GAG GTG GCA AGG
446 GAC TGG CTG CGG GTG GGA TAC GTG CTG GAC AGG CTG CTG TTC CGC
461 ATC TAC CTG CTG GCT GTG CTC GCT TAC AGC ATC ACC CTG GTC ACT

```
476  CTC TGG TCC ATT TGG CAT TAT TCT CAC CAC CAT CAT CAC CAC CAT
491  CAT CAC CAC tga GCG GCC GCA
```

5' to 3' nucleotide sequence of the 5-HT_3R-C-His_{10}. The numbers correspond to the codons starting from the ATG start codon until the TGA stop codon indicated in lower cases. The membrane targeting signal sequence is indicated in italics. The underlined nucleotides correspond to the restriction sites of Hind III and Not I, respectively. For more details, see section 3.3.2.

A.2.2 Amino acid sequence

```
1    MRLCI PQVLL ALFLS MLTAP GEGSR RRATQ ARDTT QPALL RLSDH LLANY
51   KKGVR PVRDW RKPTT VSIDV IMYAI LNVDE KNQVL TTYIW YRQYW TDEFL
101  QWTPE DFDNV TKLSI PTDSI WVPDI LINEF VDVGK SPNIP YVYVH HRGEV
151  QNYKP LQLVT ACSLD IYNFP FDVQN CSLTF TSWLH TIQDI NITLW RSPEE
201  VRSDK SIFIN QGEWE LLEVF PQFKE FSIDI SNSYA EMKFY VIIRR RPLFY
251  AVSLL LPSIF LMVVD IVGFC LPPDS GERVS FKITL LLGYS VFLII VSDTL
301  PATAI GTPLI GVYFV VCMAL LVISL AETIF IVRLV HKQDL QRPVP DWLRH
351  LVLDR IAWIL CLGEQ PMAHR PPATF QANKT DDCSA MGNHC SHVGG PQDLE
401  KTPRG RGSPL PPPRE ASLAV RGLLQ ELSSI RHFLE KRDEM REVAR DWLRV
451  GYVLD RLLFR IYLLA VLAYS ITLVT LWSIW HYSHH HHHHH HHH
```

Amino acid sequence of the 5-HT_3R-C-His_{10}. The numbering does not correspond to the SwissPort entry p23979 due to conflict regions (see section 3.3.2). The 23 amino acids in italics correspond to the membrane targeting signal sequence.

A.3 Sequence of the 5-HT$_3$R-ΔCys-His$_{10}$

A.3.1 Nucleotide sequence

1 AAG CTT GCC *atg CGG CTC TGC ATC CCG CAG GTG CTG TTG GCC TTG*
13 *TTC CTT TCC ATG CTG ACA GCC CCG GGA GAA GGC* AGC CGG AGG AGG
28 GCC ACC CAG GCC CGA GAT ACC ACC CAG CCT GCT CTA CTA AGG CTG
43 TCA GAC CAC CTC CTG GCT AAC TAC AAG AAG GGG GTG CGG CCT GTG
58 CGG GAC TGG AGG AAG CCT ACT ACT GTC TCC ATT GAT GTC ATC ATG
73 TAT GCC ATC CTC AAC GTG GAT GAG AAG AAC CAG GTT CTG ACC ACC
88 TAC ATA TGG TAC CGG CAG TAC TGG ACT GAT GAG TTT CTG CAG TGG
103 ACT CCT GAG GAC TTC GAC AAT GTC ACC AAA TTG TCC ATC CCC ACA
118 GAC AGC ATC TGG GTC CCT GAC ATT CTC ATC AAT GAG TTT GTG GAC
133 GTG GGG AAG TCT CCG AAC ATT CCT TAT GTG TAC GTG CAT CAT CGA
148 GGT GAA GTT CAG AAC TAC AAG CCC TTG CAA TTG GTG ACC GCC TGT
163 AGC CTT GAC ATC TAC AAC TTC CCC TTT GAT GTG CAG AAC TGT TCT
178 CTG ACT TTC ACC AGC TGG CTG CAC ACC ATC CAG GAC ATC AAC ATT
193 ACT CTG TGG CGA TCA CCG GAA GAA GTG AGG TCT GAC AAG AGC ATC
208 TTC ATA AAT CAG GGC GAG TGG GAG CTG CTG GAG GTG TTC CCC CAG
223 TTC AAG GAG TTC AGC ATA GAT ATC AGT AAC AGC TAT GCA GAA ATG
238 AAG TTC TAC GTG ATC ATC CGC CGG AGG CCT TTA TTC TAT GCA GTC
253 AGC CTC TTG CTG CCC AGT ATC TTC CTC ATG GTC GTC GAC ATT GTG
268 GGC TTT TCC CTG CCC CCG GAC AGT GGT GAG AGA GTC TCT TTC AAG
283 ATC ACA CTC CTT CTG GGA TAC TCA GTC TTC CTC ATC ATC GTG TCA
298 GAC ACA CTG CCG GCA ACG GCC ATC GGT ACC CCC CTC ATT GGT GTC
313 TAC TTT GTG GTG TCC ATG GCT CTA CTA GTG ATA AGC CTC GCT GAG
328 ACC ATC TTC ATT GTG CGG CTG GTG CAT AAG CAG GAC CTA CAG CGG
343 CCA GTA CCT GAC TGG CTG AGG CAC CTG GTC CTA GAC AGA ATA GCC
358 TGG ATC CTC TCC CTA GGG GAG CAG CCT ATG GCC CAT AGA CCC CCA
373 GCC ACC TTC CAA GCC AAC AAG ACT GAT GAC TCC TCA GGT TCT GAT
388 CTC CTC CCA GCC ATG GGA AAC CAC TCC AGC CAT GTT GGA GGG CCC
403 CAG GAC TTG GAG AAG ACC CCA AGG GGC AGA GGT AGC CCT CTT CCA
418 CCA CCA AGG GAG GCC TCA CTG GCT GTG CGT GGT CTC TTG CAA GAG
433 CTA TCC TCC ATC CGC CAC TTC CTG GAG AAG CGG GAT GAG ATG CGG
448 GAG GTG GCA AGG GAC TGG CTG CGG GTG GGA TAC GTG CTG GAC AGG
463 CTG CTG TTC CGC ATC TAC CTG CTG GCT GTG CTC GCT TAC AGC ATC

```
478  ACC CTG GTC ACT CTC TGG TCC ATT TGG CAT TAT TCT CAC CAT CAC
493  CAT CAC CAT CAC CAT CAC CAT tga GCG GCC GC
```

5' to 3' nucleotide sequence of the 5-HT_3R-ΔCys-His_{10} where all cysteines were replaced by serine except the two that form the disulfide bridge. The numbers correspond to the codons starting from the ATG start codon until the TGA stop codon indicated in lower cases. The membrane targeting signal sequence is indicated in italics. The underlined nucleotides correspond to the restriction sites of Hind III, EcoR V, BamH I and Not I, respectively. For more details, see section 4.3.2 and figure 4.3.a.

A.3.2 Amino acid sequence

```
1    MRLCI PQVLL ALFLS MLTAP GEGSR RRATQ ARDTT QPALL RLSDH LLANY
51   KKGVR PVRDW RKPTT VSIDV IMYAI LNVDE KNQVL TTYIW YRQYW TDEFL
101  QWTPE DFDNV TKLSI PTDSI WVPDI LINEF VDVGK SPNIP YVYVH HRGEV
151  QNYKP LQLVT ACSLD IYNFP FDVQN CSLTF TSWLH TIQDI NITLW RSPEE
201  VRSDK SIFIN QGEWE LLEVF PQFKE FSIDI SNSYA EMKFY VIIRR RPLFY
251  AVSLL LPSIF LMVVD IVGFS LPPDS GERVS FKITL LLGYS VFLII VSDTL
301  PATAI GTPLI GVYFV VSMAL LVISL AETIF IVRLV HKQDL QRPVP DWLRH
351  LVLDR IAWIL SLGEQ PMAHR PPATF QANKT DDSSG SDLLP AMGNH SSHVG
401  GPQDL EKTPR GRGSP LPPPR EASLA VRGLL QELSS IRHFL EKRDE MREVA
451  RDWLR VGYVL DRLLF RIYLL AVLAY SITLV TLWSI WHYSH HHHHH HHHH
```

Amino acid sequence of the 5-HT_3R-ΔCys-His_{10}. Cys162 and Cys176 form a disulfide bridge (this numbering do not correspond to the SwissPort entry p23979 due to conflict regions, see section 4.3.2). All other Cysteines were replaced by Serine. The 23 amino acids in italics correspond to the membrane targeting signal sequence.

Bibliography

[1] J. P. Changeux and S. J. Edelstein. Allosteric receptors after 30 years. *Neuron*, 21(5):959–80, 1998.

[2] T. P. Kenakin, R. A. Bond, and T. I. Bonner. Definition of pharmacological receptors. *Pharmacol Rev*, 44(3):351–62, 1992.

[3] C. Ludwig and A. Schmidt. Das Verhalten der Gase, welche mit dem Blut durch den reizbaren Säugetiermuskel strömen. *Arb Physiol Anstalt Leipzig*, 3:1, 1869.

[4] B. M. Twarog. Serotonin: History of a discovery. *Comp Biochem Physiol C*, 91(1):21–4, 1988.

[5] V. Erspamer. Historical introduction: The Italian contribution to the discovery of 5-hydroxytryptamine (enteramine, serotonin). *J Hypertens Suppl*, 4(1):S3–5, 1986.

[6] M. M. Rapport, A. A. Green, and I. H. Page. Crystalline serotonin. *Science*, 108:329–330, 1948.

[7] M. M. Rapport, A. A. Green, and I. H. Page. Partial purification of the vasoconstrictor in beef serum. *J Biol Chem*, 174(2):735–741, 1948.

[8] M. M. Rapport. The discovery of serotonin. *Perspect Biol Med*, 40(2):260–73, 1997.

[9] K. E. Hamlin and F. E. Fischer. The synthesis of 5-hydroxytryptamine. *J Am Chem Soc*, 73(10):5007–5008, 1951.

[10] P. M. Whitaker-Azmitia. The discovery of serotonin and its role in neuroscience. *Neuropsychopharmacology*, 21(2 Suppl):2S–8S, 1999.

[11] A. Carlsson. A half-century of neurotransmitter research: Impact on neurology and psychiatry (Nobel lecture). *ChemBioChem*, 2(7-8):484, 2001.

[12] M. Naughton, J. B. Mulrooney, and B. E. Leonard. A review of the role of serotonin receptors in psychiatric disorders. *Hum Psychopharmacol*, 15(6):397–415, 2000.

[13] E. C. Azmitia. Serotonin neurons, neuroplasticity, and homeostasis of neural tissue. *Neuropsychopharmacology*, 21(2 Suppl):33S–45S, 1999.

[14] M. Jouvet. Sleep and serotonin: An unfinished story. *Neuropsychopharmacology*, 21(2 Suppl):24S–27S, 1999.

[15] M. D. Gershon. Review article: Roles played by 5-hydroxytryptamine in the physiology of the bowel. *Alimentary Pharmacology and Therapeutics*, 13:15–30, 1999.

[16] F. Chaouloff, O. Berton, and P. Mormede. Serotonin and stress. *Neuropsychopharmacology*, 21(2 Suppl):28S–32S, 1999.

[17] A. Martinez, P. M. Knappskog, and J. Haavik. A structural approach into human tryptophan hydroxylase and its implications for the regulation of serotonin biosynthesis. *Curr Med Chem*, 8(9):1077–91, 2001.

[18] T. J. Kappock and J. P. Caradonna. Pterin-dependent amino acid hydroxylases. *Chem Rev*, 96(7):2659–2756, 1996.

[19] H. Tamir and M. D. Gershon. Serotonin-storing secretory vesicles. *Ann N Y Acad Sci*, 600:53–66; discussion 67, 1990.

[20] M. C. Boadle-Biber. Regulation of serotonin synthesis. *Prog Biophys Mol Biol*, 60(1):1–15, 1993.

[21] P. P. Humphrey. The characterization and classification of neurotransmitter receptors. *Ann N Y Acad Sci*, 812:1–13, 1997.

[22] P. M. Vanhoutte, E. A. Barnard, G. J. Cosmides, P. P. Humphrey, M. Spedding, and T. Godfraind. International union of pharmacology committee on receptor nomenclature and drug classification. *Pharmacol Rev*, 46(2):111–6, 1994.

[23] P. Humphrey, M. Spedding, and P. Vanhoutte. Receptor classification and nomenclature: The revolution and the resolution. *Trends Pharmacol Sci*, 15(7):203–4, 1994.

[24] D. Hoyer, D. E. Clarke, J. R. Fozard, P. R. Hartig, G. R. Martin, E. J. Mylecharane, P. R. Saxena, and P. P. Humphrey. International union of pharmacology classification of receptors for 5-hydroxytryptamine (serotonin). *Pharmacol Rev*, 46(2):157–203, 1994.

[25] M. O. Ortells and G. G. Lunt. Evolutionary history of the ligand-gated ion-channel superfamily of receptors. *Trends Neurosci*, 18(3):121–7, 1995.

[26] J. H. Gaddum and Z. P. Picarelli. Two kinds of tryptamine receptor. *Br J Pharmacol*, 12(3):323–8, 1957.

[27] R. Schulz and C. Cartwright. Effect of morphine on serotonin release from myenteric plexus of the guinea pig. *J Pharmacol Exp Ther*, 190(3):420–30, 1974.

[28] W. Schaumann. Inhibition by morphine of the release of acetylcholine from the intestine of the guinea-pig. *Br J Pharmacol*, 12(1):115–8, 1957.

[29] P. B. Bradley, G. Engel, W. Feniuk, J. R. Fozard, P. P. Humphrey, D. N. Middlemiss, E. J. Mylecharane, B. P. Richardson, and P. R. Saxena. Proposals for the classification and nomenclature of functional receptors for 5-hydroxytryptamine. *Neuropharmacology*, 25(6):563–76, 1986.

[30] D. Hoyer, J. P. Hannon, and G. R. Martin. Molecular, pharmacological and functional diversity of 5-HT receptors. *Pharmacol Biochem Behav*, 71(4):533–54, 2002.

[31] N. M. Barnes and T. Sharp. A review of central 5-HT receptors and their function. *Neuropharmacology*, 38(8):1083–1152, 1999.

[32] P. Gaspar, O. Cases, and L. Maroteaux. The developmental role of serotonin: News from mouse molecular genetics. *Nat Rev Neurosci*, 4(12):1002–12, 2003.

[33] A. Nicke, H. G. Baumert, J. Rettinger, A. Eichele, G. Lambrecht, E. Mutschler, and G. Schmalzing. P2X(1) and P2X(3) receptors form stable trimers: A novel structural motif of ligand-gated ion channels. *EMBO J*, 17(11):3016–3028, 1998.

[34] G. Girdler and B. S. Khakh. ATP-gated P2X channels. *Curr Biol*, 14(1):R6, 2004.

[35] C. Vial, J. A. Roberts, and R. J. Evans. Molecular properties of ATP-gated P2X receptor ion channels. *Trends Pharmacol Sci*, 25(9):487–93, 2004.

[36] D. R. Madden. The structure and function of glutamate receptor ion channels. *Nat Rev Neurosc*, 3(2):91–101, 2002.

[37] N. Armstrong, Y. Sun, G. Q. Chen, and E. Gouaux. Structure of a glutamate-receptor ligand-binding core in complex with kainate. *Nature*, 395(6705):913–7, 1998.

[38] C. Rosenmund, Y. Stern-Bach, and C. F. Stevens. The tetrameric structure of a glutamate receptor channel. *Science*, 280(5369):1596–9, 1998.

[39] L. P. Wollmuth and A. I. Sobolevsky. Structure and gating of the glutamate receptor ion channel. *Trends Neurosci*, 27(6):321–8, 2004.

[40] E. Gouaux. Structure and function of AMPA receptors. *J Physiol*, 554(Pt 2):249–53, 2004.

[41] T. Nakagawa, Y. Cheng, E. Ramm, M. Sheng, and T. Walz. Structure and different conformational states of native AMPA receptor complexes. *Nature*, 433(7025):545–9, 2005.

[42] A. V. Maricq, A. S. Peterson, A. J. Brake, R. M. Myers, and D. Julius. Primary structure and functional expression of the $5HT_3$ receptor, a serotonin-gated ion channel. *Science*, 254(5030):432–7, 1991.

[43] S. Rajendra, J. W. Lynch, and P. R. Schofield. The glycine receptor. *Pharmacology and Therapeutics*, 73(2):121–146, 1997.

[44] R. Enz and G. R. Cutting. Molecular composition of $GABA_C$ receptors. *Vision Research*, 38(10):1431–1441, 1998.

[45] T. Grutter and J. P. Changeux. Nicotinic receptors in wonderland. *Trends Biochem Sci*, 26(8):459–63, 2001.

[46] M. L. Jensen, A. Schousboe, and P. K. Ahring. Charge selectivity of the Cys-loop family of ligand-gated ion channels. *J Neurochem*, 92(2):217–25, 2005.

[47] J. A. van Hooft, A. D. Spier, J. L. Yakel, S. C. R. Lummis, and H. P. M. Vijverberg. Promiscuous coassembly of serotonin 5-HT_3 and nicotinic $\alpha 4$ receptor subunits into Ca^{2+}-permeable ion channels. *Proc Natl Acad Sci USA*, 95(19):11456–11461, 1998.

[48] J. L. Eisele, S. Bertrand, J. L. Galzi, A. Devillersthiery, J. P. Changeux, and D. Bertrand. Chimeric nicotinic serotonergic receptor combines distinct ligand-binding and channel specificities. *Nature*, 366(6454):479–483, 1993.

[49] V. V. Koltchine, Q. Ye, S. E. Finn, and N. L. Harrison. Chimeric $GABA_A$/glycine receptors: Expression and barbiturate pharmacology. *Neuropharmacology*, 35(9-10):1445–56, 1996.

[50] C. Bouzat, F. Gumilar, G. Spitzmaul, H. L. Wang, D. Rayes, S. B. Hansen, P. Taylor, and S. M. Sine. Coupling of agonist binding to channel gating in an ACh-binding protein linked to an ion channel. *Nature*, 430(7002):896–900, 2004.

[51] T. Grutter, L. Prado de Carvalho, D. Virginie, A. Taly, M. Fischer, and J. P. Changeux. A chimera encoding the fusion of an acetylcholine-binding protein to an ion channel is stabilized in a state close to the desensitized form of ligand-gated ion channels. *C R Biol*, 328(3):223–34, 2005.

[52] K. Brejc, W. J. van Dijk, R. V. Klaassen, M. Schuurmans, J. van der Oost, A. B. Smit, and T. K. Sixma. Crystal structure of an ACh-binding protein reveals the ligand- binding domain of nicotinic receptors. *Nature*, 411(6835):269–276, 2001.

[53] M. V. Jones and G. L. Westbrook. The impact of receptor desensitization on fast synaptic transmission. *Trends Neurosci*, 19(3):96–101, 1996.

[54] J. Monod, J. Wyman, and J. P. Changeux. On the nature of allosteric transitions: A plausible model. *J Mol Biol*, 12:88–118, 1965.

[55] L. H. Tecott, A. V. Maricq, and D. Julius. Nervous system distribution of the serotonin 5-HT_3 receptor mRNA. *Proc Natl Acad Sci USA*, 90(4):1430–4, 1993.

[56] I. Maurer and H. P. Volz. Cell-mediated side effects of psychopharmacological treatment. *Arzneimittelforschung*, 51(10):785–92, 2001.

[57] M. C. Miquel, M. B. Emerit, A. Nosjean, A. Simon, P. Rumajogee, M. J. Brisorgueil, E. Doucet, M. Hamon, and D. Verge. Differential subcellular localization of the 5-HT_3-A_s receptor subunit in the rat central nervous system. *Eur J Neurosci*, 15(3):449–57, 2002.

[58] J. A. van Hooft and H. P. M. Vijverberg. 5-HT_3 receptors and neurotransmitter release in the CNS: A nerve ending story? *Trends Neurosc*, 23(12):605–610, 2000.

[59] A. J. Greenshaw and P. H. Silverstone. The non-antiemetic uses of serotonin 5-HT_3 receptor antagonists. Clinical pharmacology and therapeutic applications. *Drugs*, 53(1):20–39, 1997.

[60] L. Farber, U. Haus, M. Spath, and S. Drechsler. Physiology and pathophysiology of the 5-HT_3 receptor. *Scand J Rheumatol Suppl*, (119):2–8, 2004.

[61] M. D. Ferrari. 5-HT_3 receptor antagonists and migraine therapy. *J Neurol*, 238 Suppl 1:S53–6, 1991.

[62] P. Feyer, J. S. Zimmermann, O. J. Titlbach, A. Buchali, M. Hinkelbein, and V. Budach. Radiotherapy-induced emesis. An overview. *Strahlenther Onkol*, 174 Suppl 3:56–61, 1998.

[63] H. Schworer, H. Munke, F. Stockmann, and G. Ramadori. Treatment of diarrhea in carcinoid syndrome with ondansetron, tropisetron, and clonidine. *Am J Gastroenterol*, 90(4):645–8, 1995.

[64] P. Hrycaj. Serotonin type 3 receptor antagonist tropisetron in the treatment of chronic inflammatory rheumatic conditions–preliminary clinical experience. *Scand J Rheumatol Suppl*, (119):55–8, 2004.

[65] L. W. Fu and J. C. Longhurst. Activated platelets contribute to stimulation of cardiac afferents during ischaemia in cats: role of 5-HT_3 receptors. *J Physiol*, 544(Pt 3):897–912, 2002.

[66] S. M. Fung and M. J. Ferrill. Treatment of bulimia nervosa with ondansetron. *Ann Pharmacother*, 35(10):1270–3, 2001.

[67] M. C. Buhot, S. Martin, and L. Segu. Role of serotonin in memory impairment. *Ann Med*, 32(3):210–21, 2000.

[68] S. Bhatnagar, L. M. Sun, J. Raber, S. Maren, D. Julius, and M. F. Dallman. Changes in anxiety-related behaviors and hypothalamic-pituitary-adrenal activity in mice lacking the 5-HT-3A receptor. *Physiol Behav*, 81(4):545–55, 2004.

[69] S. Bhatnagar, N. Nowak, L. Babich, and L. Bok. Deletion of the 5-HT_3 receptor differentially affects behavior of males and females in the Porsolt forced swim and defensive withdrawal tests. *Behav Brain Res*, 153(2):527–35, 2004.

[70] B. Niesler, B. Frank, J. Kapeller, and G. A. Rappold. Cloning, physical mapping and expression analysis of the human 5-HT_3 serotonin receptor-like genes *HTR3C*, *HTR3D* and *HTR3E*. *Gene*, 310:101–11, 2003.

[71] A. M. Karnovsky, L. F. Gotow, D. D. McKinley, J. L. Piechan, C. L. Ruble, C. J. Mills, K. A. Schellin, J. L. Slightom, L. R. Fitzgerald, C. W. Benjamin, and S. L. Roberds. A cluster of novel serotonin receptor 3-like genes on human chromosome 3. *Gene*, 319:137–48, 2003.

[72] A. E. Dubin, M. G. Erlander, A. Huvar, R. Huvar, and L. K. Buehler. New DNA molecule encoding human 5-HT3-C protein for modifying the function of a serotonin 5-HT3-A receptor, 2001.

[73] G. W. Boyd, P. Low, J. I. Dunlop, L. A. Robertson, A. Vardy, J. J. Lambert, J. A. Peters, and C. N. Connolly. Assembly and cell surface expression of homomeric and heteromeric 5-HT3 receptors: The role of oligomerization and chaperone proteins. *Mol Cell Neurosc*, 21(1):38–50, 2002.

[74] G. W. Boyd, A. I. Doward, E. F. Kirkness, N. S. Millar, and C. N. Connolly. Cell surface expression of 5-hydroxytryptamine type 3 receptors is controlled by an endoplasmic reticulum retention signal. *J Biol Chem*, 278(30):27681–7, 2003.

[75] P. A. Davies, M. Pistis, M. C. Hanna, J. A. Peters, J. J. Lambert, T. G. Hales, and E. F. Kirkness. The 5-HT_{3B} subunit is a major determinant of serotonin-receptor function. *Nature*, 397(6717):359–363, 1999.

[76] C. A. Brady, I. M. Stanford, I. Ali, L. Lin, J. M. Williams, A. E. Dubin, A. G. Hope, and N. M. Barnes. Pharmacological comparison of human homomeric 5-HT_{3A} receptors versus heteromeric 5-$HT_{3A/3B}$ receptors. *Neuropharmacology*, 41(2):282–4, 2001.

[77] G. Hapfelmeier, C. Tredt, R. Haseneder, W. Zieglgansberger, B. Eisensamer, R. Rupprecht, and G. Rammes. Co-expression of the 5-HT_{3B} serotonin receptor subunit alters the biophysics of the 5-HT_3 receptor. *Biophys J*, 84(3):1720–1733, 2003.

[78] N. Hussy, W. Lukas, and K. A. Jones. Functional properties of a cloned 5-hydroxytryptamine ionotropic receptor subunit: Comparison with native mouse receptors. *J Physiol*, 481 (Pt 2):311–23, 1994.

[79] J. A. van Hooft, A. P. Kreikamp, and H. P. Vijverberg. Native serotonin 5-HT_3 receptors expressed in *Xenopus* oocytes differ from homopentameric 5-HT_3 receptors. *J Neurochem*, 69(3):1318–21, 1997.

[80] M. C. Miquel, M. B. Emerit, J. A. Gingrich, A. Nosjean, M. Hamon, and S. el Mestikawy. Developmental changes in the differential expression of two serotonin 5-HT_3 receptor splice variants in the rat. *J Neurochem*, 65(2):475–83, 1995.

[81] M. B. Emerit, M. P. Martres, M. C. Miquel, S. el Mestikawy, and M. Hamon. Differentiation alters the expression of the two splice variants of the serotonin 5-HT_3 receptor-A mRNA in NG108-15 cells. *J Neurochem*, 65(5):1917–25, 1995.

[82] R. Ranganathan, S. C. Cannon, and H. R. Horvitz. MOD-1 is a serotonin-gated chloride channel that modulates locomotory behaviour in *C. elegans*. *Nature*, 408(6811):470–5, 2000.

[83] I. Putrenko, M. Zakikhani, and J. A. Dent. A family of acetylcholine-gated chloride channel subunits in *Caenorhabditis elegans*. *J Biol Chem*, 280(8):6392–8, 2005.

[84] H. C. Neijt, H. P. Vijverberg, and J. Van den Bercken. The dopamine response in mouse neuroblastoma cells is mediated by serotonin $5HT_3$ receptors. *Eur J Pharmacol*, 127(3):271–4, 1986.

[85] H. M. Jacocks and B. M. Cox. Serotonin-stimulated release of [3H]dopamine via reversal of the dopamine transporter in rat striatum and nucleus accumbens: A comparison with release elicited by potassium, N-methyl-D-aspartic acid, glutamic acid and D-amphetamine. *J Pharmacol Exp Ther*, 262(1):356–64, 1992.

[86] A. D. Campbell, D. E. Womer, and J. R. Simon. The 5-HT_3 receptor agonist 1-(m-chlorophenyl)-biguanide interacts with the dopamine transporter in rat brain synaptosomes. *Eur J Pharmacol*, 290(2):157–62, 1995.

[87] E. Schlicker, M. Kathmann, H. J. Exner, M. Detzner, and M. Gothert. The 5-HT_3 receptor agonist 1-(m-chlorophenyl)-biguanide facilitates noradrenaline release by blockade of α2-adrenoceptors in the mouse brain cortex. *Naunyn Schmiedebergs Arch Pharmacol*, 349(1):20–4, 1994.

[88] C. Allgaier, P. Warnke, A. P. Stangl, and T. J. Feuerstein. Effects of 5-HT receptor agonists on depolarization-induced [3H]-noradrenaline release in rabbit hippocampus and human neocortex. *Br J Pharmacol*, 116(2):1769–74, 1995.

[89] R. L. Klein, E. Sanna, S. J. McQuilkin, P. J. Whiting, and R. A. Harris. Effects of 5-HT_3 receptor antagonists on binding and function of mouse and human $GABA_A$ receptors. *Eur J Pharmacol*, 268(2):237–46, 1994.

[90] J. H. Ye, R. Schaefer, W. H. Wu, P. L. Liu, V. K. Zbuzek, and J. J. McArdle. Inhibitory effect of ondansetron on glycine response of dissociated rat hippocampal neurons. *J Pharmacol Exp Ther*, 290(1):104–11, 1999.

[91] R. M. Eglen, E. H. Wong, A. Dumuis, and J. Bockaert. Central 5-HT_4 receptors. *Trends Pharmacol Sci*, 16(11):391–8, 1995.

[92] J. H. Ye, W. C. Mui, J. Ren, T. E. Hunt, W. H. Wu, and V. K. Zbuzek. Ondansetron exhibits the properties of a local anesthetic. *Anesth Analg*, 85(5):1116–21, 1997.

[93] R. M. Parker, K. R. Bentley, and N. M. Barnes. Allosteric modulation of 5-HT_3 receptors: focus on alcohols and anaesthetic agents. *Trends Pharmacol Sci*, 17(3):95–9, 1996.

[94] A. M. Brown, A. G. Hope, J. J. Lambert, and J. A. Peters. Ion permeation and conduction in a human recombinant 5-HT_3 receptor subunit (h5-HT_{3A}). *J Physiol*, 507 (Pt 3):653–65, 1998.

[95] A. G. Hope, D. L. Downie, L. Sutherland, J. J. Lambert, J. A. Peters, and B. Burchell. Cloning and functional expression of an apparent splice variant of the murine 5-HT_3 receptor A subunit. *Eur J Pharmacol*, 245(2):187–92, 1993.

[96] M. I. Sepulveda, S. C. Lummis, and I. L. Martin. The agonist properties of m-chlorophenylbiguanide and 2-methyl-5-hydroxytryptamine on 5-HT_3 receptors in N1E-115 neuroblastoma cells. *Br J Pharmacol*, 104(2):536–40, 1991.

[97] J. A. Peters, H. M. Malone, and J. J. Lambert. Ketamine potentiates 5-HT_3 receptor-mediated currents in rabbit nodose ganglion neurones. *Br J Pharmacol*, 103(3):1623–5, 1991.

[98] N. Unwin. Structure and action of the nicotinic acetylcholine receptor explored by electron microscopy. *FEBS Lett*, 555(1):91–5, 2003.

[99] V. I. Tsetlin and F. Hucho. Snake and snail toxins acting on nicotinic acetylcholine receptors: Fundamental aspects and medical applications. *FEBS Lett*, 557(1-3):9–13, 2004.

[100] R. W. Janes. α-Conotoxins as selective probes for nicotinic acetylcholine receptor subclasses. *Curr Opin Pharmacol*, 5(3):280–92, 2005.

[101] P. H. Celie, I. E. Kasheverov, D. Y. Mordvintsev, R. C. Hogg, P. van Nierop, R. van Elk, S. E. van Rossum-Fikkert, M. N. Zhmak, D. Bertrand, V. Tsetlin, T. K. Sixma, and A. B. Smit. Crystal structure of nicotinic acetylcholine receptor homolog AChBP in complex with an α-conotoxin PnIA variant. *Nat Struct Mol Biol*, 12(7):582–8, 2005.

[102] A. Karlin. Emerging structure of the nicotinic acetylcholine receptors. *Nat Rev Neurosci*, 3(2):102–114, 2002.

[103] W. G. Conroy, L. F. Ogden, and D. K. Berg. Cluster formation of α7-containing nicotinic receptors at interneuronal interfaces in cell culture. *Neuropharmacology*, 39(13):2699–2705, 2000.

[104] N. P. Barrera, P. Herbert, R. M. Henderson, I. L. Martin, and J. M. Edwardson. Atomic force microscopy reveals the stoichiometry and subunit arrangement of 5-HT_3 receptors. *Proc Natl Acad Sci USA*, 102(35):12595–12600, 2005.

[105] R. Hovius, A. P. Tairi, H. Blasey, A. Bernard, K. Lundstrom, and H. Vogel. Characterization of a mouse serotonin 5-HT_3 receptor purified from mammalian cells. *J Neurochem*, 70(2):824–34, 1998.

[106] R. M. McKernan, N. P. Gillard, K. Quirk, C. O. Kneen, G. I. Stevenson, C. J. Swain, and C. I. Ragan. Purification of the 5-hydroxytryptamine 5-HT_3 receptor from Ncb20 cells. *J Biol Chem*, 265(23):13572–13577, 1990.

[107] F. G. Boess, R. Beroukhim, and I. L. Martin. Ultrastructure of the 5-hydroxytryptamine(3) receptor. *J Neurochem*, 64(3):1401–1405, 1995.

[108] A. Miyazawa, Y. Fujiyoshi, and N. Unwin. Structure and gating mechanism of the acetylcholine receptor pore. *Nature*, 423(6943):949–955, 2003.

[109] N. Unwin. Refined structure of the nicotinic acetylcholine receptor at 4Å resolution. *J Mol Biol*, 346(4):967–89, 2005.

[110] A. Cha, G. E. Snyder, P. R. Selvin, and F. Bezanilla. Atomic scale movement of the voltage-sensing region in a potassium channel measured via spectroscopy. *Nature*, 402(6763):809–813, 1999.

[111] P. Schwille, U. Haupts, S. Maiti, and W. W. Webb. Molecular dynamics in living cells observed by fluorescence correlation spectroscopy with one- and two-photon excitation. *Biophys J*, 77(4):2251–65, 1999.

[112] C. Chamberlain and K. M. Hahn. Watching proteins in the wild: Fluorescence methods to study protein dynamics in living cells. *Traffic*, 1(10):755–62, 2000.

[113] R. Y. Tsien. The green fluorescent protein. *Annu Rev Biochem*, 67:509–44, 1998.

[114] N. C. Shaner, R. E. Campbell, P. A. Steinbach, B. N. Giepmans, A. E. Palmer, and R. Y. Tsien. Improved monomeric red, orange and yellow fluorescent proteins derived from *Discosoma* sp. red fluorescent protein. *Nat Biotechnol*, 22(12):1567–72, 2004.

[115] J. Farinas and A. S. Verkman. Receptor-mediated targeting of fluorescent probes in living cells. *J Biol Chem*, 274(12):7603–6, 1999.

[116] L. W. Miller, J. Sable, P. Goelet, M. P. Sheetz, and V. W. Cornish. Methotrexate conjugates: A molecular in vivo protein tag. *Angew Chem Int Ed*, 43(13):1672–1675, 2004.

[117] K. M. Marks, P. D. Braun, and G. P. Nolan. A general approach for chemical labeling and rapid, spatially controlled protein inactivation. *Proc Natl Acad Sci USA*, 101(27):9982–7, 2004.

[118] A. Keppler, S. Gendreizig, T. Gronemeyer, H. Pick, H. Vogel, and K. Johnsson. A general method for the covalent labeling of fusion proteins with small molecules *in vivo*. *Nat Biotechnol*, 21(1):86–9, 2003.

[119] A. Keppler, M. Kindermann, S. Gendreizig, H. Pick, H. Vogel, and K. Johnsson. Labeling of fusion proteins of O^6-alkylguanine-DNA alkyltransferase with small molecules in vivo and in vitro. *Methods*, 32(4):437–44, 2004. 1046-2023 Journal Article.

[120] A. Juillerat, C. Heinis, I. Sielaff, J. Barnikow, H. Jaccard, B. Kunz, A. Terskikh, and K. Johnsson. Engineering substrate specificity of O^6-alkylguanine-DNA alkyltransferase for specific protein labeling in living cells. *ChemBioChem*, 6(7):1263–1269, 2005.

[121] N. George, H. Pick, H. Vogel, N. Johnsson, and K. Johnsson. Specific labeling of cell surface proteins with chemically diverse compounds. *J Am Chem Soc*, 126(29):8896–7, 2004.

[122] L. Vivero-Pol, N. George, H. Krumm, K. Johnsson, and N. Johnsson. Multicolor imaging of cell surface proteins. *J. Am. Chem. Soc.*, 127(37):12770–12771, 2005.

[123] B. A. Griffin, S. R. Adams, and R. Y. Tsien. Specific covalent labeling of recombinant protein molecules inside live cells. *Science*, 281(5374):269–72, 1998.

[124] J. Nakanishi, N. Takahiro, S. Moritoshi, and O. Takeaki. Imaging of conformational changes of proteins with a new environment-sensitive fluorescent probe designed for site-specific labeling of recombinant proteins in live cells. *Anal. Chem*, 73:2920–2928, 2001.

[125] G. Gaietta, T. J. Deerinck, S. R. Adams, J. Bouwer, O. Tour, D. W. Laird, G. E. Sosinsky, R. Y. Tsien, and M. H. Ellisman. Multicolor and electron microscopic imaging of connexin trafficking. *Science*, 296(5567):503–507, 2002.

[126] W. Ju, W. Morishita, J. Tsui, G. Gaietta, T. J. Deerinck, S. R. Adams, C. C. Garner, R. Y. Tsien, M. H. Ellisman, and R. C. Malenka. Activity-dependent regulation of dendritic synthesis and trafficking of AMPA receptors. *Nat Neurosci*, 7(3):244–53, 2004.

[127] I. Chen, M. Howarth, W. Y. Lin, and A. Y. Ting. Site-specific labeling of cell surface proteins with biophysical probes using biotin ligase. *Nat Methods*, 2(2):99–104, 2005.

[128] M. Howarth, K. Takao, Y. Hayashi, and A. Y. Ting. Targeting quantum dots to surface proteins in living cells with biotin ligase. *P Natl Acad Sci USA*, 102(21):7583–7588, 2005.

[129] D. A. Dougherty. Unnatural amino acids as probes of protein structure and function. *Curr Opin Chem Biol*, 4(6):645–52, 2000.

[130] E. Ilegems, H. M. Pick, and H. Vogel. Monitoring mis-acylated tRNA suppression efficiency in mammalian cells via EGFP fluorescence recovery. *Nucleic Acids Res*, 30(23):e128, 2002.

[131] L. Wang and P. G. Schultz. Expanding the genetic code. *Angew Chem Int Ed*, 44(1):34–66, 2005.

[132] I. Chen and A. Y. Ting. Site-specific labeling of proteins with small molecules in live cells. *Curr Opin Biotechnol*, 16(1):35–40, 2005.

[133] L. W. Miller and V. W. Cornish. Selective chemical labeling of proteins in living cells. *Curr Opin Chem Biol*, 9(1):56–61, 2005.

[134] T. Gronemeyer, G. Godin, and K. Johnsson. Adding value to fusion proteins through covalent labelling. *Curr Opin Biotechnol*, 16(4):453–8, 2005.

[135] E. Hochuli, H. Dobeli, and A. Schacher. New metal chelate adsorbent selective for proteins and peptides containing neighbouring histidine residues. *J Chromatogr*, 411:177–84, 1987.

[136] S. A. McMahan and R. R. Burgess. Single-step synthesis and characterization of biotinylated nitrilotriacetic acid, a unique reagent for the detection of histidine-tagged proteins immobilized on nitrocellulose. *Anal Biochem*, 236(1):101–6, 1996.

[137] A. N. Kapanidis, Y. W. Ebright, and R. H. Ebright. Site-specific incorporation of fluorescent probes into protein: Hexahistidine-tag-mediated fluorescent labeling with (Ni^{2+}: Nitrilotriacetic acid)(n)-fluorochrome conjugates. *J Am Chem Soc*, 123(48):12123–12125, 2001.

[138] T.A. Keller, C. Duschl, D. Kröger, A. Sévin, S. Cervigni, P. Dumy, and H. Vogel. Reversible oriented immobilization of histidine-tagged proteins on gold surfaces using a chelator thioalkane. *Supramol Sci*, 2:155–160, 1995.

[139] E. A. Jares-Erijman and T. M. Jovin. FRET imaging. *Nat Biotechnol*, 21(11):1387–95, 2003.

[140] B.W. van der Meer, G. Cocker, and S.Y.S. Chen. *Resonance energy transfer: Theory and data*. VCH Publishers, New York, 1994.

[141] J. R. Lakowicz. *Principles of Fluorescence Spectroscopy*. Plenum Publishers, New-York, second edition, 1999.

[142] H. Pick, A. K. Preuss, M. Mayer, T. Wohland, R. Hovius, and H. Vogel. Monitoring expression and clustering of the ionotropic $5HT_3$ receptor in plasma membranes of live biological cells. *Biochemistry*, 42(4):877–84, 2003.

[143] B. Meyer. *Investigation of the Neurokinin-1 receptor by fluorescence techniques*. PhD thesis, Swiss Federal Institut of Technology of Lausanne (EPFL), 2005.

[144] H. Gutfreund. *Kinetics for the life sciences: Receptors, transmitters and catalysts*. Cambridge University Press, 1995.

[145] T. Wohland, K. Friedrich, R. Hovius, and H. Vogel. Study of ligand-receptor interactions by fluorescence correlation spectroscopy with different fluorophores: Evidence that the homopentameric 5-hydroxytryptamine type 3As receptor binds only one ligand. *Biochemistry*, 38(27):8671–8681, 1999.

[146] P. Vallotton, A. P. Tairi, T. Wohland, K. Friedrich-Benet, H. Pick, R. Hovius, and H. Vogel. Mapping the antagonist binding site of the serotonin type 3 receptor by fluorescence resonance energy transfer. *Biochemistry*, 40(41):12237–42, 2001.

[147] C. Schreiter, R. Hovius, M. Costioli, H. Pick, S. Kellenberger, L. Schild, and H. Vogel. Characterization of the ligand-binding site of the serotonin 5- HT_3 receptor - the role of glutamate residues 97, 224, and 235. *J Biol Chem*, 278(25):22709–22716, 2003.

[148] J. E. Hale. Irreversible, oriented immobilization of antibodies to cobalt-iminodiacetate resin for use as immunoaffinity media. *Anal Biochem*, 231(1):46–49, 1995.

[149] D. C. Reeves and S. C. R. Lummis. The molecular basis of the structure and function of the 5-HT_3 receptor: A model ligand-gated ion channel. *Mol Memb Biol*, 19:11–26, 2002.

[150] A. P. Tairi, R. Hovius, H. Pick, H. Blasey, A. Bernard, A. Surprenant, K. Lundstrom, and H. Vogel. Ligand binding to the serotonin $5HT_3$ receptor studied with a novel fluorescent ligand. *Biochemistry*, 37(45):15850–15864, 1998.

[151] S. H. White and W. C. Wimley. Membrane protein folding and stability: Physical principles. *Annu Rev Biophys Biomol Struct*, 28:319–365, 1999.

[152] H. Sprong, P. van der Sluijs, and G. van Meer. How proteins move lipids and lipids move proteins. *Nat Rev Mol Cell Biol*, 2(7):504–13, 2001.

[153] C. A. Maggi and T. W. Schwartz. The dual nature of the tachykinin NK1 receptor. *Trends Pharmacol Sci*, 18(10):351–5, 1997.

[154] K. L. Pierce, R. T. Premont, and R. J. Lefkowitz. Seven-transmembrane receptors. *Nature Reviews Molecular Cell Biology*, 3(9):639–650, 2002.

[155] S. Weiss. Fluorescence spectroscopy of single biomolecules. *Science*, 283(5408):1676–83, 1999.

[156] P. Tinnefeld and M. Sauer. Branching out of single-molecule fluorescence spectroscopy: Challenges for chemistry and influence on biology. *Angew Chem Int Ed*, 44(18):2642–2671, 2005.

[157] J. Meier, C. Vannier, A. Serge, A. Triller, and D. Choquet. Fast and reversible trapping of surface glycine receptors by gephyrin. *Nat Neurosci*, 4(3):253–60, 2001.

[158] A. Kusumi, Y. Sako, and M. Yamamoto. Confined lateral diffusion of membrane receptors as studied by single particle tracking (nanovid microscopy). Effects of calcium-induced differentiation in cultured epithelial cells. *Biophys J*, 65(5):2021–40, 1993.

[159] M. Dahan, S. Levi, C. Luccardini, P. Rostaing, B. Riveau, and A. Triller. Diffusion dynamics of glycine receptors revealed by single-quantum dot tracking. *Science*, 302(5644):442–5, 2003.

[160] S. Weiss. Measuring conformational dynamics of biomolecules by single molecule fluorescence spectroscopy. *Nat Struct Biol*, 7(9):724–9, 2000.

[161] A. Ishijima and T. Yanagida. Single molecule nanobioscience. *Trends Biochem Sci*, 26(7):438–44, 2001.

[162] H. P. Lu, L. Xun, and X. S. Xie. Single-molecule enzymatic dynamics. *Science*, 282(5395):1877–82, 1998.

[163] S. N. Xie. Single-molecule approach to enzymology. *Single Mol*, 2(4):229–236, 2001.

[164] A. Sonnleitner, G. J. Schütz, and T. Schmidt. Free brownian motion of individual lipid molecules in biomembranes. *Biophys J*, 77(5):2638–42, 1999.

[165] Y. Sako, S. Minoghchi, and T. Yanagida. Single-molecule imaging of EGFR signalling on the surface of living cells. *Nat Cell Biol*, 2(3):168–72, 2000.

[166] G. J. Schütz, G. Kada, V. P. Pastushenko, and H. Schindler. Properties of lipid microdomains in a muscle cell membrane visualized by single molecule microscopy. *EMBO J*, 19(5):892–901, 2000.

[167] G. J. Schütz, V. P. Pastushenko, H. J. Gruber, H. Knaus, B. Pragl, and H. Schindler. 3D imaging of individual ion channels in live cells at 40 nm resolution. *Single Mol*, (1):25–31, 2000.

[168] L. Groc, M. Heine, L. Cognet, K. Brickley, F. A. Stephenson, B. Lounis, and D. Choquet. Differential activity-dependent regulation of the lateral mobilities of AMPA and NMDA receptors. *Nat Neurosci*, 7(7):695–6, 2004.

[169] K. Suzuki, K. Ritchie, E. Kajikawa, T. Fujiwara, and A. Kusumi. Rapid hop diffusion of a G protein-coupled receptor in the plasma membrane as revealed by single-molecule techniques. *Biophys J*, 88(5):3659–3680, 2005.

[170] R. Iino, I. Koyama, and A. Kusumi. Single molecule imaging of green fluorescent proteins in living cells: E-cadherin forms oligomers on the free cell surface. *Biophys J*, 80(6):2667–2677, 2001.

[171] G. Seisenberger, M. U. Ried, T. Endress, H. Buning, M. Hallek, and C. Brauchle. Real-time single-molecule imaging of the infection pathway of an adeno-associated virus. *Science*, 294(5548):1929–1932, 2001.

[172] V. T. Nguyen, Y. Kamio, and H. Higuchi. Single-molecule imaging of cooperative assembly of gamma-hemolysin on erythrocyte membranes. *EMBO J*, 22(19):4968–79, 2003.

[173] N. Watanabe and T. J. Mitchison. Single-molecule speckle analysis of Aactin filament turnover in lamellipodia. *Science*, 295(5557):1083–1086, 2002.

[174] D. Choquet and A. Triller. The role of receptor diffusion in the organization of the postsynaptic membrane. *Nat Rev Neurosci*, 4(4):251–65, 2003.

[175] T. A. Blanpied, D. B. Scott, and M. D. Ehlers. Dynamics and regulation of clathrin coats at specialized endocytic zones of dendrites and spines. *Neuron*, 36(3):435–49, 2002.

[176] M. Rosenberg, J. Meier, A. Triller, and C. Vannier. Dynamics of glycine receptor insertion in the neuronal plasma membrane. *J Neurosci*, 21(14):5036–44, 2001.

[177] M. Moransard, L. S. Borges, R. Willmann, P. A. Marangi, H. R. Brenner, M. J. Ferns, and C. Fuhrer. Agrin regulates rapsyn interaction with surface acetylcholine receptors, and this underlies cytoskeletal anchoring and clustering. *J Biol Chem*, 278(9):7350–9, 2003.

[178] M. B. Emerit, E. Doucet, M. Darmon, and M. Hamon. Native and cloned 5-HT_{3A}(S) receptors are anchored to F-actin in clonal cells and neurons. *Mol Cell Neurosci*, 20(1):110–24, 2002.

[179] L. Fleury, J.-M. Segura, G. Zumofen, B. Hecht, and U. P. Wild. Nonclassical photon statistics in single-molecule fluorescence at room temperature. *Phys Rev Lett*, 84(6):1148–1151, 2000.

[180] S. A. Rosenberg, M. E. Quinlan, J. N. Forkey, and Y. E. Goldman. Rational motions of macromolecules by single-molecule fluorescence microscopy. *Acc. Chem. Res.*, (38):583–593, 2005.

[181] G. S. Harms, L. Cognet, P. H. M. Lommerse, G. A. Blab, and T. Schmidt. Autofluorescent proteins in single-molecule research: Applications to live cell imaging microscopy. *Biophys J*, 80(5):2396–2408, 2001.

[182] G. J. Schütz, H. Schindler, and T. Schmidt. Single-molecule microscopy on model membranes reveals anomalous diffusion. *Biophys J*, 73(2):1073–1080, 1997.

[183] S. Milon. Etude du comportement diffusif des protéines ancrées à un GPI dans des membranes biologiques par FCS (fluorescence correlation spectroscopy). Technical report, EPFL, 2000.

[184] E. Ilegems, H. Pick, C. Deluz, S. Kellenberger, and H. Vogel. Noninvasive imaging of 5-HT_3 receptor trafficking in live cells: From biosynthesis to endocytosis. *J. Biol. Chem.*, 279(51):53346–53352, 2004.

[185] A. Taly, M. Delarue, T. Grutter, M. Nilges, N. Le Novere, P. J. Corringer, and J. P. Changeux. Normal mode analysis suggests a quaternary twist model for the nicotinic receptor gating mechanism. *Biophys J*, 88(6):3954–65, 2005.

[186] A. Mitra, T. D. Bailey, and A. L. Auerbach. Structural dynamics of the M4 transmembrane segment during acetylcholine receptor gating. *Structure*, 12(10):1909–18, 2004.

[187] H. A. Lester, M. I. Dibas, D. S. Dahan, J. F. Leite, and D. A. Dougherty. Cys-loop receptors: New twists and turns. *Trends Neurosci*, 27(6):329–36, 2004.

[188] M. H. Akabas, D. A. Stauffer, M. Xu, and A. Karlin. Acetylcholine receptor channel structure probed in cysteine-substitution mutants. *Science*, 258(5080):307–10, 1992.

[189] J. Horenstein, D. A. Wagner, C. Czajkowski, and M. H. Akabas. Protein mobility and GABA-induced conformational changes in $GABA_A$ receptor pore-lining M2 segment. *Nat Neurosci*, 4(5):477–85, 2001.

[190] J. F. Leite, M. P. Blanton, M. Shahgholi, D. A. Dougherty, and H. A. Lester. Conformation-dependent hydrophobic photolabeling of the nicotinic receptor: electrophysiology-coordinated photochemistry and mass spectrometry. *Proc Natl Acad Sci USA*, 100(22):13054–9, 2003.

[191] P. J. Corringer, N. Le Novere, and J. P. Changeux. Nicotinic receptors at the amino acid level. *Annu Rev Pharmacol Toxicol*, 40:431–458, 2000.

[192] L. M. Mannuzzu, M. M. Moronne, and E. Y. Isacoff. Direct physical measure of conformational rearrangement underlying potassium channel gating. *Science*, 271(5246):213–6, 1996.

[193] A. Cha and F. Bezanilla. Characterizing voltage-dependent conformational changes in the *Shaker* K^+ channel with fluorescence. *Neuron*, 19(5):1127–40, 1997.

[194] M. Li, R. A. Farley, and H. A. Lester. An intermediate state of the γ-aminobutyric acid transporter GAT1 revealed by simultaneous voltage clamp and fluorescence. *J Gen Physiol*, 115(4):491–508, 2000.

[195] H. P. Larsson, A. V. Tzingounis, H. P. Koch, and M. P. Kavanaugh. Fluorometric measurements of conformational changes in glutamate transporters. *Proc Natl Acad Sci USA*, 101(11):3951–6, 2004.

[196] Y. Chang and D. S. Weiss. Site-specific fluorescence reveals distinct structural changes with GABA receptor activation and antagonism. *Nat Neurosci*, 5(11):1163–8, 2002.

[197] D. S. Dahan, M. I. Dibas, E. J. Petersson, V. C. Auyeung, B. Chanda, F. Bezanilla, D. A. Dougherty, and H. A. Lester. A fluorophore attached to nicotinic acetylcholine receptor βM2 detects productive binding of agonist to the $\alpha\delta$ site. *Proc Natl Acad Sci USA*, 101(27):10195–200, 2004.

[198] E. Ilegems, H. Pick, C. Deluz, S. Kellenberger, and H. Vogel. Ligand binding transmits conformational changes across the membrane-spanning part to the intracellular side of the 5-HT_3 serotonin receptor. *ChemBioChem*, In press, 2005.

[199] Q. Shan, S. T. Nevin, J. L. Haddrill, and J. W. Lynch. Asymmetric contribution of α and β subunits to the activation of $\alpha\beta$ heteromeric glycine receptors. *J Neurochem*, 86(2):498–507, 2003.

[200] A. Campos-Caro, S. Sala, J. J. Ballesta, F. Vicente-Agullo, M. Criado, and F. Sala. A single residue in the M2-M3 loop is a major determinant of coupling between binding and gating in neuronal nicotinic receptors. *Proc Natl Acad Sci USA*, 93(12):6118–23, 1996.

[201] C. M. Deane and S. C. Lummis. The role and predicted propensity of conserved proline residues in the 5-HT_3 receptor. *J Biol Chem*, 276(41):37962–6, 2001.

[202] T. L. Kash, A. Jenkins, J. C. Kelley, J. R. Trudell, and N. L. Harrison. Coupling of agonist binding to channel gating in the $GABA_A$ receptor. *Nature*, 421(6920):272–5, 2003.

[203] A. K. Bera, M. Chatav, and M. H. Akabas. $GABA_A$ receptor M2-M3 loop secondary structure and changes in accessibility during channel gating. *J Biol Chem*, 277(45):43002–43010, 2002.

[204] J. W. Lynch, N. L. Han, J. Haddrill, K. D. Pierce, and P. R. Schofield. The surface accessibility of the glycine receptor M2-M3 loop is increased in the channel open state. *J Neurosci*, 21(8):2589–99, 2001.

[205] J. W. Lynch, S. Rajendra, K. D. Pierce, C. A. Handford, P. H. Barry, and P. R. Schofield. Identification of intracellular and extracellular domains mediating signal transduction in the inhibitory glycine receptor chloride channel. *EMBO J*, 16(1):110–20, 1997.

[206] R. Croxen, C. Newland, D. Beeson, H. Oosterhuis, G. Chauplannaz, A. Vincent, and J. Newsom-Davis. Mutations in different functional domains of

the human muscle acetylcholine receptor α subunit in patients with the slow-channel congenital myasthenic syndrome. *Hum Mol Genet*, 6(5):767–74, 1997.

[207] M. H. Akabas, C. Kaufmann, P. Archdeacon, and A. Karlin. Identification of acetylcholine receptor channel-lining residues in the entire M2 segment of the α subunit. *Neuron*, 13(4):919–27, 1994.

[208] H. Zhang and A. Karlin. Contribution of the β subunit M2 segment to the ion-conducting pathway of the acetylcholine receptor. *Biochemistry*, 37(22):7952–64, 1998.

[209] G. Wilson and A. Karlin. Acetylcholine receptor channel structure in the resting, open, and desensitized states probed with the substituted-cysteine-accessibility method. *Proc Natl Acad Sci USA*, 98(3):1241–8, 2001.

[210] D. C. Reeves, E. N. Goren, M. H. Akabas, and S. C. R. Lummis. Structural and electrostatic properties of the 5-HT_3 receptor pore revealed by substituted cysteine accessibility mutagenesis. *J Biol Chem*, 276(45):42035–42042, 2001.

[211] E. Neher and B. Sakmann. Single-channel currents recorded from membrane of denervated frog muscle-fibers. *Nature*, 260(5554):799–802, 1976.

[212] B. Sakmann and E. Neher. *Single-Channel Recording*. Kluwer Academic / Plenum Publishers, 2^{nd} edition, 1997.

[213] L. B. Cohen and B. M. Salzberg. Optical measurement of membrane potential. *Rev Physiol Biochem Pharmacol*, 83:35–88, 1978.

[214] H. M. Shapiro. Membrane potential estimation by flow cytometry. *Methods*, 21(3):271–9, 2000.

[215] S. Panicker, H. Cruz, C. Arrabit, and P. A. Slesinger. Evidence for a centrally located gate in the pore of a serotonin-gated ion channel. *J. Neurosci.*, 22(5):1629–1639, 2002.

[216] V. Derkach, A. Surprenant, and R. A. North. 5-HT_3 receptors are membrane ion channels. *Nature*, 339(6227):706–9, 1989.

[217] J. A. van Hooft, A. R. Kooyman, A. Verkerk, R. G. van Kleef, and H. P. Vijverberg. Single 5-HT_3 receptor-gated ion channel events resolved in N1E-115 mouse neuroblastoma cells. *Biochem Biophys Res Commun*, 199(1):227–33, 1994.

[218] J. A. van Hooft and H. P. Vijverberg. Phosphorylation controls conductance of 5-HT_3 receptor ligand-gated ion channels. *Receptors Channels*, 3(1):7–12, 1995.

[219] W. P. Hu, X. H. You, B. C. Guan, L. Q. Ru, J. G. Chen, and Z. W. Li. Substance P potentiates 5-HT_3 receptor-mediated current in rat trigeminal ganglion neurons. *Neurosci Lett*, 365(2):147–52, 2004.

[220] G. Hapfelmeier, R. Haseneder, K. Lampadius, G. Rammes, R. Rupprecht, and W. Zieglgansberger. Cloned human and murine serotonin$_{3A}$ receptors expressed in human embryonic kidney 293 cells display different single-channel kinetics. *Neurosci Lett*, 335(1):44–8, 2002.

[221] C. H. Gill, J. A. Peters, and J. J. Lambert. An electrophysiological investigation of the properties of a murine recombinant 5-HT_3 receptor stably expressed in HEK 293 cells. *Br J Pharmacol*, 114(6):1211–21, 1995.

[222] S. Mochizuki, A. Miyake, and K. Furuichi. Ion permeation properties of a cloned human 5-HT_3 receptor transiently expressed in HEK 293 cells. *Amino Acids*, 17(3):243–55, 1999.

[223] S. P. Kelley, J. I. Dunlop, E. F. Kirkness, J. J. Lambert, and J. A. Peters. A cytoplasmic region determines single-channel conductance in 5-HT_3 receptors. *Nature*, 424(6946):321–4, 2003.

[224] W. Hanke and W.-R. Schlue. *Planar lipid bilayer: Methods and applications*. Academic Press, London, 1993.

[225] H. Nyquist. Thermal agitation of electric charge in conductors. *Phys Rev*, (32):110–113, 1928.

[226] P. Lauger. Shot noise in ion channels. *Biochim Biophys Acta*, 413(1):1–10, 1975.

[227] F. J. Sigworth. Open channel noise. I. Noise in acetylcholine-receptor currents suggests conformational fluctuations. *Biophys J*, 47(5):709–720, 1985.

[228] S. Nekolla, C. Andersen, and R. Benz. Noise-analysis of ion current through the open and the sugar-induced closed state of the lamb channel of *Escherichia-Coli* outer-membrane : Evaluation of the sugar binding-kinetics to the channel interior. *Biophys J*, 66(5):1388–1397, 1994.

[229] F. Wohnsland and R. Benz. 1/f-noise of open bacterial porin channels. *J Membrane Biol*, 158(1):77–85, 1997.

[230] S. M. Bezrukov and M. Winterhalter. Examining noise sources at the single-molecule level: 1/f noise of an open maltoporin channel. *Phys Rev Lett*, 85(1):202–205, 2000.

[231] Z. Siwy and A. Fulinski. Origin of $1/f^{\alpha}$ noise in membrane channel currents. *Phys Rev Lett*, 89(15), 2002.

[232] P. Lauger. Structural fluctuations and current noise of ionic channels. *Biophys J*, 48(3):369–373, 1985.

[233] D. O. D. Mak and W. W. Webb. Molecular dynamics of alamethicin transmembrane channels from open-channel current noise analysis. *Biophys J*, 69(6):2337–2349, 1995.

[234] P. A. Borea, A. Dalpiaz, S. Gessi, and G. Gilli. Thermodynamics of 5-HT_3 receptor binding discriminates agonistic from antagonistic behaviour. *Eur J Pharmacol*, 298(3):329–34, 1996.

[235] P. A. Borea, K. Varani, S. Gessi, P. Gilli, and G. Gilli. Binding thermodynamics at the human neuronal nicotine receptor. *Biochem Pharmacol*, 55(8):1189–97, 1998.

[236] B. E. Cohen, T. B. McAnaney, E. S. Park, Y. N. Jan, S. G. Boxer, and L. Y. Jan. Probing protein electrostatics with a synthetic fluorescent amino acid. *Science*, 296(5573):1700–1703, 2002.

[237] B. E. Cohen, A. Pralle, X. Yao, G. Swaminath, C. S. Gandhi, Y. N. Jan, B. K. Kobilka, E. Y. Isacoff, and L. Y. Jan. A fluorescent probe designed for studying protein conformational change. *Proc Natl Acad Sci USA*, 102(4):965–70, 2005.

Acknowledgements

It would never have been possible to achieve all the work presented here without the help of many persons to whom I want to address all my gratitude.

First of all, I would like to thank Professor Horst Vogel for giving me the opportunity to join his lab for the PhD thesis. I really appreciated the independence he gave me to pursue my project but also his availability for discussions and advices in this very interdisciplinary environment. I would like also to thank him for letting me travelling and participating to very interesting international conferences.

I especially want to thank Ruud Hovius who coached me these last years. He taught me nearly everything in the field of biophysics and answered all my questions always with the same patience. His availability and enthusiasm have been very pleasant and contributed a lot to my motivation.

My thanks go also to Jean-Manuel Segura for his assistance in all questions, for teaching me the bases of single molecule spectroscopy and single particle tracking, and for his incredible patience for data analysis. Collaborating with him was always very enjoyable.

I would like to thank Daniel Abankwa for careful reading of parts of the manuscript, as well as Christophe Danelon, Ruud Hovius and Jean-Manuel Segura. My thanks also to Lorraine, for all the grammatical corrections. I would also like to thank Joerg Grandl and Christoph Schreiter for introducing me to the world of electrophysiology, Christophe Danelon for all the work he performed for the noise analysis treatment, Nina Dixit for the cysteine-less construct, Cédric Deluz for his devotion in the lab and help with ordering materials, and Verena Tabet for all the administrative procedures. Of course, I thank all the members of the Vogel lab, present and former, for the nice atmosphere and for all the parties, who made working in this institute a pleasure. Moreover, I would like to thank all my friends who were of great support.

And last but not least, I would like to thank my parents and my sister for their love, encouragement and support throughout these years.

Curriculum Vitæ

Emmanuel G. Guignet
Born on December 20, 1977 in Orbe, Switzerland
Citizen of Essertes, VD, Switzerland

since 2001	PhD thesis under supervision of Prof. Horst Vogel at the Institute of Chemical Sciences and Engineering of ETH Lausanne, Switzerland.
1996 – 2001	Chemical engineering at ETH Lausanne, Switzerland. **Sygenta Monthey Prize**, recompensing the best results in the Chemistry section.
1993 – 1996	Maturité fédérale C, Gymnase CESSNOV in Yverdon-les-Bains, Switzerland. Prize of mathematics, physics and best general results.
1984 – 1993	Primary and secondary school in Grandson, Switzerland.